Russian Original Vol. 35, No. 5, November, 1973

May, 1974

SATEAZ 35(5) 977-1062 (1973)

SOVIET ATOMIC ENERGY

АТОМНАЯ ЭНЕРГИЯ
(ATOMNAYA ÉNERGIYA)

TRANSLATED FROM RUSSIAN

CONSULTANTS BUREAU, NEW YORK

SOVIET ATOMIC ENERGY

Soviet Atomic Energy is a cover-to-cover translation of *Atomnaya Énergiya*, a publication of the Academy of Sciences of the USSR.

An arrangement with Mezhdunarodnaya Kniga, the Soviet book export agency, makes available both advance copies of the Russian journal and original glossy photographs and artwork. This serves to decrease the necessary time lag between publication of the original and publication of the translation and helps to improve the quality of the latter. The translation began with the first issue of the Russian journal.

Consultants Bureau journals appear about six months after the publication of the original Russian issue. For bibliographic accuracy, the English issue published by Consultants Bureau carries the same number and date as the original Russian from which it was translated. For example, a Russian issue published in December will appear in a Consultants Bureau English translation about the following June, but the translation issue will carry the December date. When ordering any volume or particular issue of a Consultants Bureau journal, please specify the date and, where applicable, the volume and issue numbers of the original Russian. The material you will receive will be a translation of that Russian volume or issue.

Subscription
$80 per volume (6 Issues)
2 volumes per year
(Add $5 for orders outside the United States and Canada.)

Single Issue: $30
Single Article: $15

CONSULTANTS BUREAU, NEW YORK AND LONDON

227 West 17th Street
New York, New York 10011

Davis House
8 Scrubs Lane
Harlesden, NW10 6SE
England

Published monthly. Second-class postage paid at Jamaica, New York 11431.

Soviet Atomic Energy is abstracted or indexed in *Applied Mechanics Reviews, Chemical Abstracts, Engineering Index, INSPEC—Physics Abstracts and Electrical and Electronics Abstracts, Current Contents,* and *Nuclear Science Abstracts.*

SOVIET ATOMIC ENERGY

A translation of *Atomnaya Énergiya*

May, 1974

Volume 35, Number 5 November, 1973

CONTENTS

CONTENTS

(continued)

The Russian press date (podpisano k pechati) of this issue was 10/25/1973. Publication therefore did not occur prior to this date, but must be assumed to have taken place reasonably soon thereafter.

ARTICLES

BILIBINO NUCLEAR POWER STATION

V. M. Abramov, A. V. Bondarenko,
A. A. Vaimugin, L. V. Gurevich,
V. V. Dolgov, O. V. Komissarov,
M. E. Minashin, P. A. Nikolenko,
A. L. Simonyan, G. A. Sosenkov,
E. I. Strel'tsov, A. I. Suvorov,
A. P. Suvorov, Yu. G. Kharizomenov,
and V. N. Sharapov

UDC 621.039:621.039.311.2

A nuclear-fueled space heat and electric power generating plant (the Bilibino ATÉTs [nuclear thermal electric power station]) is being built in the Soviet Union on the Chukchi peninsula (Chukotka), near the village of Bilibino. The function of this power station will be to supply electric power to the Bilibino–Chaun mining and industrial district, and to supply space heat to the village of Bilibino.

The development of the northeastern polar regions of the USSR, which are rich in minerals, is directly connected with the expansion of the power resources and power base in those areas. The lack of

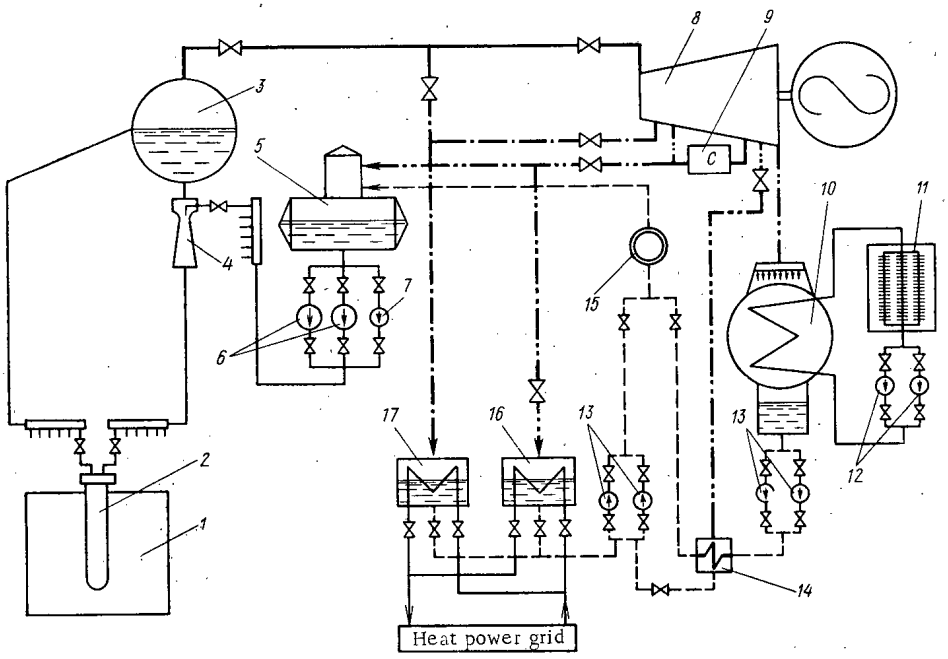

Fig. 1. Basic flowsheet of Bilibino nuclear-fueled heat power and electric power generating station (ATÉTs): 1) reactor; 2) fuel channel; 3) separator drum; 4) mixer with effective head; 5) deaerator; 6) working feedwater pumps; 7) emergency feedwater pump; 8) turbogenerator; 9) interseparator; 10) turbine condenser; 11) radiator coolers; 12) pumps serving radiator coolers; 13) hotwell pumps; 14) low-pressure reheater; 15) iron-trapping filter; 16) basic power grid reheater; 17) peak-load power-grid reheater.

Translated from Atomnaya Énergiya, Vol. 35, No. 5, pp. 299-304, November, 1973. Original article submitted April 4, 1973.

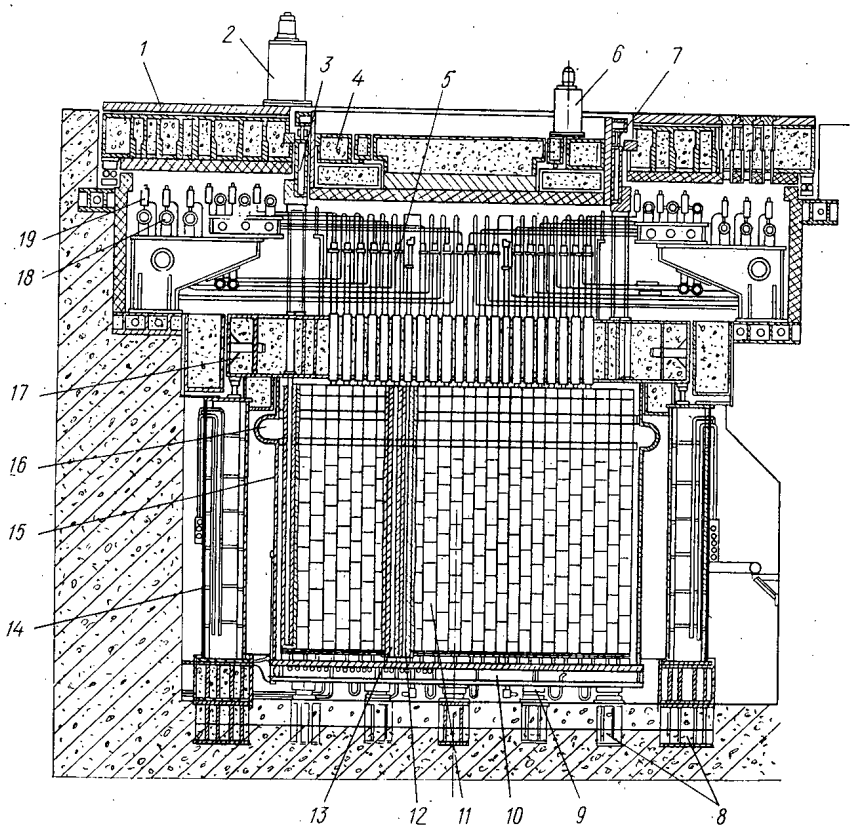

Fig. 2. Longitudinal cross section through reactor: 1) top side cover; 2) power drive for large rotating cover; 3) central frame with supports; 4) central rotating cover; 5) standpipes; 6) power drive for small rotating cover; 7) roller support; 8) sunken foundation supports; 9) load-bearing members; 10) bottom support plate; 11) stacking; 12) control and scram channel; 13) fuel channel; 14) biological shielding tank; 15) reactor vessel; 16) temperature expansion compensator; 17) top cover plate; 18) ganged headers with working pipes; 19) check valves.

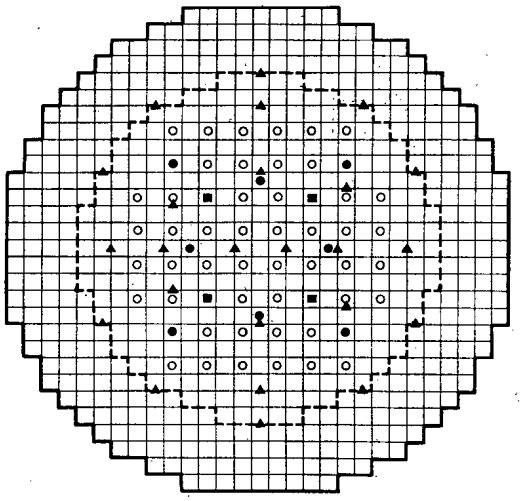

Fig. 3. Reactor pile loading arrangement: ●) scram rods (total 8); ■) automatic control rods (4); ○) manual control rods (48); ▲) neutron flux monitors (24); – – – –) boundary of reactor core.

local power resources and the high cost of shipping in fossil fuels conspire against engineering cost feasibility of even medium-level industrial operations in the area without recourse to a nuclear power station [1, 2].

As design and planning work on the Bilibino ATÉTs has shown, savings in fuel expenses can prove sufficient to compensate for the rise in construction costs of nuclear power stations, paying off construction costs within a span of six to seven years, not longer.

General Description of Power Station

The Bilibino nuclear power station is designed on the modular principle, and will consist of four identical reactor–turbine power units. The electric power output of each power unit is 12 MW, and each power unit will produce, in addition, as much as 25 Gcal/h heat. The thermal output of the reactor is 62 MW, at steam capacity 96 tons/h. All four reactors will be housed in a common reactor department.

The construction of the power station building rests on a foundation of monolithic reinforced concrete pads with

prethawing of the foundation soil. The outside wall of the reactor hall is constructed with aluminum panels, in order to lower construction costs. The presence of four nuclear chain reactors within a single reactor hall, and the absence of additional concrete walls, has prompted a need to use a containerized method in reloading of fuel channels. Spent channels in the reactors are unloaded and transferred to storage pools located in the reactor hall by means of a special shielded container. The positioning of the four reactors within a single common reactor hall imposes stringent requirements on the effectiveness and reliability of the biological shielding of reactors, if normal radiation conditions are to be maintained on the premises of the nuclear power station.

Thermal Power Arrangement

A single-loop thermal power system with a saturated steam cycle (Fig. 1) is employed at the Bilibino nuclear power station. The steam–water mixture is fed from the reactor to a separator drum. Steam is fed from there under 65 kg/cm^2 pressure and at temperature 280°C directly to the turbine. An intermediate separator installed between the high-pressure and low-pressure cylinders of the turbine fulfills the task of drying the steam working in the turbine.

The condensate downstream of the turbine condenser passes through a desalting filter, and then through a low-pressure reheater to an atmospheric deaerator. The water stream is moved along, at temperature 104°C, via the action of a feedwater pump and enters the natural-circulation loop.

Heat from the turbine condenser is carried off by the water circulating through the special loop and cooled by outside air in radiator coolers.

Water belonging to the heat grid system and intended for the village Bilibino is heated in the basic reheaters and peak-load reheaters fed with steam from controlled and uncontrolled taps on the turbines.

The station turbines were developed and fabricated in Czechoslovakia, and the radiator type cooler were developed and fabricated in Hungary.

Reactor Design Features

A channel type graphite-moderated water-cooled reactor with tubular fuel elements was the type selected for the Bilibino power station. Reactors of that type have been giving excellent service at the World's First Nuclear Power Station [3] and at the Belyi Yar nuclear power station [4]. These reactors are distinguished by their easy-to-fabricate design modules, restricted size, and weight, features which enable them to be built on a construction site situated far from main railway lines. In reactors of this type, the coolant does not suffer contamination by radioactive fission products, and that is particularly important when dealing with the single-loop thermal power arrangement of the nuclear power station.

The reactor system flowsheet appears in Fig. 2. The reactor is sunk in a pit. The graphite stacking consists of 200 × 200 mm cross section graphite slugs arranged on an underlying steel foundation plate and shaped as a cylinder 6 m in diameter and 5.2 m high. Uncooled steel bars are set in the peripheral graphite slugs to provide added stiffening. The entire graphite stacking assembly is housed within a steel pressure-tight containment shell welded to the top and bottom plates of the reactor and filled with nitrogen gas.

The fuel channels and channels with control and scram system rods are embedded in the stacking and form the cylindrical core, 4.2 m in diameter and 3 m in height. The reactor when fully loaded accommodates a total of 273 fuel channels and 60 control and scram channels. Two dozen β-emission rhodium sensors are installed between fuel channels to monitor the spatial distribution of neutrons throughout the active region in the graphite stacking. The in-pile arrangement of channels is mapped in the diagram in Fig. 3.

The top of the stacking, of total thickness 1 m, is one of the components of the reactor's biological shielding. Along with the graphite, the stacking also contains sandwiched layers of cast iron.

The plate on top of the stacking performs the function of a load-carrying metal structure for the channels and for the piping runs accompanying the channels. The plate is in three sections, and is laid down on the annular biological shielding tank, which is filled with water. Pipes running through the plate have standpipes welded to them, to accommodate the channels. The center of the plate is filled with iron–serpentinite concrete [5]. The additional biological shielding placed above the intake and outflow pipe conduit channels is made of the same concrete mix. The center of this shield is made in the form of two rotating cylindrical covers, a large one and a smaller one nested within it (the latter eccentrically placed). The small cover features a reloading hole which is plugged while the reactor is on power. Access to any channel for unloading purposes is open with the reactor shut down, by rotating the small and large covers.

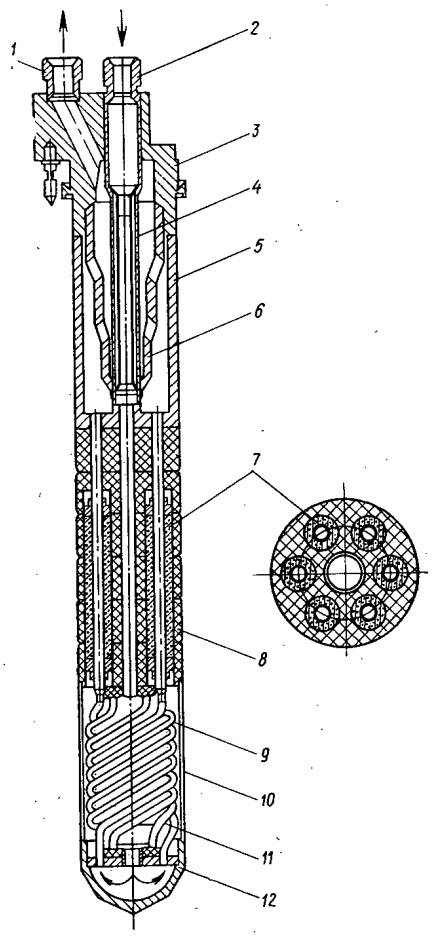

Fig. 4. Fuel channel arrangement: 1) pipe connection – outlet for steam–water mixture; 2) water inlet pipe connection; 3) head; 4) downcomer tube; 5) body of top mixing chamber; 6) stepped biological shielding plug; 7) fuel element; 8) graphite sleeve; 9) linear expansion compensation joint; 10) shielding jacket; 11) distance spacing piece; 12) bottom distributor chamber.

Fuel Channels and Control-Scram Channels

The reactor fuel channel consists of six fuel elements, plus incoming and outgoing steel tubes (Fig. 4). A 25×1 mm diameter tube runs the entire length through the center of the channel. Water flows down this tube to the bottom chamber of the channel and from there through six tubes fabricated in the form of helical temperature elongation compensators (expansion pieces), and thereby gains access to the interior of the fuel elements. The steam–water mixture emerging from the fuel elements is collected in an annular chamber and moves from there to the channel exit. A stepped steel shielding plug with overlagging cross section over the height of the plug is placed in the chamber to avert streaming (leakage) of radiation over the chamber.

The tubular-design fuel elements are arranged around the center tube of the channel in graphite sleeves. The fuel-element tubes are made of grade 0Kh18N10T steel, and dimensioned $\phi 12 \times 0.6$ mm and $\phi 20 \times 0.3$ mm. Uranium–molybdenum alloy (9 wt.% molybdenum) is dispersed (~50 vol.%) in the magnesium matrix inside the tubes. The fuel channels extend 7.7 m in length, and weigh ~150 kg.

The channels for the control and scram rods are welded structures made from six $\phi 9.4 \times 0.6$ mm steel tubes enclosed in graphite sleeves. The poison rod is placed in the inner gas-filled cavity of the channel. The rods are moved up and down by cable drives. The poison rod contains boron steel (2 wt.% boron) bushes 39×3 mm in diameter. Heat given off in the rod is taken up by the water circulating through the channel tubes (three downflow tubes and three riser tubes). The cooling loop for the rods terminates at the deaerator. Loop circulation is forced, pressure ~10 kg/cm^2. Cooling keeps the temperature of the poison rods from rising above 700°C.

Natural Circulation Loop

Reliance on natural coolant circulation to pick up in-pile heat enhances the operational reliability of the reactor, simplifies reactor operation, cuts down equipment costs, and cuts down on the power needed to run the power station proper. The reactor's natural circulation loop consists of six independent subloops terminating in a separator drum. Each subloop consists of a downcomer header converting into a horizontal distributor header ($\phi 219 \times 12$ mm), a group of fuel channels included in parallel, and an assembled horizontal header converting into an uptake tube ($\phi 219 \times 12$ mm). The reactor fuel channels are divided into six groups, according to the subloops they are associated with. The two central groups (in terms of their placement in the core in plan view) comprise 61 fuel channels, two in-between groups comprise 104 fuel channels, and the two peripheral groups account for 108 fuel channels.

The steam–water mixture from the fuel channels is collected in the assembled headers and moves through the uptake main pipes to the separator drum, where the steam is directed to the turbine, and the water separated from the mixture (at t_s) is routed to the downflow main pipes.

Feedwater is supplied to the loop via special mixers installed on the main downcomer lines. The mixers are arranged in a jet-pump system, so that a certain effective head can be built up in them; the working medium is the feedwater. Under steam generation conditions, the effective head of the mixer is not greater than 8–9% of the dynamic head developed in the loop. It is important to note that the mixer carries out several operations while the reactor is being started up and cooled down: the mixer makes it possible to remove air from the subloops alternately while the reactor is being prepared for startup; the

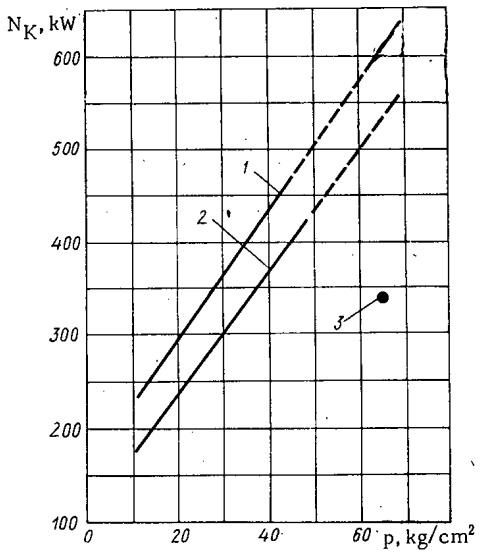

Fig. 5. Dependence of limiting power output of fuel channel N_K on coolant pressure: 1, 2) plotted respectively for cosinusoidal and uniform heat generation over length of channel; 3) working point for peak-power channel.

mixer sets the working direction of circulation before the power level is raised; it maintains circulation flow through the loop under deep cooldown conditions.

Reactor Physical Characteristics

For the first reactor loading, 3% uranium enrichment in most of the fuel channels was decided upon. Some of the channels (about 20% of them) were placed on the periphery of the reactor in order to equalize the power distribution field, and contain slightly enriched (3.3%) uranium. Over the entire course of the first campaign (until partial reloading), the radial variation factor of the heat released k_r will not exceed 1.3. k_r rises to about 1.5 in partial reloading of the channels, because of fuel burnup. The variation factor over the height of the reactor is 1.35. The total uranium loading in the reactor is 7.2 tons, and that includes 220 kg ^{235}U. A reactor with that loading has a reactivity margin $\Delta K/K \approx 11\%$ when cold, and that is compensated by the manually activated control rods.

That reactivity margin means an average output of 5.1 MW days/kg heat power when the reactor is operating at rated power. The average power output from the fuel is about 8 MW days/kg in steady-state loading.

Hydraulic and Heat Transfer Characteristics

The relative heat loading level of the reactors in the Bilibino power station is quite high. The highest power output of a fuel channel is 340 kW. The specific heat flux is ~0.75 MW/m^2. The temperature rating of a fuel element is not in excess of 340°C.

Reliability of heat extraction from the fuel channel has been studied experimentally on a special test stand simulating the reactor's natural circulation loop. The test stand included two full-scale mockups of fuel channels with electrically heated simulators of fuel elements. Evolution of heat over the length of the simulated fuel elements was cosinusoidal and uniform. Circulation parameters in the channels were investigated on that test stand at pressures from 10 to 70 kg/cm^2, and factors tending to limit channel power output were ascertained. It was found that when a certain limiting power output level N_{lim} is attained oscillations in flowrate take place within the fuel element flow passages, and that impairs optimum heat removal from the element. The level of that limiting channel power output depends, in the specific natural circulation loop, on the pressure, on the pattern of heat generation over the length of the fuel elements (Fig. 5), and on the amount of flow throttling.

A certain optimum degree of throttling ensuring the highest value of the limiting power output over the working range of pressures was found to exist in the case of channels operating in the natural circulation loop. Over the range of pressures 60-70 kg/cm^2, optimum throttling is achieved by throttling the flow with an orifice plate having the characteristic $\Delta P_{op} = 8000\, G_{op}^2$ (here ΔP_{op} is expressed in kg/m^2, G_K is the rate of coolant flow through the channel, in kg/sec; the inlet water temperature is 250°C). These orifice plates are installed in the fuel channels at the inlet to the fuel element flow passages.

At the rated pressure 65 kg/cm^2, a coolant flowrate 2000-2100 kg/h through the fuel channels with peak power 340 kW is brought about. The percentage content of steam by weight at the exit is ~30%, when the average steam content taken over the entire reactor pile is 17% at the exit. The margin for the boundary of the region of stable operating conditions was determined, for that channel, with due cognizance of the different pattern of heat generation (1.73-1.57 in terms of power, 2.45-1.8 in terms of pressure). These reserves in limiting power are responsible for the high reliability of the reactor core from the standpoint of heat performance.

The nature of the transient processes in the startup and cooldown modes of operation was investigated on the test stand, and emergency power reduction response was also investigated on the test stand. The findings were that the downcomer portion of the channel can become attacked by steam in some situations, when the power level is lowered in an emergency procedure, and circulation can be cut off with ensuing overheating of the fuel elements. These phenomena can occur when 4% or more of the total channel

power is transferred from the graphite to the downcomer tube. The danger of a stoppage in circulation increases if the pressure in the loop builds up during a transient. Heat input to the downcomer tube from the stack graphite is kept under 1% of the power output in the reactors of the Bilibino power station in order to forestall cutoff of circulation through the fuel channels. This is achieved by increasing the gas clearance between the downcomer tube and the sleeve of the fuel channel. Experiments staged on the test stand in that mode of heat transfer, with all of the other diverse unfavorable factors operating, revealed that the transient developed normally. At the same time, two pressure controllers were installed on the steam line to the turbine in order to improve the circulation transient in the reactor loop; these pressure controllers act to lower the pressure in the loop by 2-3 kg/cm^2 after the turbine check valve is closed, when the emergency control system is energized.

At the present time, construction work on the Bilibino electric power and space heat nuclear-fueled plant is in its final phases: installation of equipment is being completed, preparations are underway for the physical startup and power startup of the first power generating unit. And the day is not far off when the first Soviet polar nuclear-fueled electric power and space heat generating plant will be in service in the frozen expanses of the far north of the USSR.

LITERATURE CITED

1. V. M. Abramov et al., IV Geneva (1971) Conference on the Peaceful Uses of Atomic Energy, P/713 (USSR).
2. V. M. Abramov et al., Small and Medium Power Reactors, 1970., IAEA, Vienna (1971), p. 363.
3. G. N. Ushakov, The First Nuclear Electric Power Generating Station (Experience in construction and operation) [in Russian], Gosenergoizdat, Moscow (1959).
4. N. P. Dollezhal' et al., At. Énerg., 27, 379 (1969).
5. A. Ya. Veselkin et al., ibid., 20, 76 (1966).

THE VALUE OF PLUTONIUM IN AN EVOLVING NUCLEAR POWER SYSTEM

S. V. Bryunin, Yu. I. Koryakin,
V. L. Lokshin, V. I. Runin,
and S. Ya. Chernavskii

UDC 621.039.003.5.54

The future growth of nuclear energy will be accompanied by significant qualitative changes in its structure. These will include the introduction of nuclear power plants with fast reactors and the creation of systems closed with respect to the fuel; in these systems the secondary nuclear fuel (plutonium) producible in a nuclear power plant will become one of the basic forms of consumable fuel resources. Under these conditions the necessity of selection of a rational strategy for the production and consumption of plutonium poses the problem of the determination of the value of plutonium in an evolving nuclear power system.

In technical-economic calculations plutonium is not infrequently considered only from the point of view of production, or only from the point of view of consumption. In the first case the nuclear power plant is regarded as having the twofold purpose of the production of plutonium and electrical energy, and the cost of the plutonium is determined by the spacing of the values of the electrical energy and the producible plutonium. Here the plutonium is considered as a commercial product of the system independent of the method and effectiveness of its future use. In the second case the price of plutonium is determined by comparing it to uranium with respect to its effectiveness from a power-producing and neutron physics standpoint, when used in a reactor of one type or another. Here the plutonium is considered as a source of neutrons and of energy independent of the means and costs of obtaining it.

Both approaches possess the shortcoming of considering the nuclear power plant as an isolated object, either for the production or consumption of plutonium; this does not give the capability of correctly taking into account the interactions of the processes of production and consumption of plutonium. As a result, the plutonium indices determined in this way do not reflect completely the true costs and benefits connected with the production and consumption of plutonium, and its consequent value in the national economy.

The cycle of production, reprocessing, and consumption of plutonium connects all the nuclear power plants and activities of the external fuel cycle into a single nuclear power system. It is therefore appropriate to consider the value of plutonium as a system concept, and to determine this quantity starting from the premise that the plutonium in a nuclear power system is doubly internal, both as a product and as a resource. The plutonium is produced and consumed within the nuclear power system, and outside of this system it has no use-value.*

As a consequence of the evolution of nuclear power and the evolving of the processes of production and consumption of plutonium over time, the value of plutonium possesses a dynamical property; that is, it can change in time.

The systems approach to the value of plutonium permits a more correct determination of the technical-economic characteristics of the separate nuclear power plants and activities of the external fuel cycle, and with the appropriate technical premises permits one to optimally select the output and method of producing the plutonium in a nuclear power plant during the period of its operation.

*We are talking about power reactor plutonium produced and consumed in significant quantity.

Translated from Atomnaya Énergiya, Vol. 35, No. 5, pp. 305-309, November, 1973. Original article submitted July 2, 1973.

In the following we will consider a nuclear power system which is closed with respect to plutonium; that is, a system which does not exchange plutonium with other systems. Then the plutonium is an intermediate product which circulates within the system.

The value of plutonium in the system is a function of the value of the end product of the nuclear power system (electrical energy), and is equal to the partial derivative, at its minimum, of the total cost in the system (for a given electrical energy output) with respect to the quantity of plutonium within the system. In other words, the value of plutonium reflects the reaction, in the financial expression, of the nuclear power system (balanced with respect to plutonium) to the onset of an imbalance of plutonium within the system. With a correct accounting of the external connections of the nuclear power system, the value of plutonium can be determined from an analysis of the nuclear power system, including within the system the entire complex of activities from the mining of the natural uranium to the production of electrical energy.

The most important purpose of the planning of nuclear power is the determination of that structure which would guarantee a minimum of national-economic costs in the system while realizing the required output of the product, electrical energy. Here the quantitative expression for the value of plutonium appears as one of the governing conditions, and the determination of the value of plutonium is one of the problems of optimally planning a nuclear power system; it can be formulated in this way: to find a quantitative estimate of the value of plutonium such that it characterizes the optimal (in the sense mentioned above) nuclear power system with given restrictions on its development.

The systems approach to the determination of the value of plutonium is given in [1, 2], and the structure of the developing nuclear power system is provisionally given without its optimization. In [3] is given an estimate of the value of plutonium for a series of specific structures of the nuclear power system of the USA.

In its most general form, questions of the optimization of the national-economic system and the determination of the value of resources is considered by Kontorovich, Nemchinov, Novozhilov, et al. [4, 5].

In the present work, the presented problem is solved using a linear mathematical model of the nuclear power system which is described in [6], where the method of linear programing is used to analyze the system.

The following problem is solved: in the calculational period from t = 1 to t = T to find the vector x^0 (where x characterizes a definite sequence of introduction of nuclear power plants) such that the functional

$$(C, x) \to \min \tag{1}$$

with the constraints

$$Ax = b. \tag{2}$$

In the expression (1), C is a vector of given costs, each component of which characterizes the total given costs for the construction and operation associated with the corresponding component of the structure vector x, while the expression in parenthesis is a scalar product. In the expression (2), A is a matrix of technological coefficients, and b is a constraint vector. Thus the coefficients of the matrix characterize the participation of the corresponding component of x in one of the constraint conditions. Amongst such restrictions as the balance (during the years of the calculated period) of the output, of the producible electrical energy and the consumption of natural uranium, there is present in the model dynamical restrictions connecting the production and consumption of plutonium with the structure components. The problem formulated by the functional (1) within the constraints (2) corresponds, as is well known, to the complementary linear programing problem: to find a vector of estimates y^0 such that

$$(y, b) \to \max \tag{3}$$

with

$$Ay \leqslant C. \tag{4}$$

It is apparent from (3) and (4) that the vector of estimates y is a vector of estimates of consumable and producible resources.

According to a known theorem of linear programing

$$(C, x^0) = (y^0, b). \tag{5}$$

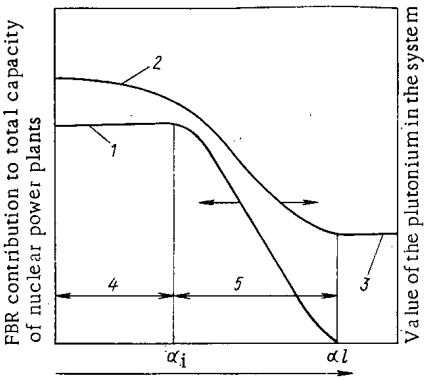

Fig. 1. The nature of the influence of a relative increase in cost of fast breeder reactors (FBR) on their contribution to the total capacity of the nuclear power plants (1) and the value of plutonium in the system (2); the value of plutonium when used only in thermal reactors (3); the region where α has an insignificant influence (4); the region where α has a significant influence (5).

From Eq. (5) it follows that the plutonium component of the vector y^0 is the desired dynamical value of plutonium (its value in a closed cycle), and it is determined by the use of programs for the solution of linear programing problems.

One of the fundamental factors influencing the determination of the value of plutonium is the productivity of the nuclear power plants. Depending on the technical assumptions made the productivity of the nuclear power plant with respect to plutonium can vary within wide limits. In this connection, in a variety of problems concerned with the determination of the value of plutonium, it becomes necessary to determine the optimal productivity of the nuclear power plants. The optimal plutonium productivity of nuclear reactors with a definite technology arises from decreasing the fuel burnup and increasing the amount of primary nuclear fuel involved in the fuel cycle while increasing the plutonium production, and also depends on the relationship between the value of plutonium and the cost of the primary nuclear fuel.

The problem of the optimal productivity can be solved on two hierarchial levels: through the consideration, in the nuclear power system, of nuclear power plants having a wide range of productivities, and by means of an analysis of the technical-economic indices of the individual nuclear power plants, taking into account the dynamical value of plutonium in the nuclear power system.

A preliminary determination of the optimal productivity of the nuclear power plants enters into the problem of the first level; there enters in the problem of the second level the increase of this productivity by the system of utilization during the operation of the reactor, and the optimization of the parameters of the nuclear reactors and the nuclear power plants, in such a way as to guarantee the optimal productivity.

We present below some results of calculations of the value of fissionable plutonium in a nuclear power system, for different assumptions concerning its future development. Variants of a two-component structure of the nuclear power system are considered, consisting on the one hand of thermal uranium reactors together with thermal plutonium reactors, and on the other hand consisting of thermal uranium reactors with fast breeder reactors. In the latter case, the year in which fast reactors are first widely introduced is varied, and the volume of natural uranium reserved involved is also varied. These are the most indicative variants for the analysis of the value of plutonium.

The all-thermal hypothesis of the development of the nuclear power system when there is no consumption of plutonium is not considered, since the solution of the given problem is obvious in this case (the value of the plutonium in such a system is zero). The calculation is performed according to a mathematical model described in [6]; the calculational period is from 1980 to the years 2000 to 2010.

When plutonium is used as a nuclear fuel in thermal reactors it acquires a positive value which, if the conditions of functioning of the nuclear power plants are maintained, is constant during the calculated period. The effect of using plutonium in this case consists in decreasing the total given costs in the nuclear power system, and decreasing the consumption of natural uranium, in comparison with the thermal model in which the plutonium in the fuel cycle is not recovered. The magnitudes of these effects are relatively small (up to 10%).

The analysis of the value of plutonium in a nuclear power system with a two-component structure containing fast reactors possesses the most interest.* Calculations show that the value of plutonium depends on the effectiveness of the use of the fast breeders in the nuclear power system, and this in its turn is determined by the year of their introduction and technical-economic indicators.

Figure 1 shows the influence, on the contribution of fast breeder reactors (FBR) in the system, of a relative excess of capital cost (α) of fast breeder reactors, in comparison to thermal reactors; the figure also shows the influence of α on the plutonium. The year of introduction of the fast breeder reactors is held fixed. The action of the factor α on the structure of the nuclear power system does not of course occur

* In the present paper questions concerning fast converter reactors are not considered; these possess an independent character and require separate discussion.

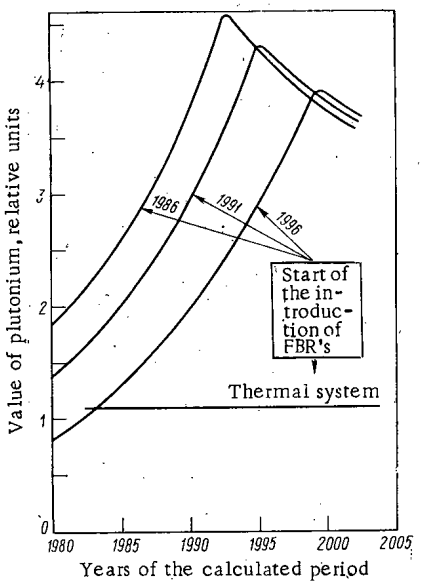

Fig. 2. Influence of the time of initial introduction of fast breeder reactors into a nuclear power system on the value of plutonium.

in an isolated fashion, but depends on other factors, the most important of which are the breeding coefficient of the fast breeder reactor, the possible limitations of resources (or the cost of natural uranium), and the time of the external fuel cycle. It is possible to identify two characteristic values of α: α_i and α_l. The region of variation $1 \leq \alpha \leq \alpha_i$ is characterized by an insignificant influence of the relative increase in cost of fast breeder reactors on their contribution to the total capacity of the nuclear power plants. In this region of variation of α the nuclear power plants with fast breeder reactors are unconditionally effective, and their introduction is determined by technical capabilities and by limitations on plutonium. However, the value of plutonium decreases somewhat with an increase in the relative capital cost of fast reactors. If the quantity α lies within the interval $\alpha_i \leq \alpha \leq \alpha_l$, the contribution of the fast breeder reactors decreases with increase in α. The quantity α_l characterizes the limit point for the competitive capability of nuclear power plants with fast breeder reactors.

With increasing α the value of plutonium naturally falls, and is zero for α_l, if the plutonium is not used in thermal reactors, or is the magnitude of the corresponding worth in the thermal hypothesis using plutonium, described above. The larger the scale of development of nuclear power, the larger the influence of the magnitude of α on the structure and the need for uranium, inasmuch as the "weight" of the fast reactors increases and the system becomes more sensitive to the value of α.

The decrease in capital cost of fast reactors, which leads to an increase in the contribution of fast reactors, contributes also to the decrease in costs in the reprocessing of plutonium on account of the capability of construction of larger enterprises in the external fuel cycle. This in its turn leads to an increase in the value of plutonium. One should note that the value of plutonium in a system with economical fast reactors can be several times greater than the value of plutonium in a nuclear power system which is being developed only with thermal reactors.

One of the most important factors determining the effectiveness of fast reactors (and consequently the value of plutonium) is the time at which these reactors are introduced into the system.

Figure 2 presents the results of calculations of the system value of plutonium as a function of the year of introduction of fast breeder reactors into a two-component structure. From Fig. 2 it follows that, although up to the introduction of fast reactors, the plutonium in the system is not used, the value of the plutonium during this period is not equal to zero, since it is assumed to be used in the calculational period. The value of plutonium increases as we approach the point of beginning its use (it increases with a rate determined by the discount cost coefficient), and the value reaches its maximum at the moment of maximum deficiency. Introducing the fast reactors at a later period of time leads to a decrease in the value of plutonium in the initial period of time, as is apparent from Fig. 2. A significant period of storage results in delaying the moment of maximum deficiency of plutonium, decreasing the absolute magnitude of its maximum worth.

The economic indicators of the production of uranium and of its reserves are the most important factors determining the value of the plutonium worth. As calculations show (Fig. 3), even insignificant limitations on the consumption of uranium in a nuclear power system lead to increasing by several times the absolute magnitude of the value of plutonium.

The analysis of the variation of the value of plutonium in a developing nuclear power system permits one to draw the following conclusions:

when fast breeder reactors are present in the system during the calculational period, it is not, as a rule, advisable to use plutonium in thermal reactors;

the value of plutonium, when evaluated for a closed cycle, can be used in the development of technical policy in the development of means of producing, reprocessing, and consuming plutonium;

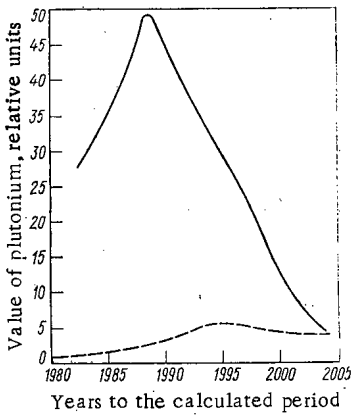

Fig. 3. Influence of limitations on uranium on the value of plutonium in a nuclear power system with fast breeder reactors being introduced from the year 1986 on. – – – –) without limitations; ——) with limitations on consumption before the year 2000.

the increase of its value in the period preceding the wide introduction of fast breeder reactors shows that it is feasible and permissible to have higher direct costs for the production and reprocessing of plutonium during this period;

the high magnitude of the value of plutonium in a system with the two-component structure consisting of thermal uranium reactors plus fast breeder reactors indicates that, especially in the case of the early introduction of fast reactors and of their significant contribution ($\alpha \leq \alpha_i$), it is advisable to increase the production of plutonium in thermal reactors during the period preceding the wide introduction of fast reactors. Technically this problem can be solved by using gas-cooled uranium–graphite reactors possessing a flexible fuel cycle. The use of dense metallic uranium fuel can also assist in increasing the production of plutonium;

in connection with the dynamical character of the value of plutonium in a system with a two-component structure, the problem of the variation throughout the prediction period, of the productivity of the thermal reactors producing the plutonium has been correctly formulated. The optimal productivity of such a reactor should be determined on the basis of the value of plutonium in the system.

LITERATURE CITED

1. A. I. Leypunskii et al., "Method of effectively using fuel in a nuclear power system with fast reactors," At. Énerg., 31, No. 4, 383-392 (1971).
2. V. V. Orlov, "Optimization criterion for nuclear reactors," Preprint FÉI-286, Obninsk (1971).
3. D. Deonigi, "Calculational model for estimating the role of nuclear power in the USA power system," Atomnaya Tekhnika za Rubezhom, No. 4, 3-7 (1971).
4. V. S. Nemchinov, Social Value and the Planning of Prices [in Russian], Nauka, Moscow (1971).
5. V. V. Novozhilov, "Problems of the Measurements of Costs and Results in Optimal Planning [in Russian], Nauka, Moscow (1972).
6. A. D. Virtser, G. B. Levental', and S. Ya. Chernavskii, "Mathematical model for the long-term prediction of the development of nuclear power systems according to economic criteria," At. Énerg., 33, No. 6, 955-960 (1972).

DISTORTION OF THE TEMPERATURE FIELD OF THE ACTIVE ZONE (CORE) OF A FAST REACTOR WHEN THE HEAT RELEASE IN THE FUEL PACKS IS DISRUPTED

Yu. K. Buksha, Yu. E. Bagdasarov, and I. A. Kuznetsov

UDC 621.039.5.17.5

One of the several possible emergency situations which may develop in a fast reactor is a "local" emergency associated with the departure of one or more of the fuel packs from normal operation. The timely detection and removal of the causes of such an emergency is one of the chief problems in ensuring the safety of fast reactors. In order to solve this problem it is essential to study the processes taking place in the failed pack and establish the ways in which the emergency may possibly spread to the neighboring packs. In this paper we shall consider the change taking place in the temperature distribution of a BN-600 reactor as a result of an increase in the hydraulic impedance of individual fuel packs [1].

The flow of coolant through the pack may be reduced as a result of a number of causes: the clogging of the through sections with impurities precipitating from the coolant, the swelling of the fuel elements during the burnup of the fuel, or the partial closing of the through sections by foreign objects which may for some reason or other have fallen into the reactor. When the flow of coolant through individual packs is reduced and the temperature in the packs is increased, some of the heat evolved in these packs is transmitted to the neighboring packs by heat conduction. The temperature distribution in the failed packs is accordingly distorted relative to that expected under normal conditions. Under certain conditions the outlet temperature of the coolant thus fails to characterize the thermal state of the pack [2]. The question as to the most appropriate method of monitoring the operation of all the fuel packs in a fast reactor has never yet been solved. Among possible methods we may mention the use of thermal probes (detectors) placed at the outlet from the packs; the question as to the reliability of the information obtained from these thermocouples is of very great importance.

Three factors interfere with the reliable monitoring of the state of the pack by reference to the outlet temperature: the fall in coolant temperature in the failed pack at the upper end screen (and in the case of low powers in the upper section of the active zone as well), the large temperature difference across the cross section of the pack due to heat conduction, and the mixing of the sodium emerging from the failed pack with the colder sodium of the neighboring packs.

Let us estimate the quasisteady-state temperature distribution of the coolant with respect to the height and radius of the active zone (operating at various powers) in the case of a reduced flow through one pack (or group of packs), allowing for the transmission of heat to the neighboring, normally cooled packs. In making this estimation we use the following model. We assume that heat transfer in the radial direction occurs solely by virtue of heat conduction (the effect of the interchannel mixing of the coolant may be allowed for by increasing the effective thermal conductivity).

The reactor is homogenized with respect to heat evolution and thermal conductivity. The effective thermal conductivity is determined from the condition that the true temperature drop of the coolant with respect to the radius of the failed pack should equal the drop calculated from the effective thermal conductivity:

Translated from Atomnaya Énergiya, Vol. 35, No. 5, pp. 311-314, November, 1973. Original article submitted March 21, 1972; revision submitted April 4, 1973.

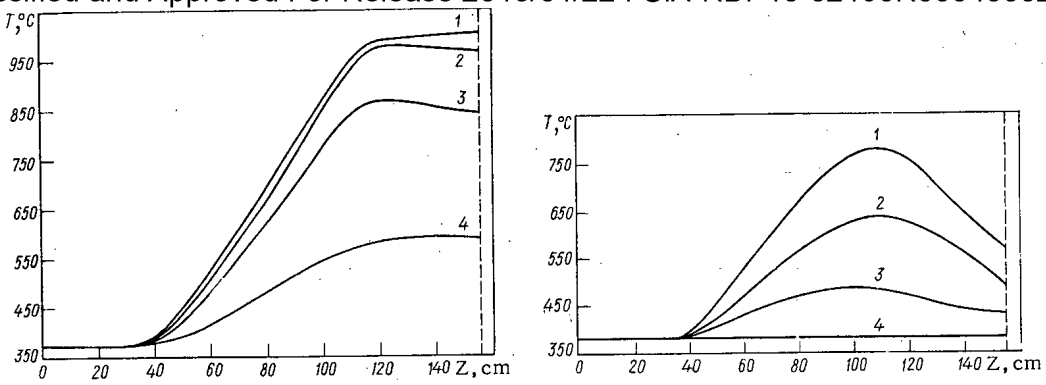

Fig. 1. Distribution of the sodium temperature T with respect to the height of the failed pack for a nominal flow of sodium and a reactor power equal to 100 and 2% of the nominal value (a and b, respectively): 1) in the center; 2) average over the cross section; 3) at the edge; 4) at a fair way from the failed pack in an unperturbed part of the active zone.

$$\lambda_{\text{eff}} = \frac{R^2}{4\int\limits_0^R \frac{\pi r\, dr}{\int\limits_0^{2\pi} \lambda(r, \varphi)\, d\varphi}}, \tag{1}$$

where R is the radius of the pack. It follows from Eq. (1) that the effective thermal conductivity is the result of averaging the thermal conductivity with respect to angle and the thermal resistance with respect to radius. For the geometry and materials of the active zone in reactors of the BN-600 or BN-350 types Eq. (1) may be simplified to a fair accuracy as follows:

$$\lambda_{\text{eff}} = \sum_i \lambda_i \varepsilon_i, \tag{2}$$

where λ_i, ε_i are respectively the thermal conductivity and the volumetric proportions of the components of the active zone.

The degrees of heating of the coolant in all packs of the reactor except the failed one are regarded as equalized by virtue of throttling. This circumstance has little effect on the temperature distribution in the failed pack, since its zone of influence is limited to a single row of packs only (this will be demonstrated later). We neglect the nonuniformity of the heat evolution with respect to the radius of the reactor; this neglect also has little effect on the results, as the diameter of the pack is small by comparison with the reactor diameter.

After making these assumptions, the temperature field of the moving coolant may be described by the equation

$$\lambda_{\text{eff}} \frac{1}{r} \cdot \frac{\partial}{\partial r} r \frac{\partial T(r, z)}{\partial r} + q_v(z) = vc\gamma\varepsilon \frac{\partial T(r, z)}{\partial z}. \tag{3}$$

Here in the failed pack $v = v_1$ and in the reactor $v = v_2$, where v_1, v_2 are the velocities of the coolant in the failed pack and in the rest of the reactor, respectively; ε is the volumetric proportion of the coolant.

In view of its relatively low value, we neglect heat transfer in an axial direction by heat conduction. The boundary conditions are

$$\left.\frac{\partial T(r, z)}{\partial r}\right|_{r=0} = 0; \tag{4}$$

$$\left.\frac{\partial T(r, z)}{\partial r}\right|_{r=R_1-0} = \left.\frac{\partial T(r, z)}{\partial r}\right|_{r=R_1+0}; \tag{5}$$

$$T(r, z)|_{r=R_1-0} - T(r, z)|_{r=R_1+0} = -\lambda_{\text{eff}} R_t \left.\frac{\partial T(r, z)}{\partial r}\right|_{r=R_1+0}; \tag{6}$$

$$\left.\frac{\partial T(r, z)}{\partial r}\right|_{r=R_2} = 0; \tag{7}$$

$$T(r, 0) = T_0. \tag{8}$$

Here R_1 and R_2 are the equivalent radius of the failed pack and the reactor, respectively; R_t is the thermal resistance of the walls of the failed and neighboring packs.

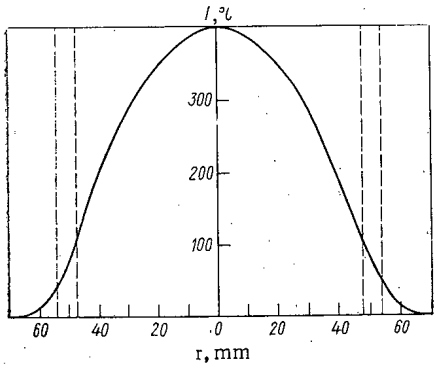

Fig. 2

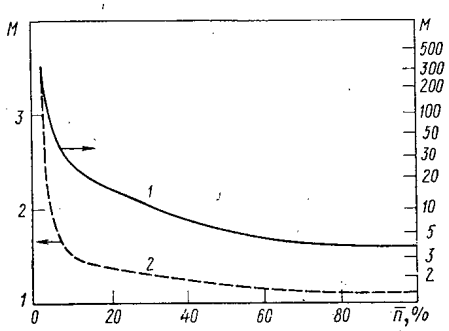

Fig. 3

Fig. 2. Distribution of the sodium temperature T with respect to the radius of the reactor r in the outlet section of the active zone for a nominal flow of sodium and a reactor power of 2%. The vertical axis gives the temperature, counting from the temperature at the reactor outlet.

Fig. 3. Ratio M of the maximum deviation of the sodium temperature in the failed pack from the mean temperature at the reactor outlet to the deviation recorded by the sensor as a function of the reactor power $\bar{n}$: 1) allowing for mixing with the sodium of the neighboring packs; 2) without so allowing.

In the upper and lower reflectors the heat evolution is distributed exponentially with respect to height, and in the active zone of the reactor on a cosinusoidal law. The problem was solved by the network method, using a finite difference scheme of the second order of approximation.

Figures 1-3 present some characteristic results of the calculation for two working modes of the reactor: for a nominal flow of sodium through the reactor and for a nominal heating of the sodium in the reactor, operating at various powers. The flow of coolant through the failed pack was chosen so that, in the absence of heat transfer between the packs, a fairly high degree of heating occurred (up to the boiling point). In this way allowance is made for the consequences of any increase in the hydraulic impedance of an individual pack in the reactor operating at various powers – for example, an increase up to a point at which a dangerous temperature difference develops. Figures 1a and b show the distribution of the maximum sodium temperature in the failed pack (on the axis) with respect to the height of the reactor (the horizontal axis representing the distance from the entrance to the lower end screen), and also similar relationships for the mixed mean sodium temperature measured over the cross section of the failed pack, the temperature at the edge of the pack, and the sodium temperature in the rest of the reactor at a fair distance from the failed pack, assuming a nominal sodium flow and a reactor power of 100 and 2% of the nominal value. It follows from the calculations that the maximum temperature distribution with respect to the height of the failed pack is only of a monotonic nature at high power. At low power there is a fall in the sodium temperature of the failed pack within the upper end screen, and under certain conditions in the upper part of the active zone as well. The temperature drop is due to the fact that, in these regions, the outflow of heat to neighboring packs exceeds the outflow of heat due to heat evolution in the fuel elements. This effect appears most strongly for the nominal flow of coolant through the reactor. At nominal power the sodium temperature on the axis of the pack reaches its maximum value at the outlet of the active zone; in the upper end screen it is approximately constant with respect to height. The mixed mean temperature in the end screen falls by 25°C owing to the increase in the temperature drop over the cross section of the failed pack.

As the power is reduced, the maximum of the coolant temperature moves toward the center of the active zone. Owing to the large temperature drop over the cross section of the pack the mixed mean temperature of the sodium is much lower than the maximum temperature in this section. Figure 2 shows the distribution of sodium temperature over the radius of the reactor in the outlet section of the active zone for a power of 2% nominal and a nominal flow of coolant through the reactor. The temperature is reckoned from the temperature at the outlet from the reactor (vertical axis); the broken lines denote the boundaries between the failed pack and the pack neighboring it. We see from Fig. 2 that the "zone of influence" of the failed pack does not extend any further than one row of neighboring packs.

In the operating modes under consideration the difference between the maximum coolant temperature in the pack and the mixed mean temperature in the outlet section equals 45-295°C in the power range 100-2% nominal. For nominal heating these differences are much smaller; for the same powers they amount to 45-150°C.

The mixed mean temperature of the coolant in the failed pack can only be established if the temperature sensor is introduced directly into the pack; otherwise mixing with the colder sodium of the neighboring packs is inevitable. If the temperature sensor is brought close to the pack the effect of mixing with the neighbor diminishes, but fails to vanish altogether. In any case mixing still occurs between the sodium of the failed pack and the sodium emerging from the nearby "windows" of the six packs surrounding it. If we accept that the flow of sodium is uniformly distributed between the outlet windows, we may consider that a flow of "cold" sodium equal to the flow of one normally working pack is mixed with the sodium of the failed pack. Since the zone of influence of the failed pack does not extend beyond one row of surrounding packs, we obtain the following expression for the heating of the coolant in the failed pack, allowing for mixing at the outlet:

$$\theta = \frac{n - n_T + n + \frac{n_T}{6}}{C(G_1 + G_2)}, \tag{9}$$

where n is the power of the pack, n_T is the fraction of the power of the failed pack lost as a result of thermal transfer to neighboring packs, C is the heat capacity (specific heat) of the coolant, G_1, G_2 is the flow of coolant through the failed and normal packs, respectively.

Remembering that

$$n_T = n - CG_1\theta_1,$$

we may rewrite Eq. (9) thus:

$$\theta = \bar{n}\,\frac{\theta_1 \frac{5}{6}\cdot\frac{\bar{G}_1}{\bar{n}} + \frac{7}{6}\theta_{nom}}{\bar{n}\left(\frac{\bar{G}_1}{\bar{n}}\right) + \bar{G}_2}, \tag{10}$$

where θ_1 is the heating of the sodium in the failed pack, θ_{nom} is the heating of the sodium in the reactor for a nominal flow and power, $\bar{n}$ is the power of the pack referred to the nominal, $\bar{G}_1$ is the flow of coolant through the failed pack, $\bar{G}_2$ is the flow of coolant through the reactor, referred to the nominal value.

The temperature sensor situated at the outlet from the pack responds to a diminution in the sodium flow through the pack and indicates a certain deviation of the temperature from the original value. It should be noted that well inside the pack this deviation may be far greater. The ratio of the actual deviation of the maximum sodium temperature in the failed pack from the initial sodium temperature at the outlet from the pack to the deviation recorded by the sensor is indicated in Fig. 3 as a function of power, with or without allowing for the mixing factor. Curve 1 is plotted on a logarithmic scale with due allowance for the mixing of the sodium from the failed pack with the sodium of neighboring packs (with minimum dilution), curve 2 without allowing for mixing. It follows from Fig. 3 that a sensor placed directly at the head of the pack may give a fairly accurate result for a power of over 30% nominal.

In reactor working conditions with nominal heating the error in the readings of the temperature sensors is not so great as in the case of nominal flow, but it is sufficient to produce a considerably distorted picture of the true position within the failed pack.

LITERATURE CITED

1. A. I. Leipunskii et al., At. Énerg., 25, 403 (1968).
2. A. Fridland, "Relation between maximum core temperatures and thermocouple outlet readings for failures subassemblines," Intern. Conf. on Safety of Fast Breeder Reactors (Aix-en-Provence, France, 1967).

NEUTRON CHARACTERISTICS OF THE VVR-M REACTOR CORE

V. M. Pasechnik, A. F. Rudik, Yu. I. Krasik, S. S. Lomakin, V. I. Kulikov, A. V. Shelenin, and G. G. Panfilov

UDC 621.039.519:621.039.55

For the choice, design, and correct utilization of an in-reactor monitoring system, it is necessary to know the energy spectrum and the absolute and relative densities of the neutron flux at various points of the reactor.

The spectral parameters and the absolute density of the thermal neutron flux in the VVR-M reactor were measured by means of activation detectors containing the ^{176}Lu, ^{151}Eu, ^{63}Cu, ^{197}Au, and ^{59}Co isotopes. The found parameters of the thermal neutron field were used for calibrating the fission chambers by means of which the relative density distribution of the neutron flux was measured at various points of the reactor core.

Leutecium and europium detectors were used in the form of aluminum alloys, where their percentage by weight was equal to 15 and 0.8%, respectively. The copper, gold, and cobalt detectors consisted of foils with a thickness of 50, 3, and 10 μ, respectively. The detector diameter was equal to 3 mm. The screening numbers for resonance neutrons G_r and Westcott's parameter S_0 were borrowed from [1].

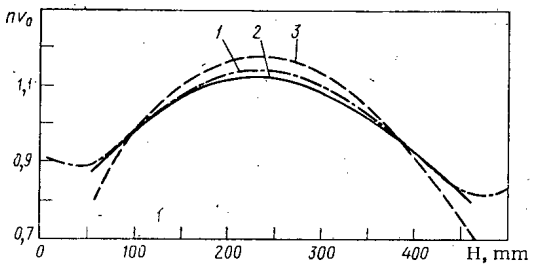

Fig. 1. Relative density distributions of the thermal neutron flux along the height of a dry experimental channel nv_0, measured by means of copper foils (1), thermal neutron fission chambers (2), and fast neutron fission chambers (3).

The detectors were irradiated by means of thin-walled nickel vials with a diameter of 5 mm, which were provided with notches for sandwiching in the detectors. The activities of the lutecium, copper, and europium detectors, measured by means of a γ-scintillation device with an integral discriminator, were used for determining the spectral indices I_{Cu}^{Lu} and I_{Cu}^{Eu} and the cadmium ratio with respect to copper R_{Cd}. The index I_{Cu}^{Lu}, which characterizes the hardening of the neutron spectrum, is determined by the relationship

TABLE 1. Spectral Characteristics of the Neutron Field in Fuel Elements with Different Degrees of Depletion

Depletion, rel. units*	R_{Cd}	I_{Cu}^{Lu}	T_n [°K]
1,0	7,15±0,14	0,96±0,01	345±10
0,5	9,28±0,18	0,94±0,01	332±10

* "Fresh" fuel is denoted by 1.0; 0.5 denotes fuel with 50%-depletion with respect to ^{235}U.

TABLE 2. Values of nv_0 in a Dry Experimental Channel of the Reactor

Reactor power level, kW	$nv_0 \times 10^{12}$, neutron/cm^2·sec	
	with respect to gold	with respect to cobalt
300	2,22±0,11	2,20±0,11
500	3,62±0,18	3,37±0,17
900	7,10±0,36	6,84±0,34

Translated from Atomnaya Énergiya, Vol. 35, No. 5, pp. 315-316, November, 1973. Original article submitted October 23, 1972; revision submitted May 24, 1973.

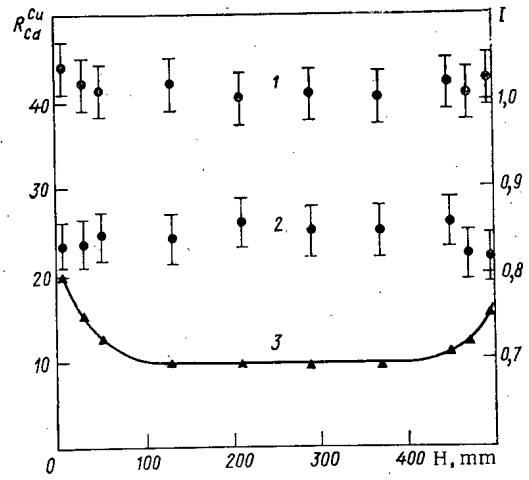

Fig. 2. Distributions of the spectral characteristics I_{Cu}^{Eu} (1) and I_{Cu}^{Lu} (2) and the cadmium ratio with respect to copper R_{Cd} (3) along the height of the channel.

$$I_{Cu}^{Lu} = \left(\frac{As^{Lu}}{As^{Cu}}\right)_x \Big/ \left(\frac{As^{Lu}}{As^{Cu}}\right)_0,$$

where the numerator and the denominator constitute the ratios of saturation activities of lutecium and copper detectors, measured in the unknown and the calibration spectra [2]. The value of I_{Cu}^{Eu} was determined in a similar manner. The neutron temperature T_n was determined from Westcott's relationships [3, 4] on the basis of data on the spectral index I_{Cu}^{Lu} and the cadmium ratio.

Figures 1-4 show the data obtained in the dry experimental channels and the fuel elements in the reactor core by means of detectors and fission chambers. The sensitivity of the thermal neutron fission chamber was $2 \cdot 10^{-17}$ A/(neutron /cm^2 · sec).

The distribution of the cadmium ratio with respect to copper (see Fig. 2) shows that the relationship between thermal and resonance neutrons along the channel is constant in its middle section. The relative distribution of R_{Cd} along a fuel element is also constant, retaining its character even after considerable fuel depletion.

Table 1 provides the values of I_{Cu}^{Lu}, R_{Cd}, and T_n for the middle section of fuel elements with different degrees of depletion. It is evident that the spectral characteristics, especially R_{Cd}, depend on the fuel depletion.

The absolute values of the thermal neutron flux were measured in the reactor channels by means of gold and cobalt films. The relative density of the neutron flux was determined by means of the expression

$$nv_0 = \frac{KNs}{gG_{th} + rSG_r},$$

where K is a coefficient which characterizes the detector and the counter efficiency, and Ns is the specific saturation activity (pulses/sec · g).

The density of a thermal neutron flux with the mean velocity $\bar{v}$ is equal to $n\bar{v} = 1.128\sqrt{(T_n/T_0)}nv_0((R-1)/R$, where R is the cadmium ratio for a 1/v-detector.

Table 2 provides the results obtained in measuring the absolute density of the neutron flux by means of gold and cobalt films for different power levels of the reactor.

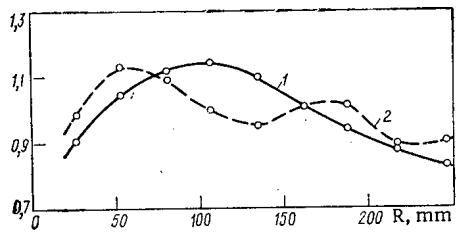

Fig. 3

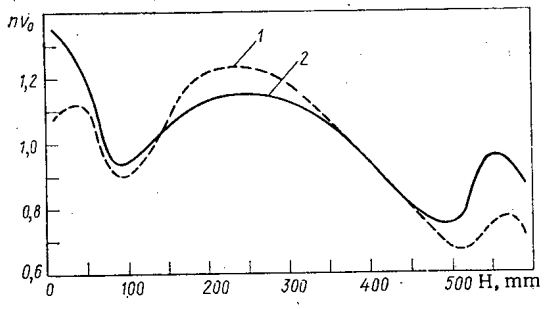

Fig. 4

Fig. 3. Relative density distributions of the thermal neutron flux along the height of a fuel element nv_0, measured by means of copper foils for depleted (1) and "fresh" (2) fuel elements.

Fig. 4. Relative density distributions of the thermal neutron flux along the core radius nv_0, measured by means of a fission chamber for the old (1) and the new (2) core.

The errors in measuring the spectral indices and the cadmium ratio are not larger than 1 and 2%, respectively. The error in determining T_n comprises the errors in I_{Cu}^{Lu}, R_{Cd}, the self-shielding factors for thermal and resonance neutrons, and the characteristics of the calibration spectrum. The total error in measuring the neutron temperature amounts to approximately 3%. The error in determining the absolute density of the thermal neutron flux is not larger than 5%.

Water circulation through the core was not interrupted during the measurements. The core temperature was maintained at 20 ± 1°C. The composition of the reactor core chosen on the basis of neutron field measurements in the core yielded an increase of approximately 10% in the absolute neutron fluxes in horizontal beams at the same power level (Fig. 4). The new arrangement consists of annular zones composed of fuel elements with different degrees of depletion.

LITERATURE CITED

1. W. Zjip, Report RCN-37 (1965).
2. S. S. Lomakin et al., SNIIP Transactions [in Russian], Vol. 12, Atomizdat, Moscow (1970), p. 230.
3. C. Westcott, AECL-1101 (1960).
4. C. Westcott, Second Geneva Conference, 1958, Report 202.

STABILITY OF SYSTEMS FOR CONTROLLING POWER DISTRIBUTION IN A NUCLEAR REACTOR

E. V. Filipchuk, P. T. Potapenko, and A. N. Kosilov

UDC 621.039.515

The rapid development of nuclear power engineering is making heavy demands on materials. Accordingly, with a view to increasing the efficiency, the control systems of modern reactors have to meet much more exacting requirements than in the initial development stage.

There is a marked tendency at the present time towards constructing larger and more powerful reactors. These changes have necessitated a qualitatively new approach to the control of a reactor as an object with distributed parameters (in particular, all modern reactors are provided with systems of in-reactor control).

Hsu and Bailey [1] give a systematic review of many papers on the spatial dynamics of the neutron field of a reactor. The present paper utilizes the so-called adiabatic model of a reactor in which the spatial and temporal components of the neutron flux are assumed separable. This is, of course, an approximation. It is permissible when discussing neutron field control, since control is a slow process compared with the time required for the field to redistribute in response to a local change of reactivity, and also because the neutron field deviates only slightly from the steady-state distribution [2].

Conditions are obtained in [3] for the stability of the steady-state power distribution in a reactor in which there is no control system. Engineering aspects of this problem are also considered in Hitchcock's monograph [4].

The present paper describes an engineering method of analyzing the stability of an automatic system for controlling the power distribution in a reactor. The mathematical model used in the analysis relates to a reactor with a stable spatial power distribution in which the dynamics of the internal feedback loops can be neglected. Thus, in comparison with the dynamics of power distribution control, the negative feedback loop due to the Doppler effect is assumed inertialness, and effects associated with xenon poisoning are ignored as slow acting.

In order to stabilize and optimize the neutron field the active zone is split up into several regions each of which contains a neutron sensor and a compensating rod of the control system. The power of each region is stabilized by this rod, which will be referred to below as a local regulator. In operation all the local regulators are coupled together through the reactor.

The automatic control of power distribution in a reactor thus means that we are dealing with a multiloop control system. The first problem to be solved in the design of such a system is that of control stability.

In contrast to [5] we shall analyze the system without artificial couplings between the local regulators. The structure of the system is illustrated in Fig. 1, where the indices denote the numbers of the local regulators; W_D and W are the transfer functions of the sensor and the regulator. The power settings n_0 on the local regulator meters are in accordance with the required form of power distribution calculated from an appropriate optimality criterion.

The reactor transfer matrix H, interrrelating the neutron flux change δn at the sensor positions with changes in the multiplication coefficient in the cells δk or with displacements of the rods, can be

Translated from Atomnaya Énergiya, Vol. 35, No. 5, pp. 317-321, November, 1973. Original article submitted November 13, 1972.

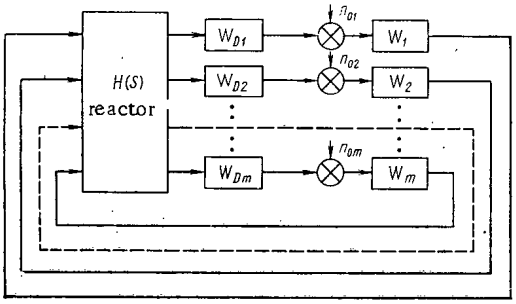

Fig. 1. Block diagram of control system.

represented in the following form in the adiabatic model

$$H = W_0 A, \tag{1}$$

where A is a numerical matrix found from static calculations or from experiment; W_0 is the transfer function of a "point" reactor. Thus,

$$\delta n = H \delta k,$$

and for the steady state

$$\delta n = A \delta k.$$

For a reactor with a negative power reactivity the matrix A is determined by experimentally measuring the flux increments with all the sensors in response to displacements of the auxiliary rods of the local regulators. In the present treatment of the problem the amplification coefficient for transfer function W_0 must, clearly, be taken equal to unity.

Using (1) the matrix equation of the system shown in Fig. 1 can be written in the form

$$[E + W_0 DWA]\,\delta n = W_0 DWA \delta n_0. \tag{2}$$

Here D and W are diagonal matrices constructed from the transfer functions of the sensors and the local regulators; E is the unit matrix; δn_0 and δn are vectors denoting the changes in the setting and in the neutron flux.

We introduce new coordinates related to the old by a nondegenerate transformation matrix C:

$$\delta n_0 = CN_0; \quad \delta n = CN.$$

In the new system of coordinates Eq. (2) can be written

$$C^{-1}[E + W_0 DWA]\,CN = C^{-1} W_0 DWACN_0. \tag{3}$$

The transfer functions of the sensors and the local regulators are naturally taken to be the same, when the matrices W and D will be scalars. Allowing for this, Eq. (3) transforms in the following manner:

$$[E + W_0 DWC^{-1}AC]\,N = W_0 DWC^{-1}ACN_0. \tag{4}$$

If the canonical basis of matrix A is taken as the matrix C, then, as is well known,

$$C^{-1}AC = \Lambda$$

gives in place of matrix A its canonical, ultimately simple form Λ. Depending on the eigenvalue spectrum of matrix A there are five ways of going from the initial system to the equivalent [6].

Let us consider in more detail the case when the control system maintains an equalized power distribution, i.e., the neutron flux is the same at all sensor positions. Utilizing the properties of the divgrad operator, which describes neutron diffusion [7], it is readily shown that the matrix A is symmetric.

The matrix Λ for a symmetric A is diagonal, the elements of its main diagonal being the (real) eigenvalues λ_i of matrix A. It follows from (4) that the multidimensional control system decomposes into m (the number of local regulators) one-dimensional systems which differ from each other only in the sections with amplification coefficients $\lambda_1, \lambda_2, \ldots, \lambda_m$.

In accordance with (2) the stability of the initial system is determined by the characteristic equation

$$\det [E + W_0 DWA] = 0. \tag{5}$$

Since the transition from the initial system to the equivalent system is effected by a similitude transformation, the roots of their characteristic equations coincide:

$$\det [E + W_0 DW\Lambda] = \prod_{i=1}^{m} [1 + W_0 DW\lambda_i] = 0. \tag{6}$$

In this manner, the characteristic equation of the equivalent system has decomposed into m characteristic equations of equivalent separate systems

$$1 + W_0 DW\lambda_i = 0, \quad i = 1, 2, 3, \ldots m. \tag{7}$$

Thus, a necessary and sufficient condition for the stability of the system is that each of the m separate systems be stable.

If all λ_i are real and positive, as in the present case, the discussion may be restricted to the stability of the separate system with $\lambda_{i\,max}$.

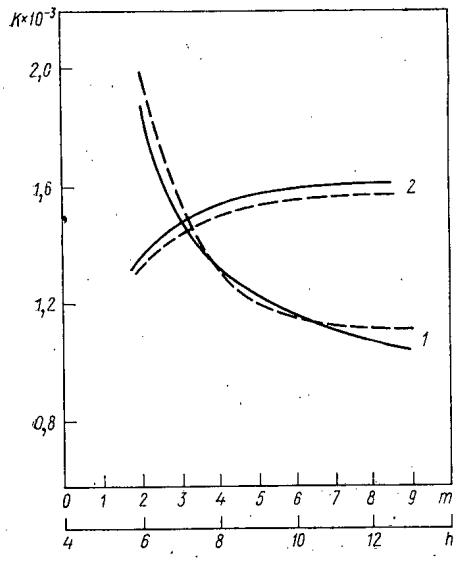

Fig. 2

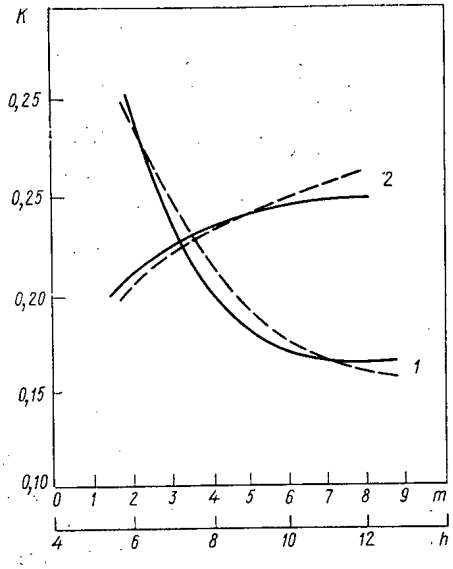

Fig. 3

Fig. 2. Threshold amplification coefficient K of local regulators with transfer function W_1 vs number of regulators m and distance between them h. ——) theory; – – – –) analog simulation.

Fig. 3. Threshold amplification coefficient K of local regulators with transfer function W_2 vs number of regulators m and distance between them h.

We cite the numerical results of a study which we made on the stability of control for a specific reactor with parameters: diameter of active zone 52 (all linear dimensions will be expressed in neutron migration lengths), diameter of equalized zone (the control zone) 32. Control is effected at a nominal power at which the power reactivity amounts to 1 cent at a 1% power deviation.

Figure 2 shows plots of K, the threshold amplification coefficient of the local regulators corresponding to the stability boundary, vs: (1) the number m of local regulators for a fixed pitch h between them, and (2) the pitch h for a fixed m. These results are obtained for slow-acting local regulators, the transfer function of which in conjunction with the sensor is

$$W_1 = \frac{Ke^{-8s}}{s(40s+1)(10s+1)(2{,}5s+1)}. \tag{8}$$

In all cases the local regulators are located in the central part of the active zone at equal distances from each other.

Figure 3 shows analogous results for high-speed regulators with a transfer function

$$W_2 = \frac{K}{s(4s+1)(0.2s+1)}. \tag{9}$$

The digital-computer calculation of the eigenvalues and the analog simulation were performed on the basis of the one-group diffusion model of the active zone.

A system for controlling integral reactor power is subject to much more stringent demands than a system for controlling power distribution. In particular, the former system must be more reliable and it must be much more fast acting (by an order).

Although a system for controlling power distribution fulfills at the same time the function of an integral-power controller, it usually cannot satisfy these stringent demands. Accordingly, for the practical realization of a multiloop control system an additional special circuit for integral power control must be provided.

Let us find the numerical reactor matrix $\mathcal{A}$ allowing for the operation of an astatic (floating) integral-power controller. In this case, as before,

$$\delta n = \mathcal{A}\delta k \tag{10}$$

TABLE 1. Elements of Matrix A with Integral-power Controller off

17,8592	3,3240	4,3679	3,0642	1,6792
3,3286	18,5283	4,6221	1,7175	3,4749
3,3869	4,6245	18,0379	4,5110	4,6414
3,0853	1,7206	4,5130	18,3143	3,4248
1,6861	3,4757	4,6414	3,4240	18,5465

Eigenvalues of maxtrix A

32,4166	16,7466	16,4636	13,3600	12,2994

TABLE 2. Elements of Matrix $\mathcal{A}$ with Integral-power Controller on

14,8024	—0,0965	0,9207	—0,1810	—1,7668
—0,1317	14,6563	0,7196	—1,9562	—0,4262
1,6665	1,5805	14,9701	1,6229	1,5746
—0,1859	—1,9397	0,8238	14,8412	—0,2631
1,8033	—0,4288	0,7061	—0,2806	14,6125

Eigenvalues of matrix A

16,7465	16,1271	16,5978	13,3570	11,0541

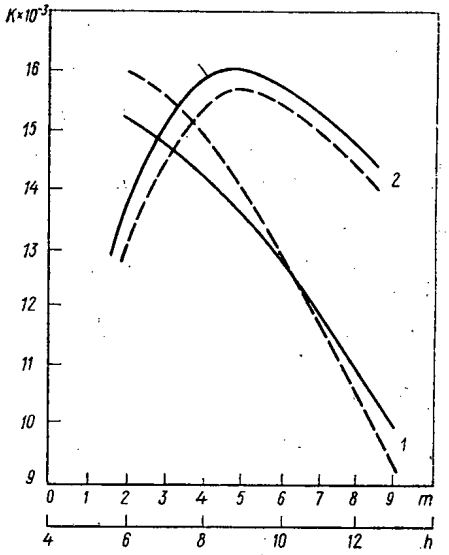

Fig. 4. Threshold amplification coefficient K of local regulators vs number of regulators m and distance between them h in the presence of an integral-power controller.

or

$$\delta n = A(\delta k + \Delta k_0), \tag{11}$$

where Δk_0 is the action vector of the integral-power controller.

Suppose an external perturbation δk is introduced only in the i-th cell. The rods of the integral-power controller compensating this local perturbation move synchronously in cells l, m, ..., p. The condition for floating control can then be written in the form:

$$\delta k_i \sum_{j=1}^{m} a_{ji} + \Delta k_0 \sum_{q} \sum_{j=1}^{m} a_{jq} = 0;\ q = l, m, \ldots p. \tag{12}$$

Here a_{ji} are the elements of matrix A.

We thus have

$$\Delta k_0 = -f_i \delta k_i, \tag{13}$$

where

$$f_i = \frac{\sum_{j=1}^{m} a_{ji}}{\sum_{q} \sum_{j=1}^{m} a_{jq}};\quad q = l, m, \ldots p. \tag{14}$$

Inserting these relationships into (11) gives

$$\delta n_i = \delta k_i A [e_i - f_i \sum_q e_q];\quad q = l, m, \ldots p,$$

where e_μ is a unit vector with a single nonzero μ-th component.

The product $A[e_i - f_i \sum_q e_q]$ is evidently the i-th column of matrix $\mathcal{A}$, and the elements of matrices $\mathcal{A}$ and A are interrelated by:

$$\alpha_{ji} = a_{ji} - f_i \sum_q a_{jq};\quad q = l, m, \ldots p. \tag{15}$$

Expressions (14) and (16) are the starting point for the construction of a machine algorithm for the calculation of matrix $\mathcal{A}$. The matrix $\mathcal{A}$ can also be found, of course, by means of direct experiments on the reactor.

As mentioned above, integral-power control must be effected in a time much shorter than for power-distribution control. The matrix $\mathcal{A}$ may then be regarded as the transfer matrix of the reactor.

The stability may now be analyzed by the method described above on setting $W_0 = 1$ and calculating the eigenvalues of $\mathcal{A}$ instead of A.

Figure 4 shows plots of the threshold amplification coefficient K for the same conditions as in Fig. 2 but with a high-speed integral-power controller present.

The influence of the integral-power controller on the static reactor matrix, on the eigenvalue spectrum, and on the stability is illustrated for example by the results of calculating the elements of the numerical matrices for m = 5 and h = 8 (Tables 1 and 2).

The integral-power controller significantly changes the reactor transfer matrix; for stability it is important that there should be an accompanying sharp reduction in the eigenvalues. A comparison of Figs. 2 and 4 shows that the integral-power controller has an even sharper influence on the stability as a result of the improved dynamic characteristics of the reactor. The above method can also be used in the case of an arbitrary (and, in particular, a nonuniform) distribution of sensors and control rods in the active zone.

In summary, a method has been described for analyzing the stability of a system for controlling the power distribution in the active zone of a reactor and the method has been extended to the case when the integral power of the regulator is stabilized by a special high-speed controller. The threshold amplification coefficient of the local regulators decreases as their number is increased. The pitch h between the regulators has a smaller effect on the stability than their number m. The high-speed integral-power controller exerts a strong stabilizing effect on the power-distribution control system.

LITERATURE CITED

1. C. Hsu and R. Bailey, Trans. Am. Nucl. Soc., 2, No. 2.
2. Kh. L. Garabedyan, in: Theory of Nuclear Reactors [in Russian], Gosatomizdat, Moscow (1963), pp. 284-318.
3. I. S. Postnikov and E. F. Sabaev, "Stability of the steady-state cycle of a power reactor in one-group diffusion approximations," At. Énerg., 24, No. 1, 38-42 (1968).
4. A. Hitchcock, Nuclear Reactor Stability [Russian translation], Gosatomizdat, Moscow (1963).
5. P. T. Potapenko, At. Énerg., 27, No. 3, 189-193 (1969).
6. O. S. Sobolev, in: Theory of Multiloop Control [in Russian], Nauka, Moscow (1967), pp. 143-161.
7. R. Varga, in: Theory of Nuclear Reactors [in Russian], Gosatomizdat, Moscow (1963), pp. 187-215.

M. Ribaric

FUNCTIONAL—ANALYTIC CONCEPTS AND STRUCTURES OF NEUTRON TRANSPORT THEORY

VOLUMES I AND II, LJUBLJANA [YUGOSLAVIA], 1973 [IN ENGLISH]

Reviewed by V. P. Kovtunenko

This monograph makes available results of many years of work by the author on applications of the arsenal of functional analysis to several problems in neutron transport theory. He develops a theory on how to determine the neutron physics properties of a medium consisting of discrete parts whose properties are known. The albedo approach lies at the basis of the theory.

The first volume is in 23 chapters grouped under five sections. The basic mathematical definitions are presented in the second volume. The first section (chapters 2-4) discuss passage of neutrons through the interface presented by a unit isolated body. Basic definitions and assumptions are put forth, the reflecting properties of the medium within a restricted span of time are estimated, continuity and invariance principles are established, and laws are established for the arbitrary retention of the albedo operator. The fourth chapter (in this section) discusses changes in the reflecting properties exhibited by the medium over an infinite time interval. The asymptotic response of the medium to a burst of bombarding neutrons is assumed. Relationships are established between physical concepts such as albedo in the stationary state, the average state over an infinite time interval, transmission, momentum reaction, etc.

The second section (chapters 5-9) takes up reflecting properties of a medium consisting of several parts. The state of the medium over a restricted time span is investigated; the nature of the composite medium is defined and the basic equation describing the state of the medium is derived. The state of a compound medium consisting of subcritical parts is treated for an infinite time interval. The seventh chapter introduces concepts determining the processes that take place in the composite medium (mean neutron distribution after an infinite number of reflections, mean number of reflections, mean time and velocity of reflection, etc.). The asymptotic properties of a medium consisting of subcritical uniformly bound particles of constant albedo over an infinitely long time interval, and the properties of a medium in a close-to-critical state are discussed in the last chapters of this section.

Measurements, experimental distribution of neutron distributions and of the reflecting characteristics of the medium, are the subject matter of the third section of the monograph (comprising chapters 10-15). The concept of linear measurement is introduced, its relationship to the concept of a linear functional is established, a definition is given of adjoint operator and adjoint equation. Measurements in the stationary state and in the dynamic state are discussed, as well as inaccuracies in measurements. A mathematical interpretation is presented for experimentally measured variables, which are determined when neutrons traverse surfaces of the particles comprising the medium. This section concludes with a discussion of indirect experimental determination of the reflecting properties of the composite medium on the basis of experimental data on the reflecting properties of the medium's constituent parts in the stationary state and in the nonstationary state.

The fourth section (chapters 16-18) discusses how the properties of the composite medium are defined and determined in terms of the properties of the constituent parts, through the use of the albedo equations. The existence of finite-dimensional approximations of the linear theory of interacting systems is demonstrated. Problems associated with calculations of the subcritical state over a finite time interval are studied. The last chapter deals with calculations leading to approximate solutions of the eigenvalue problem.

Translated from Atomnaya Énergiya, Vol. 35, No. 5, pp. 321-322, October, 1973.

The fifth section of the monograph (chapters 19-23) deals with several special topics relating to the content of the first two parts. Here we find defined the reflecting properties of the composite medium in its discrete parts in the transport approximation, states of the medium, and so on. The case where the reflecting properties of the medium and the reflecting properties of the constituent parts of the medium are nonlinear in nature are discussed in this part of the monograph. The concluding chapters establish the relationship between the proposed theory and field theory, and discuss the role played by mathematical analogs in the natural sciences.

It is demonstrated, in the monograph, that some concepts in reactor theory lend themselves well to description in function-analytical terms. Establishment of simple physical interpretations of the basic concepts of functional analysis, as done here, is also of interest. The role played by physical assumptions in determining the mathematical model to use is also demonstrated.

In view of the specificity of the treatment, the book cannot be approached as a textbook or handbook for the study of reactor theory. However, it may be found useful by physicists, who will find in it mathematical definitions of some concepts in reactor theory, and also by mathematicians, who will discover in the text physical interpretations of some traditional mathematical concepts in functional analysis.

NEW BOOKS PUBLISHED BY ATOMIZDAT

III QUARTER 1973

E. Curie. Mariya Kyuri [Marie Curie] [translated into Russian from French], 3rd Edition, Atomizdat, Moscow, 1973.

No woman scientist has ever enjoyed a popularity equal to that of Marie Curie. She was awarded ten prizes and sixteen medals. M. Curie was elected honorary member of a hundred and six scientific institutions, academies, and scientific societies. Specifically, she was an honorary member of the Society of Enthusiasts of Natural Science, [Physical] Anthropology, and Ethnography in Moscow, starting 1912 a member of the Institute of Experimental Medicine in Petersburg, Petrograd, starting 1914 an honorary member of the scientific institute in Moscow, and starting 1926 an honorary member of the USSR Academy of Sciences.

Marie Curie's biography was written by her younger daughter Eva, journalist by profession. The book was published in French in 1937 and has been through over a hundred editions in France. Moreover, the book has been translated into twenty-five languages and sometimes has come out in ten to twelve editions in the translation languages. The book has already appeared twice in print in the Russian language prior to this edition (1967 and 1968).

* * *

V. P. Krainov. Lectures on the Microscopic Theory of the Atomic Nucleus [in Russian], Moscow, 1973.

The book outlines the simplest theoretical concepts on the structure of the atomic nucleus. Attention is focused on a popular description of microscopic methods widely used in the scientific literature on the physics of the nucleus. The ground states and low-lying excited states of nuclei get the center of attention in this treatment. Methods for analyzing nuclear reactions are discussed as helpful tools in the investigation of the structure of the nucleus.

The book can be recommended as an introductory textbook for upper classes at college level and graduate students specializing in theoretical and experimental nuclear physics. It will also be useful to instructors in colleges teaching courses on theoretical physics and on the physics of the nucleus.

* * *

L. A. Matalin, V. S. Nesterenko, V. N. Smirnov, et al. Electronic Techniques in Nuclear Physics [in Russian], Atomizdat, Moscow, 1973.

This book deals with applications of up-to-date techniques in electronics and computer practice in experimental nuclear physics. Attention is centered on the design principles of electronic physics experimental equipment, and on the use of digital computers in physics experiments.

An attempt is made to throw light on the problem of acquisition, collection, and processing of data in physical experiments, from the information-processing point of view.

The book is intended for a broad range of specialists concerned with research in the fields of nuclear physics, biology, medicine, and in other related areas. The book may also prove useful to senior college undergraduates in the appropriate majors.

* * *

Translated from Atomnaya Énergiya, Vol. 35, No. 5, pp. 322, 325-6, and 331-3, November, 1973.

T. A. Germogenova, V. P. Mashkovich, V. G. Zolotukhin, and A. P. Suvorov. Neutron Albedo [in Russian], Atomizdat, Moscow, 1973.

This book is the first monograph on backscattering (albedo) of neutrons of various energies from real media (concrete, iron–water baffles, etc.). Available information and data obtained by the book's authors on the differential and integrated characteristics of neutron albedo are reviewed and analyzed, and methods used in the study of those data are discussed.

The bulk of the computer-output information obtained by the authors on the differential characteristics of the albedo of unidirectional monoenergetic sources (in the realm of isotope sources and reactor sources) is published here for the first time.

The book is intended for engineers, graduate students, undergraduates, and all scientific research workers and technicians specializing in the field of protection against ionizing radiations, or in related fields concerned with the use of radioactive sources in the various branches of science, engineering, and the national economy.

* * *

Topics in Plasma Theory. Collection of Articles, No. 7 [in Russian], Academician M. A. Leontovich (editor), Atomizdat, Moscow, 1973.

This is the seventh publication in a series of compendia of articles on advances in plasma theory, offering a unified presentation of the theory of propagation and interaction of oscillations of a continuous medium; such effects as transformation of waves in a nonhomogeneous medium, nonlinear restriction of kinetic plasma instabilities leading to the appearance of anomalous resistivity and turbulent diffusion of plasma, are discussed; the neoclassical theory of transport processes in toroidal systems is reviewed; cyclotron radiation by plasma is also discussed.

The book is written for research scientists, engineering physicists, graduate and undergraduate students, not only those specializing in plasma physics, but also those specializing in geophysics and astrophysics.

* * *

U. Ascoli-Bartoli, M. Baggiani, F. de Marco, L. A. Dushin, et al. Probing an Inhomogeneous Plasma with Electromagnetic Waves [translated into Russian from Italian], Atomizdat, Moscow, 1973.

This book comprises a survey of current methods used in research on plasma by probing the plasma with electromagnetic waves in the optical and microwave ranges of the spectrum. The authors describe techniques for determining the density, temperature, and degree of turbulence of plasma, i.e., the most important characteristics of plasma. The treatment of the optical and microwave techniques from a unified point of view is quite original. The text also contains a completely novel and hitherto unpublished body of material on applications of holographic and correlation techniques in investigations of a turbulent plasma.

This book will be useful to experimental physicists and engineers and technicians engaged in investigations of plasma.

* * *

Lasers and the Thermonuclear Problem. Collection of Translated Articles [in Russian], Academician B. B. Kadomtsev (editor), Atomizdat, Moscow, 1973.

Recently great attention has been paid to the use of lasers in creating and heating plasma, specific arrangements have been developed for setting up thermonuclear experiments involving the use of lasers, and problems relating to the interaction of extremely powerful laser radiation with matter are being considered.

The papers presented in this collection reflect the present state of research in this rapidly-developing field and will undoubtedly prove interesting to a wide circle of specialists concerned with the making and applications of lasers, plasma diagnostics, and the interaction of radiation with matter. The collection will also interest specialists in the field of plasma physics studying the retention of plasma in magnetic traps of various types.

* * *

L. A. Dushin. UHF Interferometers for Measuring Plasma Density in a Pulsed Gas Discharge [in Russian], Atomizdat, Moscow, 1973.

This is the first book which has dealt with problems relating to the working characteristics and applications of the uhf interferometer as a special instrument for studying the plasma of a pulse discharge. The author describes the operating principles, constructional aspects, and classification of various types of fast-acting interferometers, and analyzes possible measuring errors. Since interferometers incorporating lasers and photoelectric bias for recording the phase shifts differ in no way from uhf interferometers as regards operating principles, the author also describes some laser interferometers for studying pulse-type plasma, and discusses problems associated with special aspects of their use and prospective development.

The book is intended for experimental physicists and workers in technical engineering concerned with the study of plasma, and is useful to students and graduates specializing in this field.

* * *

G. A. Kasabov and V. V. Eliseev. Spectroscopic Tables for Low-Temperature Plasma, Handbook [in Russian], Atomizdat, Moscow, 1973.

These tables contain the most reliable data relating to oscillator strengths and Stark broadening parameters for a large number of spectral lines of nineteen elements widely employed in apparatus and instrument involving low-temperature plasma.

The handbook is useful to research workers concerned with methods of direct energy conversion, high-temperature hydrodynamics, the physics of shock waves, gas lasers, and gas-discharge light sources.

* * *

P. Cohen. Water Technology of Power Reactors [translated into Russian from English], Atomizdat, Moscow, 1973.

This book sets out the present state of a number of questions relating to the use of ordinary and heavy water as a coolant, moderator, and biological shield in nuclear power reactors. Methods of chemically regulating reactors, boron regulation in particular, are considered. Methods of purifying the coolant and removing radioactive waste are set out, the behavior of solid impurities and gases in the reactor circuit is considered, and so on. Considerable attention is paid to practical problems: the purification of the water at high temperatures, ion-exchange materials, purification by evaporation, in mixed ion-exchange resins, and so forth.

The book is intended for engineers and scientific workers designing and using nuclear power installations, and also for students and graduates of the higher educational establishments studying the corresponding fields.

* * *

G. V. Tsiklauri, L. I. Seleznev, and V. S. Danilin. Adiabatic Two-Phase Flows [in Russian], Atomizdat, Moscow, 1973.

This monograph is devoted to problems of high-velocity two-phase flows. Detailed attention is given to the hydrodynamics of two-phase flows of different structures (drop, bubble, foam), questions of their stability, processes of mechanical interaction, and heat and mass transfer. The results of various experimental and theoretical investigations into the adiabatic flows of two-phase media in nozzles, tubes, and jet systems are presented for a wide range of concentrations of the liquid phase (right up to unity), including the outflow of saturated and underheated liquids. Data are presented in relation to the flow and energy characteristics of nozzles and jet systems, the critical conditions of two-phase flows are analyzed, and methods are given for calculating the corresponding two-phase flows; some problems relating to the two-phase boundary layer and the separation and flow of films are also considered.

The book is intended for a wide circle of engineers and scientific workers concerned with the study of two-phase flows, and the design of new types of stationary and portable power installations; it may also be useful for students of the senior courses in power and polytechnic higher educational establishments.

* * *

A. L. Yakubovich, E. I. Zaitsev, and S. M. Przhiyalgovskii. Nuclear-Physical Methods of Analyzing Minerals [in Russian], 2nd Edition, Atomizdat, Moscow, 1973.

The authors of this book set out the physical foundations of nuclear-physical methods of analysis and the principles underlying the construction of the analytical apparatus; they consider the prospects and characteristics of laboratory methods of elementary analysis for rocks, ores, and processing products. In the second edition (the first was published in 1969) more detailed attention is given to the prospects of using semiconductor detectors of ionizing radiations in apparatus for nuclear-physical analysis, and also instrumental activation analysis. New data are presented as regards the use of the method of time selection between different radiations in radiometry, as well as additional information on the x-ray radiometric method of analyzing light rock-forming elements.

The book is intended for workers in the analytical service of industrial, scientific-research, and teaching establishments of the geological, mineral–chemical, metallurgical, and mixed persuasions.

* * *

Production of Coatings by High-Temperature Spraying (Sputtering) [translated into Russian from English], L. K. Druzhinina (editor), Atomizdat, Moscow, 1973.

This book contains papers from the Sixth International Conference on Metallization by Spraying (Sputtering) which took place in 1970 in Paris; it contains data relating to various methods of depositing coatings, using an electric arc, an oxyacetylene flame, and plasma, and to the manufacture of the equipment required for these purposes. Information is presented as to the industrial use of coatings, together with experimental investigations into the properties of coatings produced from metallic and ceramic materials in relation to the conditions of formation, the composition of the gas atmosphere, the composition of the materials deposited, and other factors. Questions as to the physicochemical interaction of the coating with the substrate, leading to firm adhesion, are also considered. Attention is given to monitoring the quality of coatings.

The book is intended for technical engineering workers, graduates, and students specializing in atomic, aviation, metallurgical, engineering, and other branches of technology.

* * *

V. I. Korobkov and V. B. Luk'yanov. Methods of Preparing Specimens and Analyzing the Results of Radioactivity Measurements [in Russian], Atomizdat, Moscow, 1973.

In solving many scientific and technical problems associated with the use of radioactive isotopes in the popular economy it is essential to measure the radioactivity of specimens prepared under laboratory conditions.

This book systematizes the most important methodical developments in specimen preparation for relative and absolute radioactivity measurements. Attention is paid to the preparation of thin substrates for specimens, particularly thin organic films.

Mathematical statistical methods are given for analyzing the results of radioactivity measurements.

The book constitutes a methodical convenience in the everyday work of students and scientific workers employing radioactive isotopes in their pursuits.

* * *

A. D. Levkovich, A. M. Lyutsko, and A. N. Pertsev. Isotopic Biointroscopy [in Russian], A. N. Pisarevskii (editor), Atomizdat, Moscow, 1973.

Isotopic introscopy is a promising method of studying processes taking place in optically opaque media. This method is of particular significance in medico-biological research. This book sets out problems encountered in the detection, transmission, recording, contrasting, and interpretation of introscopic information. A high proportion of the material is based on investigations carried out by the authors. Using the theoretical models proposed, the present state of the method, the possibilities of improving it, and the prospects of further development are all analyzed.

The book is intended for specialists of the physical, physicotechnical, and medico-biological fields concerned with the applications of isotopic introscopy in various fields of science and popular economy,

particularly in relation to isotopic diagnostics; it may also serve as a guide to the method of isotopic introscopy for the students of higher educational establishments in the corresponding fields of work.

* * *

Radiation Protection Manual for Engineers [translated into Russian from English], D. L. Broder et al. (editors), Atomizdat, Moscow, 1973.

This handbook, published under IAEA sponsorship, is in two volumes. The first volume discussed the most widely applied modern methods for calculating protection and shielding against neutron radiation and γ-radiation, while the second volume deals with forecasting of shielding and protection against radiations emitted by extended sources of different geometric configuration, methods for calculating radiation energy power distribution, temperature fields in shielding and thermal stresses, passage of radiation through channels, voids, slits, and other inhomogeneities in shielding. There are abundant tabular and graphical data needed in shielding calculations.

The handbook is intended for specialists in the physics of protection and shielding against ionizing radiations, in radiation safety, and can also be found useful by research scientists working with ionizing radiations.

* * *

N. S. Shimanskaya. Calorimetry of Ionizing Radiations [in Russian], Atomizdat, Moscow, 1973.

The book is devoted to calorimetric methods for investigating and measuring the ionizing radiations emitted by radioactive isotopes, nuclear reactors, betatrons, cyclotrons, and other nuclear facilities. Applications of calorimetric measurements in work on radiation chemistry, radiation materials science, radiation physics and nuclear physics, are discussed. A wealth of material accumulated to date on the calorimetry of ionizing radiations is reviewed.

The book is written for engineers and physicists concerned with radiometry and dosimetry of ionizing radiations, and also for senior undergraduate students and graduate students concentrating in those fields.

* * *

A. K. Sudakov. Protection of the Population against Radioactive Fallout [in Russian], 2nd Edition, Atomizdat, Moscow, 1973.

This brochure discloses the reasons for the appearance of radioactive contamination on the scene, and the nature of radioactive contamination, and its effects on humanity; it describes the characteristics of dosimetric instruments employed to ascertain the presence of radioactive contamination and the results of its action on people, on industry and equipment, on property, on foodstuffs, and on water supplies; it discusses individual and collective means of protection and shielding, measures to be taken to protect the population against exposure to radioactive materials, conditions governing survival of a population at a contaminated locality, the effect of radioactive contamination on the progress of recovery operations at foci of nuclear radiation injury.

The brochure is written for a broad range of readers and for people interested in civil defense topics, as well as for persons studying dosimetric instruments and personnel protection equipment in study circles, in civil defense courses, and at educational institutions.

* * *

V. I. Ivanov and V. P. Mashkovich. Collection of Problems on Dosimetry and Protection against Ionizing Radiations (Textbook aid for colleges) [in Russian], 2nd Edition, Atomizdat, Moscow, 1973.

This book is a second (revised and enlarged) edition of a textbook which first appeared in 1964 as an aid in seminar and practical instruction within the scope of a course in dosimetry and protection against ionizing radiations.

The problem book contains about five hundred problems. Each section begins with a list of basic formulas needed in solving the problems, and ends with more complex problems which can be used either as homework or to check the student's progress. Answers to problems are included at the end of the book; worked-out solutions are given for the most typical problems.

This is a textbook aid for students specializing in dosimetry and protection against radiations. It can also be recommended for students in allied fields, and for engineers and research workers concerned with the use of radioactive isotopes.

* * *

V. E. Levin and L. P. Kham'yanov. Recording Ionizing Radiations (Textbook for technical schools) [in Russian], 2nd Edition, Atomizdat, Moscow, 1973.

The first edition of this textbook, which appeared (1969) under the title Measurements of Nuclear Radiations, was well received by readers. The textbook has been in demand not only on the part of students at technical colleges, but also on the part of workers concerned with measurements of nuclear radiations. Methods for recording nuclear radiations are detailed in the text. Physical processes at work in radiation detectors are described, the electrical circuitry of detectors is presented, and coverage is given to techniques of spectrometry and mathematical processing of results. Coverage of new achievements in the field of recording nuclear radiations marks an addition to what was contained in the first edition.

The textbook is basically intended for students at technical colleges, but also for dosimetric technicians, laboratory technicians in physics laboratories, isotope laboratories, x-ray laboratories, nondestructive testing and quality control laboratories, and also for technicians and research people handling nuclear physics equipment, isotope equipment, and other similar equipment.

* * *

Effects of Ionizing Radiations on Cellular Membranes [in Russian], A. M. Kuzin, T. E. Pavlovskaya, and M. S. Volkovaya (editors), Atomizdat, Moscow, 1973.

The effect of radiations on biological membranes is one of the most urgent problems on the agenda of modern radiobiology. The book presents results of experimental research in radiation membranology. The effects of ionizing radiations on the physicochemical properties of artificially fashioned biopolymeric and cellular membranes are discussed. Failures of permeability of surface membranes in cells and of membranes of intracellular organells (mitochondria, nucleus) are described. Data on the effects of radiation on the functional activity of membranes, associated with localization of enzymes, ion transport, and so forth, are presented. Ultrastructural changes in membranes of irradiated nerve cells are discussed.

* * *

Yu. I. Moskalev, I. K. Dibobes, V. F. Zhuravlev, V. G. Ryadov, A. A. Moiseev, and A. V. Terman. Concept of Biological Risk in Effects of Ionizing Radiations [in Russian]. Atomizdat, Moscow, 1973.

This book is the first Soviet publication to review currently accepted concepts on the biological effects of radiation on the population over a broad range of dosages, as may occur under extreme conditions. The authors review a variety of data and cite comparative characteristics of the degree of risk due to either radiation effects at different doses or to nonradiation factors, including the use of transportation, etc.

The manuscript on which the text is based was approved by the National Radiation Protection Commission under the aegis of the Ministry of Public Health of the USSR.

The book is of unquestioned interest to a broad range of specialists whose work deals with utilization of radioactive isotopes.

* * *

ARTICLES

THERMAL OPENING OF OXIDE FUEL ELEMENTS WITH ZIRCONIUM CANS

A. T. Ageenkov, S. E. Bibikov,
E. M. Valuev, G. P. Novoselov,
and V. F. Savel'ev

UDC 621.039.54

In the rod-type fuel elements of power reactors the oxide nuclear fuel is enclosed in stainless steel or zirconium cans [1]. The opening of worked-out fuel elements and the separation of the fuel core from the constructional material of the can before regeneration of the nuclear fuel is an important technical problem. The extension of the thermal fusion of steel cans [2] to fuel elements with a zirconium can is more desirable from the point of view of the universality of the technological process. Tests [3] have shown that it is in principle quite feasible to melt the structural zirconium in the presence of the additive metal without any serious interaction taking place between the melt and the uranium dioxide. This justifies

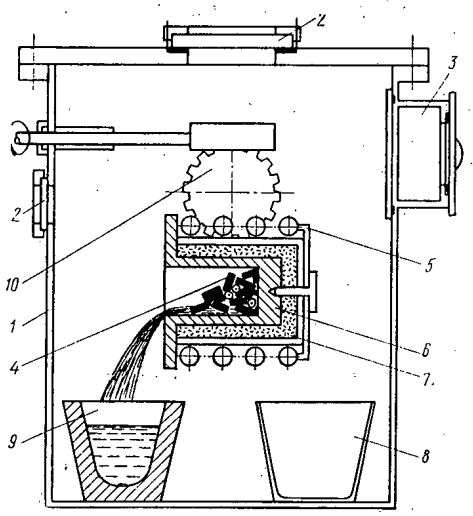

Fig. 1. Arrangement of the apparatus: 1) body of chamber; 2) inspection windows; 3) preliminary chamber; 4) UO_2 blocks; 5) inductor; 6) melting crucible; 7) insulation; 8) receiver for the UO_2 blocks; 9) mold; 10) tilting device.

TABLE 1. Thermal Opening of Fuel Elements

Material of additive	Conditions of opening		Composition of products, wt. %								
			fuel blocks				alloy casting				
	temperature, °C	time of contact of fuel with melt, min	UO_2	Zr	Fe	Cu	Zr	Fe	Cu	U	C
Fe	1050	20	95,3	4,2	0,5	—	84,8	15,0	—	0,09	0,08
The same	1150	15	93,9	5,5	0,6	—	87,0	12,8	—	0,10	0,10
" "	1200	15	94,8	4,7	0,5	—	87,8	12,0	—	0,10	0,09
" "	1270	15	97,7	2,1	0,2	—	87,2	12,6	—	0,10	0,04
" "	1320	20	92,3	7,0	0,7	—	79,8	20,0	—	0,10	0,10
" "	1400	30	93,3	6,1	0,6	—	78,8	20,5	—	0,51	0,09
Cu	1150	15	96,5	3,1	—	0,4	77,5	0,5	21,7	0,22	0,08
The same	1200	15	95,1	4,2	—	0,7	78,8	0,2	20,7	0,23	0,07
" "	1260	15	94,4	5,1	—	0,5	77,6	0,1	21,8	0,30	0,10

Translated from Atomnaya Énergiya, Vol. 35, No. 5, pp. 323-325, November, 1973. Original article submitted March 7, 1973.

TABLE 2. Distribution of Radioactive Elements and Total β- and γ-Activity in the Products Obtained by the Thermal Opening of the Fuel Elements, %

Products	Elements										Total radioactivity of the fuel elements	
	U, Pu	Rb, Cs	Sr, Ba	REE + Y	Nb	Te	I	Ru	Rh	Xe, Kr	β	γ
Fuel blocks	99,9	99,68	99,89	99,89	95,0	98,0	95,0	94,95	95,0	80—95	98,4	98,0
Alloy casting	0,1	0,2	0,1	0,1	4,99	—	—	5,0	5,0	—	1,5	2,0
Encrustation	0,002	0,12	0,01	0,01	0,01	2,0	5,0	0,05	—	—	0,01	0,02
Gas phase	—	—	—	—	—	—	—	—	—	5—20	0,06	—

a start being made into the development of the thermal process for opening oxide fuel elements with zirconium cans.

Materials and Apparatus

Unirradiated fuel elements of a water-cooled, water-moderated power reactor cut into sections 30-50 mm long were subjected to dissection in this way. The core of the fuel element was made of sintered UO_2 blocks and the can from Zr–1% Nb tubes. As additive material to reduce the melting point of the alloy, commercial iron (St. 3) was employed, or else copper of the M1 type. The opening of the fuel elements was studied in a vacuum installation with a GL-15M high-frequency generator (Fig. 1). All the operations in loading and unloading the materials were carried out through a chamber preliminarily evacuated and then filled with argon. ARV graphite crucibles were used for the experiments. First the crucible was degassed at 1400°C. Then the zirconium alloy was placed in the crucible and held at 1300-1400°C for 30 min. After this the alloy was cast into a mold. During the melting and holding period the inside of the crucible was coated with a protective layer containing zirconium carbide.

Opening of the Fuel Elements

The samples, constituting fragments of a water-cooled, water-moderated power reactor fuel element placed in sheaths of additive metal (Cu or Fe), were loaded into the prepared crucible. The samples in the crucible were heated until the onset of contact melting between the material of the fuel element can and the additive. After holding for 15-30 min the melt was decanted into a mold while the fuel was thrown into a receiver. The casting and the fuel blocks were weighed and analyzed chemically. The amounts of copper, iron, uranium, and carbon were determined in the alloy and the amounts of zirconium and additive material in the fuel.

Experiments showed that the can of the opened fuel element fused easily with the additive below 1200°C, and the resultant melt formed a molten metal pool in the crucible. The melt has an excellent flowability and passes completely out of the crucible when the latter is tilted. The casting is freely extracted from the steel mold. The alloy is extremely brittle, and its fracture surface has a silver-white

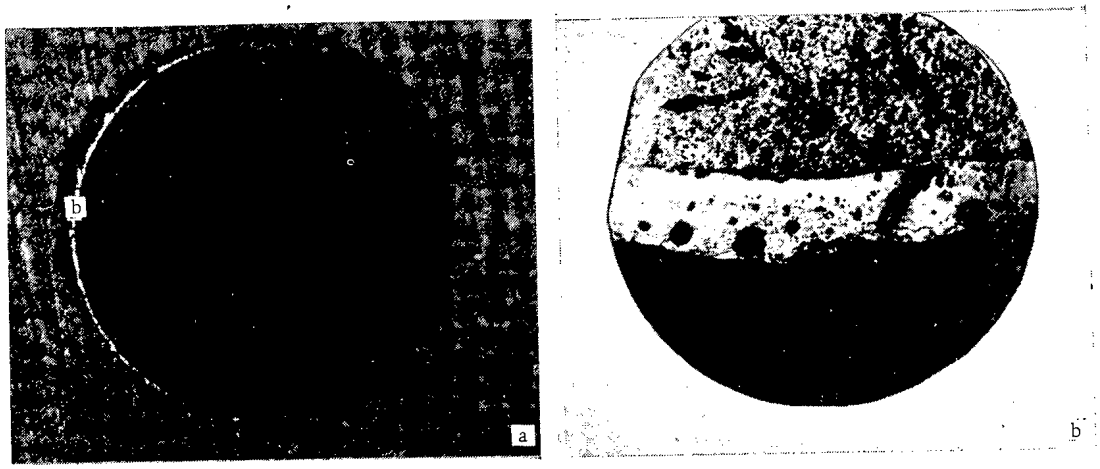

Fig. 2. Cross section of a UO_2 block after opening: a) magnified 8 times; b) 120 times.

color. The uranium dioxide blocks retain their shape during the opening process. After opening, part of the surface of the blocks is covered with a film of alloy not more than 0.1 mm thick (Fig. 2).

The results of the experiments on opening the cans are presented in Table 1. Changing the temperature from 1050 to 1300°C and the holding period from 15 to 30 min has hardly any effect on the completeness of separation of the can materials from the fuel blocks. Owing to the high flowability of the melt, most of the latter may be separated out, and only 2.1-7.0% of zirconium and 0.2-0.7% of iron or copper are left in the blocks. The transfer of uranium into the Zr–Fe or Zr–Cu melts is no greater than 0.1 and 0.3% respectively at temperatures up to 1320°C. At 1400°C the amount of uranium passing into the melt increases to 0.5%. The amount of carbon in the melt is small (0.04 to 0.10 wt. %) and does not increase in this way. Hence at temperatures up to 1400°C the protective layer of zirconium carbide formed on the inner surface of the crucible reliably protects the graphite from damage due to the melt.

Table 2 shows some computed data relating to the distribution of radioactive elements in the products obtained by thermal opening. The amount of fission products passing into the casting and encrustation is negligible. At the same time 5-20% of Xe and Kr are evolved into the gas phase during the opening.

Oxidation of the Fuel

In order to transform the UO_2 into a powdered product suitable for subsequent fluorination in a fluidized bed [4], the blocks obtained after opening were oxidized in air at 400-500°C. In all the experiments the blocks started breaking up after some 10-15 min at 400°C. The process ended in 20-30 min. The product formed a powder containing 85-97% of particles less than 10 μ in size and 3-15% of particles between 0.01 and 3 mm. Thus the alloy film on the surface of the blocks breaks up and does not prevent the oxidation of the UO_2. On oxidation of the UO_2 blocks in a fludized bed of corundum with a particle size of 500 μ, additional separation of the fuel from the alloy occurs. Fine (1-10 μ) particles of U_3O_8 are then carried out of the apparatus in the gas flow, while fragments of alloy 1-3 mm in size are accumulated in the corundum bed (2-7%) and taken out together with the latter.

LITERATURE CITED

1. A. M. Petros'yants, At. Énerg., 27, No. 4, 263 (1969).
2. G. P. Novoselov and A. T. Ageenkov, ibid., 26, No. 3, 230 (1969).
3. A. T. Ageenkov et al., ibid., 32, No. 6, 490 (1972).
4. J. Barghusen, React. Fuel Proc. Technol., 10, 309 (1967).

THERMODYNAMICAL ESTIMATION OF THE PROCESSES INVOLVED IN THE SEPARATION OF URANIUM AND PLUTONIUM HEXAFLUORIDES BY SELECTIVE CHEMICAL REDUCING AGENTS

N. P. Galkin, V. T. Orekhov, and A. G. Rybakov

UDC 621.039.59

The processes involved in the separation of UF_6–PuF_6 mixtures are of considerable interest in connection with the technology of processing the nuclear fuel of breeder reactors by the fluoride volatility method. The separation is based on the differing physical and chemical properties of the hexafluorides. There are three methods of separation which have been most widely discussed: distillation, thermal decomposition, and the use of selective chemical reducing agents. Separation by fractional distillation is clearly ineffective owing to the radiochemical and thermal instability of PuF_6 [1, 2], which leads to the gradual accumulation of PuF_4 in the apparatus. The thermal reduction of PuF_6 proceeds to a state of equilibrium; reduction by chemical reagents may be effected quantitatively and is therefore preferable.

In this paper principal attention will be directed toward chemical methods of reduction, which were discussed in earlier papers [2, 3] chiefly on the basis of experimental data.

As reducing agents for PuF_6, it is desirable to use substances having physicochemical properties differing from those of UF_6 and PuF_4; in this case the purification of the fissile materials may more easily be achieved. Analogous demands are made upon the reaction products [1]. The following substances have been proposed and studied [1-3]: freons of the methane series, CCl_3F, CCl_2F_2, $CClF_3$ (carbon tetrachloride cannot be used in view of the fact that UF_6 and CCl_4 cannot be readily separated), freon of the ethane series $C_2F_4Cl_2$, inorganic compounds H_2, Br_2, Cl_2, O_2, Xe, CO_2, SO_2, and SF_4. The most suitable substances for the separation of UF_6–PuF_6 mixtures are generally considered to be CO_2, freon-114 ($C_2F_4Cl_2$), and SF_4 [3]; however, no theoretical arguments have been presented in favor of these.

TABLE 1. Temperature Dependence of the Change in the Standard Gibbs Energy of Formation of Certain Substances ΔG^0_{fT}, kcal/mole

	CCl_3F [9]	CCl_2F_2 [9]	$CClF_3$ [9]	$C_2Cl_3F_3$ [10]	$C_2Cl_2F_4$ [10]	C_2ClF_5 [10]	OF_2 [5]	SF_6 [11]	SO_2F_2 [5]	BrF_3 [12]	XeF_2 [13]	XeF_4 [13]
T, °K	$-\Delta H^0_{f298}$											
	70,9	119,1	171,3	178,20 [14]	214,60	262,40	5,0	291,8	205,1	61,115 [15]	25,9	51,5
298	61,51	109,81	162,46	158,65	195,02	242,68	0,87	266,96	194,94	55,08	17,86	33,03
300	—	—	—	—	—	—	—	—	—	—	—	—
400	58,31	106,63	158,28	152,50	188,35	235,810	—0,55	258,40	191,54	45,09	15,15	27,83
500	55,21	103,52	155,00	145,85	181,84	229,49	—1,95	249,78	187,44	42,27	12,50	21,76
600	52,14	100,44	151,73	139,04	175,38	222,74	—3,36	241,10	183,97	39,52	9,85	15,68
700	49,10	97,36	148,46	132,55	168,97	216,19	—4,77	232,39	180,53	36,81	7,19	9,60
800	46,08	94,32	145,21	125,91	162,61	209,70	—6,18	224,96	177,76	34,13	4,53	3,52
900	43,10	91,28	141,97	119,76	156,29	203,22	—7,59	214,82	173,65	31,46	1,82	—2,55
1000	40,07	88,27	138,74	113,30	149,98	196,78	—9,00	204,73	169,64	28,81	—0,77	—8,63

Translated from Atomnaya Énergiya, Vol. 35, No. 5, pp. 327-331, November, 1973. Original article submitted February 7, 1973.

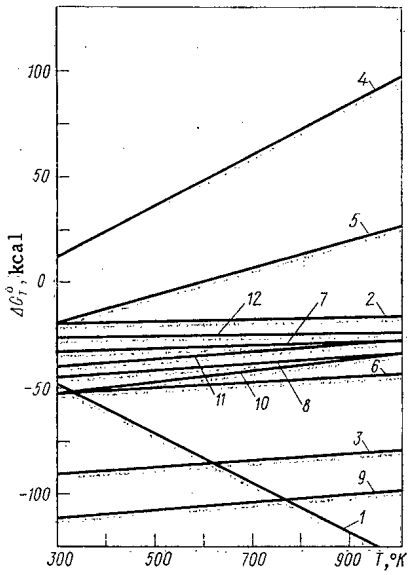

Fig. 1

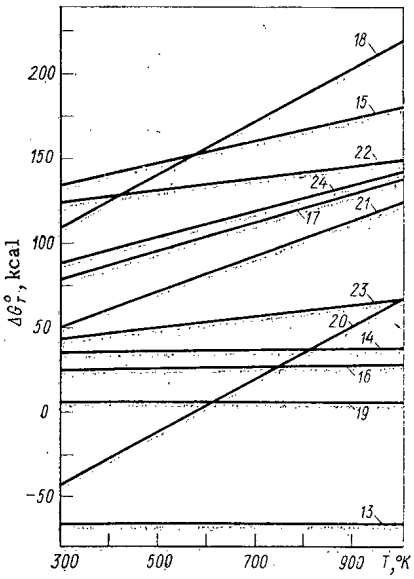

Fig. 2

Fig. 1. Change in the standard Gibbs energy ΔG_T^0 for the interaction of UF_6 with organic reagents.

Fig. 2. Change in the standard Gibbs energy ΔG_T^0 for the interaction of UF_6 with H_2, O_2, Cl_2, Br_2, I_2, and Xe.

The aim of the present investigation was to make a thermodynamical estimation of the chemical means of separating uranium and plutonium hexafluorides with various reagents. In order to achieve a more complete picture of the processes involved, the earlier-proposed substances were supplemented with freon-113 ($C_2Cl_3F_3$), freon-115 (C_2ClF_5), CO, and I_2.

It was assumed that the following reactions might take place during the process:

Freons of the ethane series

1 — $2C_2Cl_3F_3 + EF_6 = 2C_2Cl_2F_4 + EF_4 + Cl_2$;

2 — $C_2Cl_3F_3 + EF_6 = C_2ClF_5 + EF_4 + Cl_2$;

3 — $2C_2Cl_3F_3 + 3EF_6 = 2C_2F_6 + 3EF_4 + 3Cl_2$;

4 — $2C_2Cl_2F_4 + EF_6 = 2C_2ClF_5 + EF_4 + Cl_2$;

5 — $C_2Cl_2F_4 + EF_6 = C_2F_6 + EF_4 + Cl_2$;

6 — $2C_2ClF_5 + EF_6 = 2C_2F_6 + EF_4 + Cl_2$.

Freons of the methane series

7 — $2CCl_3F + EF_6 = 2CCl_2F_2 + EF_4 + Cl_2$;

8 — $CCl_3F + EF_6 = CClF_5 + EF_4 + Cl_2$;

9 — $2CCl_3F + 3EF_6 = 2CF_4 + 3EF_4 + 3Cl_2$;

10 — $2CCl_2F_2 \quad EF_6 = 2CClF_3 + EF_4 + Cl_2$;

11 — $CCl_2F_2 + EF_6 = CF_4 + EF_4 + Cl_2$;

12 — $2CF_3Cl + EF_6 = 2CF_4 + EF_4 + Cl_2$.

Inorganic reagents

13 — $H_2 + EF_6 = 2HF + EF_4$;

14 — $Cl_2 + EF_6 = 2ClF + EF_4$;

15 — $Cl_2 + 3EF_6 = 2ClF_3 + 3EF_4$;

16 — $Br_2 + EF_6 = 2BrF + EF_4$;

17 — $Br_2 + 3EF_6 = 2BrF_3 + 3EF_4$;

18 — $Br_2 + 5EF_6 = 2BrF_5 + 5EF_4$;

19 — $I_2 + EF_6 = 2IF + EF_4$;

20 — $I_2 + 5EF_6 = 2IF_5 + 5EF_4$;

21 — $I_2 + 7EF_6 = 2IF_7 + 7EF_4$;

22 — $O_2 + 2EF_6 = 2OF_2 + 2EF_4$;

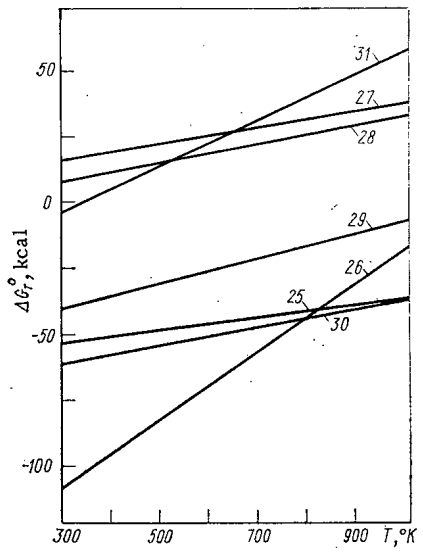

Fig. 3

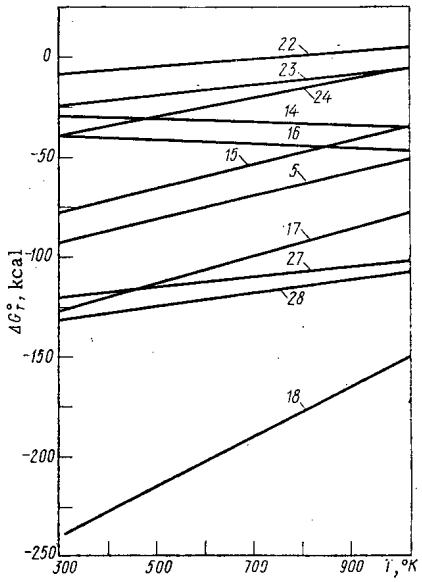

Fig. 4

Fig. 3. Change in the standard Gibbs energy ΔG_T^0 for the interaction of UF_6 with CO, CO_2, SF_4, and SO_2.

Fig. 4. Change in the standard Gibbs energy ΔG_T^0 for the interaction of PuF_6 with O_2, Cl_2, Br_2, Xe, CO_2, and $C_2Cl_2F_4$.

TABLE 2. Logarithms of K_e for Certain Reactions Leading to the Reduction of PuF_6

No. of reaction	T°, K							
	298	400	500	600	700	800	900	1000
5	67,87	46,79	34,58	26,49	20,76	16,49	13,21	10,60
14	25,09	18,81	15,17	12,78	11,09	9,83	8,87	8,12
15	47,45	39,18	28,65	21,73	16,87	13,27	10,54	8,37
16	32,26	24,18	19,47	16,35	14,16	12,54	11,26	10,26
17	95,40	60,11	45,71	36,25	29,63	24,62	20,84	17,83
18	178,70	124,85	93,66	73,14	57,96	47,73	39,53	33,00
23	17,98	11,89	8,38	6,17	4,44	3,23	2,30	1,58
24	33,98	22,48	15,35	10,68	7,39	4,95	3,09	1,61
27	90,44	65,58	51,55	42,05	35,32	30,28	26,40	23,24
28	96,33	69,70	54,20	43,99	36,62	31,18	26,98	23,65

23 — $Xe + EF_6 = XeF_2 + EF_4$;
24 — $Xe + 2EF_6 = XeF_4 + 2EF_4$;
25 — $CO + EF_6 = COF_2 + EF_4$;
26 — $2CO + 4EF_6 = 2CF_4 + 4EF_4 + O_2$;
27 — $2CO_2 + 2EF_6 = 2COF_2 + 2EF_4 + O_2$;
28 — $CO_2 + 2EF_6 = CF_4 + 2EF_4 + O_2$;
29 — $SF_4 + EF_6 = SF_6 + EF_4$;
30 — $SO_2 + EF_6 = SO_2F_2 + EF_4$;
31 — $SO_2 + 3EF_6 = SF_6 + 3EF_4 + O_2$.

As a criterion for estimating the possible occurrence and direction of any particular reaction we used the change in the standard Gibbs energy ΔG_T^0 and the equilibrium constant K_e, expressed in units of pressure for the state of an ideal gas at 1 atm. We used the following thermodynamic relations [4, 5] for the chemical reaction with stoichiometric coefficients expressed as smallest whole numbers:

$$aA + bB \rightleftarrows rR + qQ;$$
$$\Delta G_T^0 = r\Delta G_{fT}^0[R] + q\Delta G_{fT}^0[Q] - a\Delta G_{fT}^0[A] - b\Delta G_{fT}^0[B],$$

where ΔG_T^0 is the change in the standard Gibbs energy of the reaction under consideration; $\Delta G_{fT}^0[R]$ is the change in the standard Gibbs energy of formation of one mole of substance R from the elements in standard states at a temperature T and a pressure of 1 atm.

The change in the standard Gibbs energy of formation of the compounds at various temperatures was calculated from the equations [4]

$$\Delta G_{fT}^0 = \Delta H_{fT}^0 - T\Delta S_{fT}^0,$$

where

$$\Delta H_{fT}^0 = \Delta H_{f298}^0 + [H_T^0 - H_{298}^0] - \Sigma [H_T^0 - H_{298}^0]_{elem};$$
$$\Delta S_{ft}^0 = S_T^0 - \Sigma S_{Telem}^0.$$

ΔH_{f298}^0 and ΔH_{fT}^0 are the enthalpies of formation of the compounds in the standard state at 298.15°K and temperature T, respectively; $[H_T^0 - H_{298}^0]$ is the difference between the enthalpies in the standard state at temperature T and 298.15°K; ΔS_{fT}^0 is the change in the entropy of the substance with temperature.

TABLE 3. Melting and Boiling Points of the Original Substances and Reaction Products [9, 16-18].

Substance	t_m, °C	t_b, °C
Cl_2	−101,3	−34,7
ClF	−155,6	−100,1
ClF_3	−83	11,75
BrF	−33	20,0
BrF_3	8,8	127,6
BrF_5	−61,3	40,5
Br_2	−7,3	58,8
Xe	−111,8	−108,1
XeF_2	−140	—
XeF_4	114	—
CO_2	—	−78,5
COF_2	−114	−86,1
CF_4	−184	−128
$C_2Cl_2F_4$	−94	+3,7
C_2F_6	−100,6	−78,2
UF_6	64,5	56,6
PuF_6	50,8	62,3

After determining ΔG_T^0 we calculated K_e from the equation

$$\Delta G_T^0 = -RT \ln K$$

The values of the standard Gibbs energies of formation of the original reagents and the reaction products ΔG_{fT}^0 were taken from the following sources: UF_6, UF_4 [6]; PuF_6, PuF_4 [7]; CF_4, C_2F_6, HF, CO, CO_2, COF_2, SOF_2, SO_2, SF_4 [4]; ClF, ClF_3, BrF, BrF_5, IF, IF_5, IF_7 [8]. The values of $\Delta H_{f\,298}^0$ and ΔG_{fT}^0 for certain compounds not mentioned in the literature were calculated and are presented in Table 1.

First we calculated the standard Gibbs energies for the interactions between the substances and elements just mentioned and uranium hexafluoride. From the value of ΔG_T^0 for the reaction we selected substances, the interaction of which, with UF_6, was thermodynamically impossible; for such reactions the condition $\Delta G_T^0 > 10$-15 kcal had to be satisfied. Then we studied the interaction with these reducing agents. The results of the calculations are presented in Figs. 1-3. Among the organic compounds, one substance thermodynamically inert with respect to UF_6 may be freon-114 or $C_2Cl_2F_4$ (reactions 4 and 5). Since reaction 4 has a value of ΔG_T^0 = 10-100 kcal in the temperature range studied, it is clear that any estimation of the interaction should be based on reaction 5, according to which freon-114 is directly converted into C_2F_6, missing the stage of C_2ClF_5 formation.

In the reactions of all the remaining organic compounds of the ethane and methane series with UF_6 we have $\Delta G_T^0 = -120$ to -20 kcal, and the reduction of uranium by these reagents is thermodynamically quite possible. For this reason these cannot be recommended as selective reagents for the separation of UF_6 and PuF_6, and we shall pay no further attention to them. Of all the elemental substances those thermodynamically stable with respect to UF_6 are Cl_2, Br_2, O_2, and Xe. In the interaction between UF_6 and iodine with the formation of iodine monofluoride ΔG_T^0 = 2-3 kcal over the whole temperature range, which does not exclude the possibility of reducing UF_6. Hydrogen, of course, is a strong reducing agent for UF_6.

Of the inorganic compounds, only CO_2 may be recommended for separating UF_6–PuF_6 mixtures. The remaining substances (SO_2, SF_4, CO) are thermodynamically capable of reducing UF_6 at 298-1000°K. Judging by the thermodynamic data, $C_2Cl_2F_2$, SO_2, and SF_4 should reduce both hexafluorides. Certain reported results [1, 3], according to which these substances do not reduce UF_6, may be attributed to kinetic hindrances. In processing actual nuclear fuel, Ru, Rh, Mo, etc. may constitute appropriate catalysts for the interaction with UF_6.

Thus, according to the results obtained, it is reasonable to consider the interaction of PuF_6 with the following substances only: $C_2F_4Cl_2$, O_2, Cl_2, Br_2, Xe, and CO_2 (reactions 5, 14-18, 22-24, 27, 28). Figure 4 shows the temperature dependence of the standard Gibbs energy for these compounds.

All these substances except O_2 are thermodynamically suitable for separating UF_6–PuF_6 mixtures. The standard Gibbs energies of the reaction between oxygen and PuF_6 vary from −12 to +2 kcal, so that O_2 is a less energetic reducing agent for PuF_6 than all the other substances. In this case the separation conditions may be complicated by the fact that the reduction of PuF_6 will be incomplete or entirely absent.

Thermodynamic analysis gives the following substances as the best selective reducing agents for PuF_6: Cl_2, Br_2, CO_2, Xe, and $C_2Cl_4F_2$. As regards the last of these, experimental verification is still needed, since the absence of interaction with UF_6 has only been verified for temperatures above 600°K.

Table 2 shows the temperature dependence of the equilibrium constants K_e for the interactions of PuF_6 with a number of substances. Reaction 18 has a molecularity of six, and will thus probably be limited by the kinetic parameters. Hence any estimation of the interaction of the halogens Cl_2 and Br_2 with PuF_6 should be based on the formation of the mono- and trifluorides only (reactions 14-17). All the reactions except 5, 14, and 16 involve a reduction in volume; in view of this, an increase in the pressure of the system favors a shift to the right in the equilibrium. Judging by the equilibrium constants K_e, the most energetic reducing agent is CO_2 and the weakest is xenon.

Table 3 gives the physical properties of the selective reducing agents for PuF_6 and certain reaction products. It is well known that, after separation, the uranium hexafluoride and plutonium tetrafluoride have to be freed from an excess of reducing agent and the corresponding reaction products. Hence the difference in the physical properties of the compounds is of extremely important significance.

The decisive part in choosing any particular selective reducing agent for PuF_6 is played by the choice of the fluorinating agent used in the reprocessing of irradiated UO_2–PuO_2-base fuel by the fluoride-volatility method.

When using halogen fluorides under conditions preventing their thermal decomposition (in accordance with published data and the reactions studied in the present investigation) selective fluorination of the uranium takes place, while the plutonium remains in the condensed phase. When the uranium hexafluoride is contaminated with plutonium it is appropriate to use the corresponding halogen, chlorine, bromine or freon-114, as reducing agent.

On treating fuel with elemental fluorine, the hexafluorides may best be separated by means of carbon dioxide, since this and the reaction products so formed have physical properties which differ to the greatest extent from those of the actinide fluorides. In addition to this, CO_2 is used in the fluorination of fuel by halogen fluorides. The use of xenon for these purposes is undesirable, since the volatile and condensed actinide fluorides are contaminated owing to the unsatisfactory properties of the xenon fluorides so formed. Furthermore the xenon fluorides may explode spontaneously [18].

Thus the most readily accessible and universal reagent for separating a mixture of UF_6 and PuF_6 must at the present time be regarded as carbon dioxide.

LITERATURE CITED

1. P. Regnout and M. Bourgeois, Kerntechnik, No. 8/9, 388 (1965).
2. Trans. Am. Nucl. Soc., 9, No. 1, 22 (1966).
3. M. Bourgeois, Bull. Inform. Scient. et Techn. Comissar. Energie Atom., No. 128, 3-11 (1968).
4. D. Stull, E. Westram, and H. Sinke, Chemical Thermodynamics of Organic Compounds [Russian translation], Mir, Moscow (1971).
5. S. Benson, Thermochemical Kinetics [Russian translation], Mir, Moscow (1971).
6. M. Rand and O. Kubaschewski, The Thermochemical Properties of Uranium Compounds, Interscience, London (1963).
7. F. Oetting, Chem. Revs., 67, No. 3, 261 (1967).
8. Ya. A. Fialkov, Interhalide Compounds [in Russian], Izd. AN UkrSSR (1958).
9. L. V. Gurvich and G. A. Khachkaruzov, Thermodynamical Properties of Individual Substances [in Russian], Izd. AN SSSR, Moscow (1962).
10. N. P. Galkin, V. T. Orekhov, and A. G. Rybakov, Zh. Fiz. Khim., 46, No. 10, 2681 (1972); 47, No. 2, 482 (1973).
11. A. Kudchadker et al.. Ind. J. Chem., 9, No. 7, 722 (1971).
12. K. Christe et al., Spectrochim. Acta, 27a, No. 6, 931 (1971).
13. B. Weinstock et al., Inorg. Chem., 5, No. 12, 2189 (1966).
14. V. F. Tomanovskaya and B. E. Kolotova, Freons [in Russian], Khimiya, Leningrad (1970).
15. M. Kh. Karapet'yants and M. L. Karapet'yants, Fundamental Thermodynamic Constants of Inorganic and Organic Substances [in Russian], Khimiya, Moscow (1968).
16. B. P. Nikol'skii (editor), Handbook of Chemistry [in Russian], Vol. II, Goskhimizdat, Leningrad –Moscow (1963).
17. I. G. Ryss, Chemistry of Fluorine and Its Inorganic Compounds [in Russian], Goskhimizdat, Moscow (1956).
18. N. I. Gubkina, Usp. Khim., 35, No. 12, 2219 (1966).

OPTIMAL CONSTRUCTION OF INFORMATION CHANNELS IN RADIATION MONITORING SYSTEMS

A. N. Klimov, V. V. Matveev,
I. V. Makhnovskii, and B. V. Nemirovskii

UDC 539.107

The introduction of extensive systems for monitoring, for prediction, and, in a number of cases, for issuance of advisory statements naturally leads to the complication of systems and to a need for carrying out various operations for the analysis and output of information which makes centralized multichannel systems resemble specialized computers in structure and complexity [1-5]. Under these conditions, universalization of multichannel systems and optimization of their construction techniques take on particularly great importance. A single all-purpose centralized device for handling information is developed and specific monitoring of objects is provided by completion of the system with the appropriate detection units. For the realization of this situation, it is desirable to equalize all system channels through appropriate unification of output signal parameters from detection units.

As a rule, on output devices of centralized systems, digital information is displayed, indexed, and recorded, and the output of the great majority of detection units is also discrete, i.e., is determined by the number of pulses per unit time. Such an approach to system construction permits simplification of the algorithms for handling information flow and optimization of the information and measurement channels of a radiation monitoring system.

In this paper the output information flow is discussed first and then the input information flow. This order is determined by the fact that the form of information presentation to the operator decides the primary treatment of the input information flow.

Representation of Output Information Flow

In most general form, information F about the results of measurements in any channel must contain information about the channel number N, the quantitative (numerical) value of the measured parameter Π and its dimensionality R:

$$F = f(N, \Pi, R). \tag{1}$$

The value of the measured parameter is usually represented in decimal notation on the output devices of digital registers and can be given in most general form by the polynomial Π(10).

$$\Pi(10) = P_n 10^n + P_{n+1} 10^{n+1} + \ldots P_i 10^i + \ldots + P_m 10^m;$$

$$\Pi(10) = \sum_{i=n}^{i=m} P_i 10^i, \tag{2}$$

where P_i is the value of the digit in the i-th column, varying from 0 to 9; m is the highest power of ten; and n is the lowest power of ten. The quantities m and n may be negative or positive.

Multichannel systems for radiation monitoring measure various physical quantities such as γ-ray exposure dose rate, gas concentration, aerosol concentration, etc. The range of variation of absolute numerical values is considerable for all measured quantities. To a certain extent, it can be reduced by the choice of appropriate dimensionality. The first readout point of a measured parameter is always characterized by some coefficient 10^l, where l is the power of ten corresponding to the first readout point

Translated from Atomnaya Énergiya, Vol. 35, No. 5, pp. 333-337, November, 1973. Original article submitted April 4, 1973.

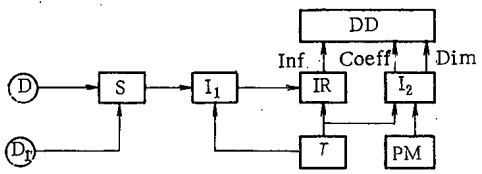

Fig. 1. Block diagram of single channel with timing: D, D_1) detection units; S) subtracter; I_1, I_2) coincidence circuits; T) timer; IR) information register; DD) digital display; PM) permanent memory.

of the measured range. For example, in measurements of the γ-ray exposure dose rate in the ranges 10^{-4}-10^{-1} or 10^{0}-10^{+3} R/h, the coefficient l is respectively -4 and 0. In this case, Eq. (2) takes the form

$$\Pi(10) = 10^{l} \sum_{i=n}^{i=m} P_i 10^{i-l}. \quad (3)$$

From Eqs. (1) and (3), information in the output of the system characterizing a measured quantity can be represented in the following manner:

$$F = f\left(N,\ 10^{l} \sum_{i=n}^{i=m} P_i 10^{i-l},\ R\right). \quad (4)$$

Consequently, information in the output of any system for radiation monitoring can be presented in the form of a channel number, a numerical value of the measured parameter, a coefficient 10^{l} characterizing the beginning of the measured range, and the dimensionality.

Representation of Input Information Flow

The detectors used in nuclear instrument manufacture convert information about ionizing radiation into an average current or into a sequence of electrical current or voltage pulses which is characterized by a repetition rate, by the number of pulses in a given period of time, by an average current, or by a total charge. Each pulse is characterized by time of appearance, by current pulse height, by a charge, or by the shape of the time distribution of the elementary charges. Any of these signal parameters can carry definite information about measured characteristics of the radiation field and accordingly varies within definite limits [6].

In radiometric equipment one ordinarily measures the flux density of particles with energies ranging from E_1 to E_2. The quantity which relates flux density of particles or quanta to pulse repetition frequency is the sensitivity. Usually the value of particle flux density is proportional to the pulse repetition rate and is measured by it. At the same time, the pulse height at the output of various types of detectors (pulse ionization chambers, proportional counters, Geiger–Muller counters, scintillation and semiconductor counters) varies over the range $(0.25 \cdot 10^{-3}$-$80)E$ volts [7]. The energy E mainly varies from 10^{-1} to 10^{+1} MeV, and the pulse height of the signals over five to six decades. With radiometric equipment one mainly measures particle flux densities for particles in an energy range (E_2-E_1) and therefore the introduction of appropriate amplifiers and pulse shapers for pulses from all types of detectors can lead to a single normalized value.

One can therefore assume there arrives at the outputs of multichannel systems sequences of pulses characterized by a counting rate n_i in some i-th channel of the system. In this case, the total load on the system is $\sum_{i=1}^{i=k} n_i$, where k is the number of channels in the system.

The timing method is the simplest and most widely used technique for recording such flows of pulses [3]. In this case, the number of pulses accumulated in a time T is $n_i T$ for ordinary channels and $(n_i - n_i')T$ for a differential channel where n_i is the count rate in the "signal + background" channel and n_i' is the count rate in the background channel.

Figure 1 shows a block diagram characterizing the timing method for a single differential channel. Here the count rates n_i and n_i' from the detection units D and D_1 are sent to the statistical subtracter S [8] and then pass through the coincidence circuit I_1 controlled by the timer T to the information register IR. Identification of the number of pulses collected and the corresponding measured quantity is accomplished by means of the timer. Representation of the information occurs on the digital display DD in the form of three quantities: the information I, the coefficient 10^{l} (K), and the dimensionality R.

At the beginning of display, a signal is sent from the timer to the coincidence circuit I_2 which also sends information about the value of the coefficient and dimensionality from some permanent memory device PM to the digital display. Values for the coefficient and dimensionality are most often entered on the front panel of the instrument.

When considering several channels, the quantities n_i and n_i' for each type of detection unity at the beginning and end of the range are different as a rule. In this case, the resultant value of the count $(n_i - n_i')T$ is also a variable quantity at the beginning of the range, for example. At the same time, it is desirable to have the quantity T the same in multichannel systems.

To have identical measurements, it is reasonable to introduce the normalizing factors β and α which respectively take into account the spread in efficiencies of detectors of different types and of detectors of the same type. Then the expression for the accumulated number of pulses N_i in a time interval T takes the form

$$N_i = (\alpha_i \beta_i n_i - \alpha_i' \beta_i' n_i')\, T. \tag{5}$$

When there is no background channel, we have

$$N_i = \alpha_i \beta_i n_i T. \tag{6}$$

Information in systems with many detection units is recorded serially [9], in parallel [3, 9], or in series-parallel [10]. The most widely used is parallel recording in which numbering and coding of detection units is carried out on a matrix basis [3, 9].

In this case, Eq. (5) is written conventionally in the form

$$N_i = \begin{vmatrix} \alpha_1\beta_1, \ldots, \alpha_{\sqrt{k}}\beta_{\sqrt{k}} \\ \alpha_{1+\sqrt{k}}\beta_{1+\sqrt{k}}, \ldots, \alpha_{2\sqrt{k}}\beta_{2\sqrt{k}} \\ \cdots\cdots\cdots\cdots \\ \alpha_{k-\sqrt{k}+1}\beta_{k-\sqrt{k}+1}, \ldots, \alpha_k\beta_k \end{vmatrix} n_i T - \begin{vmatrix} \alpha_1'\beta_1', \ldots, \alpha_{\sqrt{k}}'\beta_{\sqrt{k}}' \\ \alpha_{1+\sqrt{k}}'\beta_{1+\sqrt{k}}', \ldots, \alpha_{2\sqrt{k}}'\beta_{2\sqrt{k}}' \\ \cdots\cdots\cdots\cdots \\ \alpha_{k-\sqrt{k}+1}'\beta_{k-\sqrt{k}+1}', \ldots, \alpha_k'\beta_k' \end{vmatrix} n_i' T. \tag{7}$$

Introduction into the system of devices which realize the factors α_i and β_i makes it possible to unify the counting rates from all detection units. Then

$$\alpha_i \beta_i n_{\min_i} = \text{const};\ \alpha_i \beta_i n_{\max_i} = 10^D n_{\min_i} = \text{const},$$

where D is the number of orders of magnitude covered by a single detection unit. To have the channels identical, it is advisable to have the quantity D the same for all channels.

Consequently,

$$N_{\min_i} = \text{const};\ N_{\max_i} = 10^D N_{\min_i} = \text{const}.$$

If the quantities $\alpha_i \beta_i n_i$ and $\alpha_i' \beta_i' n_i'$ are denoted by n_{u_i} and n_{u_i}' (unified count rate), Eq. (5) takes the form

$$N_i = (n_{u_i} - n_{u_i}')\, T. \tag{8}$$

Thus the input information flow in a multichannel dosimetric system can be presented to the channels at a unified count rate by the introduction of devices which eliminate the effects of the spread in efficiency for detectors of a given type. With such an information flow, the measurement operation for any parameter is identical in all channels.

Comparison of Input and Output Information Flows

The analysis of input information flow makes it possible to simplify the measurement of the physical quantities themselves to a considerable extent. For example, the expression for the concentration of radioactive gases has the form

$$K_i = (\alpha_i \beta_i n_i - \alpha_i' \beta_i' n_i')\, T \eta_i R_i, \tag{9}$$

where η_i is a factor which takes into account the conversion from the number of accumulated pulses to the actual physical quantity; R_i is the dimensionality of the measured quantity.

Analysis of Eqs. (4) and (9) shows that these expressions are different descriptions of the measured parameter employing input and output quantities.

Comparing these equations, we write the following system of equations:

$$\left.\begin{aligned} &\sum_{i=n}^{i=m} P_i 10^{i-l} = (\alpha_i \beta_i n_i - \alpha_i' \beta_i' n_i')\, T; \\ &10^l = \eta_i; \\ &R = R_i. \end{aligned}\right\} \tag{10}$$

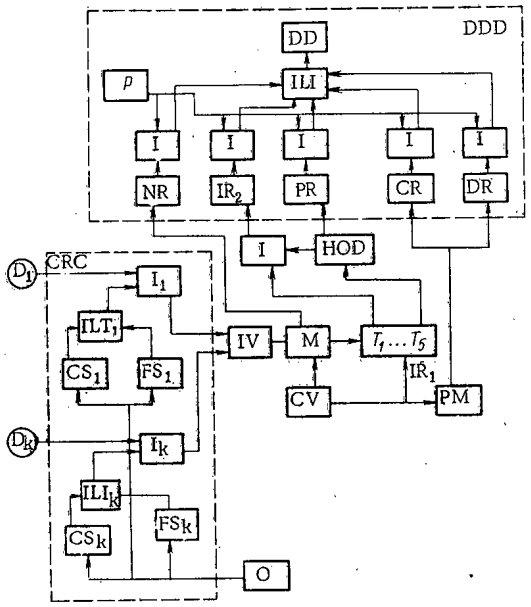

Fig. 2. Block diagram of multichannel dosimetric system with unified input and output: D_1, D_k) detection units; CRC) count rate converter; CS) coarse shaper; FS) fine shaper; ILI) collection circuit; I) coincidence circuit; IU) input unit; O) oscillator; M) memory; CU) control unit; IR) information register; T_1–T_5) tetrads; PM) permanent memory; HOD) high-order digit unit; NR, IR_2, PR, CR, DR) registers for channel number, information, decimal point, coefficient, and dimensionality, respectively; DDD) decimal digital display.

Allowing for unified input, the first equation of this system can be brought into the form

$$\sum_{i=n}^{i=m} P_i 10^{i-l} = (n_u - n'_u)\, T. \qquad (11)$$

Thus the measured quantity is made up of a variable numerical value and two constants – the dimensionality and the factor 10^l; the variable numerical value of the measured quantity is completely determined by the unified counting rate; the normalization coefficient in the absence of a background channel and with $\alpha = 1$ is found from the expression $P_i = n_{min_u}/n_{min_i}$.

Block Diagram of a Possible System

A possible version for the construction of a multichannel dosimetric system with unified input and output is shown in Fig. 2. Here the unified flow from the detection units D_1 and D_k is sent to the count rate converter CRC which is controlled by the oscillator O [11]. Each channel of the CRC includes a coarse (CS) and fine (FS) shaper producing pulses of appropriate length which are sent through the ILI circuit into the coincidence circuit I and which prevent the transmission of pulses from the detectors to the input unit IU and to the memory M. Thus a unified information flow is created at the output of the CRC.

On signal from the control unit CU, information from M is sent to the appropriate tetrads T_1–T_5 of the information register IR_1. This information is then converted in a device for determining the high-order digit and is sent through the appropriate coincidence circuit to the information register IR_2 and the decimal point register PR. At the same time, the appropriate quantities are sent from the permanent memory PM into the coefficient register CR and the dimensionality register DR. The number of the channel from which the information is being taken at this time is in the channel number register NR.

All the information stored in the static output registers NR, IR_2, PR, CR, and DR is digitized by means of the dynamic digital display DDD. As a result, the information is presented on the digital display, for example, in the form

$$151.\ 32.7 \times 10^{-4},\ \text{R/h}.$$

Conclusions

Thus the input information flow in a multichannel system for radiation monitoring can be unified. In that case, the range covered by a detection unit can be reduced to an identical value D (for example, D = 3) and, correspondingly, the counting rate in any channel at the beginning and end of the range should be identical and vary from 1 to 1000 counts/sec. Such a realization can be achieved either by means of multichannel count rate converters which eliminate the efficiency spread in different kinds of detectors (the factor β) and the efficiency spread in detectors of the same kind (factor α) or by means of devices located within the detection units themselves.

With such a solution, the output information flow can be represented by a channel number, a numerical value of the measured parameter in the form of a three-digit number with floating decimal point, a coefficient 10^l characterizing the beginning of the measurement range, and the dimensionality. The three-digit number is completely determined by the unified counting rate during a timing period that is a multiple of 10. The subrange in which the measurement is made determines the position of the decimal point in this number.

The coefficient 10^l and the dimensionality can be formed and stored in the permanent memory. It is sufficient to store only the value of l in the permanent memory to represent the factor 10^l. It is then sufficient to have a total PM capacity of 7 bits for storage in any channel of the system of quantities varying from 10^{-7} to 10^{+7} and having eight dimensionalities.

The algorithm for the measurement of any parameter is then very simple and for a time T = 100 sec reduces to the simple accumulation of pulses and their subsequent display accompanied by a numerical value for the dimensionality and the coefficient 10^l.

LITERATURE CITED

1. V. V. Matveev, Nuclear Instrument Manufacture, SNIIP Proceedings, No. 6, Atomizdat, Moscow (1967), p. 5.
2. I. S. Krasheninnikov et al., in: Standardization and Technical Progress in Nuclear Instrument Manufacture, No. 1, SNIIP, Moscow (1972), p. 16.
3. L. G. Kiselev et al., Nuclear Instrument Manufacture, SNIIP Proceedings, No. 11, Atomizdat, Moscow (1969), p. 112.
4. O. Billaniuk et al., Nucl. Instrum. and Methods, 14, 63 (1961).
5. B. Spiller, Instrum. Practice, 25, No. 9, 527 (1971).
6. V. V. Matveev, see [3], p. 27.
7. V. V. Matveev and B. I. Khazanov, Instruments for Measurement of Ionizing Radiation [in Russian], Atomizdat, Moscow (1972), p. 325.
8. V. M. Malykhin, Prib. i Tekh. Éksperim., No. 2, 167 (1964).
9. S. S. Kurochkin et al., Proceedings of the 5th Scientific and Technical Conference on Nuclear Electronics, Vol. II, Part 2, Gosatomizdat, Moscow (1963), p. 31.
10. A. F. Gertsovskii et al., Byul. Izobret., No. 5, 172 (1972).
11. A. N. Klimov et al., ibid., No. 34, 145 (1971).

GAMMA-ACTIVATION ANALYSIS METHOD FOR OXYGEN AND FLUORINE WITH DELAYED-NEUTRON RECORDING

M. M. Dorosh, N. P. Mazyukevich, A. M. Parlag, and V. A. Shkoda-Ul'yanov

UDC 543.53

The use of delayed neutrons in activation analysis allows one to significantly increase selectivity with respect to oxygen; the method successfully supplements γ- and neutron-activation methods of determining it, since one excludes here the effect of boron, fluorine, and other elemental impurities which after activation produce emissions which compete with emissions of nuclear products from the $^{16}O(\gamma, n)^{15}O$ and $^{16}O(n, p)^{16}N$ reactions. The given method is convenient to use for rapid analysis for oxygen and fluorine in large samples of metals and other substances without destroying the samples.

In order to study the physical bases of the method, we measured the output and determined the creation cross section of delayed neutrons in the reaction $^{18}O(\gamma, p)^{17}N$ in the region from threshold to 25 MeV using a betatron having intensity 30 R/min at 1 meter from the target [1], and we also measured the delayed-neutron output from heavy-oxygen water $H_2{}^{18}O$ and Teflon-4 $[CF_2]_n$ in the range 25-70 MeV on a linear electron accelerator having current of 0.01 μA [2, 3].

Recording began after saturation was achieved and was conducted for 30 sec with delay of 0.1 sec after beam turn-off. The principal detector in the counters with BF_3 had efficiency $\varepsilon = 0.33\%$; the apparatus background in the absence of the beam was $n_b = 4$ pulses/min. The heavy-oxygen water in the amount 0.98 g·mole (50% ^{18}O) was placed in an oxygenless (Plexiglas) container having internal diameter 40 mm, height 34 mm, and wall thickness 4 mm. To take account of the background and γ-absorption and

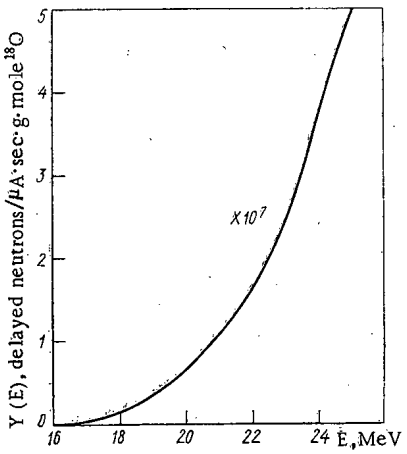

Fig. 1

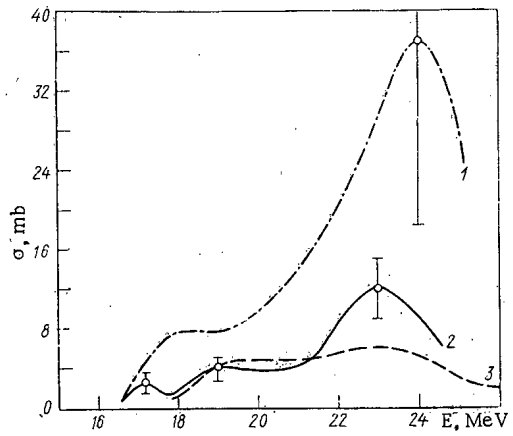

Fig. 2

Fig. 1. Output of delayed neutrons from thin ^{18}O sample reduced to absolute-ionization-chamber current.

Fig. 2. Transverse $^{18}O(\gamma, p)^{17}N$ reaction cross section: 1) data from [5]; 2) the present work; 3) data from [6]

Translated from Atomnaya Énergiya, Vol. 35, No. 5, pp. 339-342, November, 1973. Original article submitted November 29, 1972; revision submitted April 3, 1973.

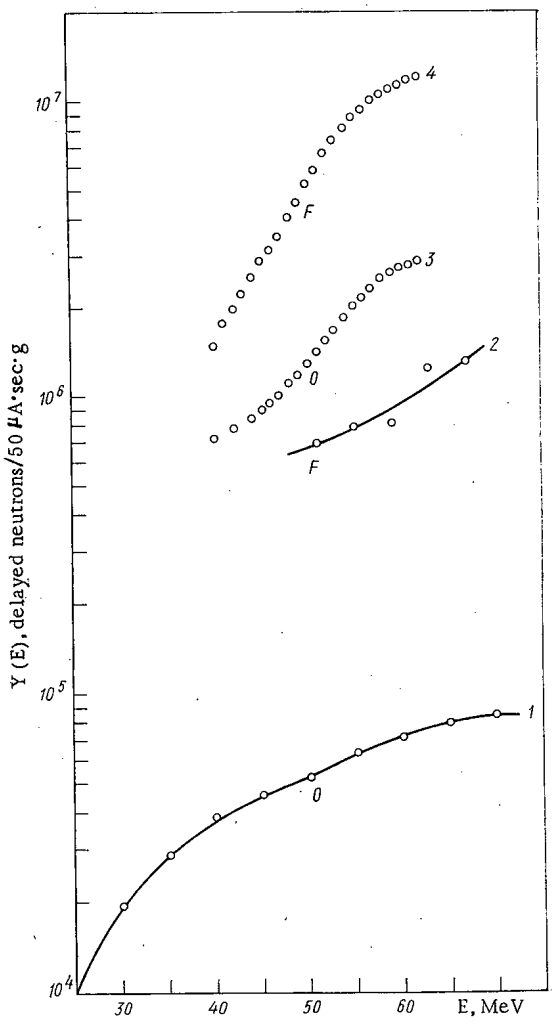

Fig. 3. Output of delayed neutrons from oxygen and fluorine: 1, 2) data from present work; 3, 4) date from [8].

TABLE 1. Sensitivity in Determining Oxygen and Fluorine

Energy, MeV	Oxygen, g		Fluorine, g	
	present work	[8]	present work	[8]
40	$2{,}70\cdot10^{-3}$	$1{,}40\cdot10^{-4}$	—	$7{,}90\cdot10^{-5}$
50	$1{,}90\cdot10^{-3}$	$0{,}80\cdot10^{-4}$	$1{,}52\cdot10^{-4}$	$3{,}64\cdot10^{-5}$
60	$1{,}60\cdot10^{-3}$	$0{,}52\cdot10^{-4}$	$1{,}30\cdot10^{-4}$	$1{,}20\cdot10^{-5}$
70	$1{,}42\cdot10^{-3}$	$0{,}28\cdot10^{-4}$	$1{,}10\cdot10^{-4}$	$0{,}92\cdot10^{-5}$

TABLE 2. Possible Accompanying Reactions

No.	Element	Reaction	Isotope content, %	Threshold, MeV	$T_{1/2}$, sec
1	B	$^{11}B(\gamma, 2p)^{9}Li$	81	31,3	0,17
2	C	$^{12}C(\gamma, 3p)^{9}Li$	100	47,3	0,17
3	Ne	$^{20}Ne(\gamma, 3p)^{17}N$	30,5	36,8	4,15
4	Na	$^{23}Na(\gamma, \alpha 2p)^{17}N$	100	34,4	4,15
5	Mg	$^{24}Mg(\gamma, \alpha 3p)^{17}N$	77	46,1	4,15
6	Al	$^{27}Al(\gamma, 2\alpha 2p)^{17}N$	100	44,5	4,15
7	U, Th	Neutron photofission	100	$n-1\div3$; $\gamma-5,1$ 5,5	0,2—60

scattering effects we used a sample identical in form, but made from ordinary water. The sample containing fluorine weighed 31 g; it was 35 mm in diameter and 20 mm in height.

Figure 1 shows the delayed-neutron output from a thin $H_2{}^{18}O$ target in the interval 16.5-24.5 MeV relative to 1 μA current in a Flowers ionization chamber and 1 mole ^{18}O. The $^{18}O(\gamma, p)^{17}N$ reaction cross section found in our work is shown in Fig. 2. The maximal value is $\sigma_{\gamma p}(E) = 12 \pm 4$ mb; the errors in determining this are determined by the statistical accuracy in measuring the output (1%), the drift of the irradiating apparatus and the measuring apparatus (4), and by the errors of the method for calculating cross section, which is about 20%. Besides this, the errors in measuring ^{18}O concentration (2%), in calibrating the neutron source (3%), and calculating the sensitivity of the absolute chamber (~5%) enter into the total errors. The position of the maximum was determined as 23.0 ± 0.5 MeV. A thorough accounting for all possible errors, and also the fact that the cross section $\sigma_{\gamma p}(E)$ which we obtained by the thick-sample method [4] agrees well with the cross section for a thin sample, allows us to conclude that the results of [5] are high and the data of [6] are somewhat low. The $^{18}O(\gamma, p)^{17}N$ reaction cross section obtained in the present work can be used in activation analysis for theoretical evaluation of the delayed-neutron output from large samples of oxygen-containing substances; this evaluation can be made using cascade theory [7].

Figure 3 shows the output of delayed neutrons from 1 g of $H_2{}^{18}O$ in the energy range 25-70 MeV and from 1 g of Teflon-4 for energies 51-67 MeV. For ease in comparing the results obtained with the delayed-neutron outputs from SiO_2 and LiF samples weighing 1 g each, measured in [8], they were reduced to a current of 50 μA, which is used in that paper and which in magnitude is typical for modern electron accelerators of various types (microtron, linear accelerator) which are capable of applied use. We should note in this energy range additional contributions to the output of delayed neutrons are made by the reactions $^{12}C(\gamma, 3p)^{9}Li$ (threshold 47.3 MeV) and $^{18}O(\gamma, 2p)^{16}C$ (threshold 29 MeV). According to our data, the delayed-neutron output from natural oxygen in the range 30-70 MeV increases from $2\cdot10^4$ to $8\cdot10^4/1/(50$ $\mu A\cdot sec)\cdot g$, i.e., by a factor of 4. This delayed-neutron output from ^{19}F in the range 51-67 MeV is 10-13 times smaller than the output from ^{18}O. But this ratio still does not determine the ratio of analysis sensitivities for oxygen and fluorine in this energy range, since for the sensitivities one must take into account the isotope content in the natural mixture.

Before moving on to evaluate the sensitivity to oxygen and fluorine, we will examine the curves for delayed-neutron output from ^{18}O and ^{19}F for the region 40-62 MeV [8], which until lately were the only ones in the literature (see Fig. 3). The nature of the curve for ^{18}O, i.e., the presence of an inflection point at E = 55 MeV, must be evidence of the fact that the cross section of the reaction $^{18}O(\gamma, p)^{17}N$ close to this point has a maximum, since despite the ever-increasing quantity (depending on $E_{\gamma_{max}}$) even of γ-quanta with energies corresponding to resonances in $\sigma_{\gamma p}(E)$, the output curve does not exhibit a steady rising, which one would expect in the absence of resonance near E = 55 MeV. On the contrary, it displays a tendency to "saturation," which for the energy range above 62 MeV may be explained by fall-off of the resonance peak. However, the literature does not indicate the existence of a resonance in this energy range for photonuclear reactions with emission of a single particle. The output curve for the $^{19}F(\gamma, 2p)$ reaction has a similar nature, while our data show an increase, which agrees with the assumption that significant variations in the $^{18}O(\gamma, p)$ and $^{19}F(\gamma, 2p)$ reaction cross sections are absent in this energy range.

There is a discrepancy (of approximately one order of magnitude) among measured values of ^{17}N activity. The discrepancy is too large to be explained by the two possible causes: discrepancy in the neutron spectra from calibrated sources and experimental geometry. Engelmann and Scherle [8] do not cite data on detector calibration, experimental geometry, and accuracy of results obtained; therefore, it appears possible to evaluate the degree to which these factors influence the results of both experiments.

We will take, following [8], as the method's sensitivity that quantity of the element which in one irradiation event gives an output equal to the magnitude of the apparatus background recorded over the measurement period. Then, we can write

$$m_{\min}(E) = \frac{n_b t_{meas}}{\varepsilon Y(E)} = \frac{606}{Y(E)},$$

where n_b = 4 pulses/min; t_{meas} = 30 sec; ε = 0.33%. The minimum determined concentration is found from the expression

$$C_{\min}(E) = \frac{m\min(E)}{m_{sam}} = \frac{606}{Y(E)\, m_{sam}}.$$

Table 1 shows the values of sensitivity calculated in this way using the experimental results of our work and of [8]. The values were obtained for electron currents of 50 μA.

The discrepancy in the data for one element is caused by the discrepancy in outputs, discussed above. With γ-quanta energies of 40-60 MeV, one can attain practically uniform irradiation of samples weighing hundreds of grams and more. Then, the minimum recorded oxygen concentration will be 10^{-3}-10^{-4}%, i.e., an amount less than the oxygen concentration in oxide film (for more common metals, 10^{-2}-10^{-3}%). Inasmuch as the removal of surface oxides when the half-life is short (4.15 sec) is a complex problem, the method is oriented to such large samples or systems, in which there is up to 10^{-3}% oxygen or from which sampling is difficult.

To eliminate the influence of an insignificant number of possible interfering reactions [3, 8] (see Table 2), one can use simple discrimination methods (according to irradiation energy and measurement duration). Several elements (Ne, U, Th) are present in pure substances in such quantities that do not influence analysis; then, reactions 4-6 (see Table 2) must have very small cross sections in comparison with those of $^{18}O(\gamma, p)$ and $^{19}F(\gamma, 2p)$. We note that the $^{18}O(\gamma, 2p)$ and $^{19}F(\gamma, 3p)$ reactions are possible with these isotopes, bringing into being the precursor of delayed neutrons ^{16}O ($T_{1/2}$ = 0.74 sec) and strengthening the necessary effect of neutron activity.

The most promising energy range for determining oxygen with delayed neutrons is 25-30 MeV, while for analyzing for fluorine it is up to 35 MeV. Existing accelerators have beam currents (50 μA and up) sufficient to reveal 10^{-4} and 10^{-5}% oxygen or fluorine, respectively (with clean surfaces), in samples weighing on the order of 1 g. By increasing the sample mass, the neutron-recording efficiency, and the analysis cyclicity, the above-mentioned theoretical value can be increased by one or two orders of magnitude.

The authors express profound gratitude to L. L. Kunin for valuable advice and to B. A. Chapyzhnikov and A. M. Vasserman for discussions of several questions concerning the present work.

LITERATURE CITED

1. M. M. Dorosh, N. P. Mazyukevich, and V. A. Shkoda-Ul'yanov, Ukr. Fiz. Zh., 17, 847 (1972).
2. M. M. Dorosh, N. P. Mazyukevich, and V. A. Shkoda-Ul'yanov, At. Énerg., 21, 163 (1966).

3. M. M. Dorosh, N. P. Mazyukevich, and V. A. Shkoda-Ul'yanov, At. Énerg., 24, 274 (1968).
4. V. A. Shkoda-Ul'yanov, in: Papers of the Conference on Nuclear Reactions at Small and Intermediate Energies (Moscow, 1957) [in Russian], Izd. AN SSSR, Moscow (1958). p. 485.
5. W. Stephens et al., Phys. Rev., 82, 511 (1951).
6. R. Kosiek et al., Z. Phys., 179, 9 (1964).
7. S. Z. Belen'kii, Cascade Processes in Cosmic Rays [in Russian], Gostekhteorizdat, Moscow–Leningrad (1948).
8. C. Engelmann and A. Scherle, J. Radioanal. Chem., 6, 235 (1970).

ABSTRACTS

RECONSTRUCTION OF THE SPECTRA OF NEUTRONS HAVING ENERGIES OF 0.4 eV-10 MeV FROM MEASUREMENTS MADE WITH A SET OF SPLITTING-ISOTOPE DETECTORS

G. G. Doroshenko, A. M. Zaitov, K. K. Koshaeva, S. N. Kraitor, E. S. Leonov, and M. Z. Tarasko

UDC 539.12.08

The article considers the possibility of reconstructing the spectra $\varphi(E)$ of neutrons in the energy range 0.4 eV-10 MeV from measurements made with a set of splitting-isotope detectors.

In the case of slow and intermediate neutrons, ^{235}U is used along with five ^{10}B filters having thicknesses of 0.1, 0.4, 1.0, 4.0, and 10 g/cm^2; in the case of fast neutrons, the ^{237}Np, ^{231}Pa, ^{236}U, and ^{238}U isotopes, as well as activated detectors with $^{32}S(n, p)$, $^{27}Al(n, p)$, and $^{27}Al(n, \alpha)$ reactions, were employed.

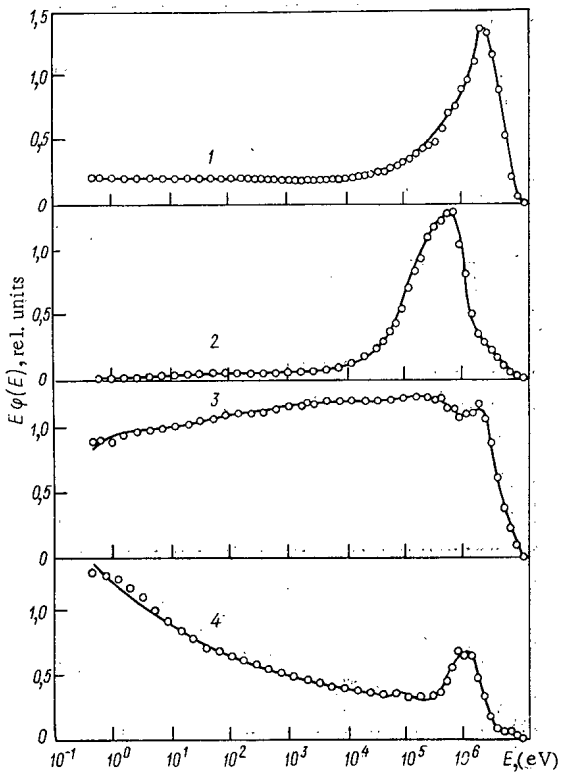

Fig. 1. Reconstruction of neutron spectra of (1) a uranium–graphite reactor, (2) a BR-5 reactor, (3) a Vinča reactor, and (4) the fission neutrons behind a carbon shield.

The mathematical formalism is based on the minimization of direction-dependent divergence. The method uses mathematical statistics and information theory. The minimum of the functional $J[N, \hat{\sigma}, \varphi] = \int N(V) \ln (N(V)dV / \int \varphi(E)\sigma(E, V)dV)$ must be determined, where N denotes the detector readings; σ denotes the efficiency of the detectors; and V denotes some parameter.

The method can be employed in the form of an iteration process which always converges to a unique, positive solution. The method makes it possible to use a rather large number of detectors and almost any number of energy intervals so that a good approximation of a spectrum is obtained. Since inversion and subtraction operations are not used in the computational algorithm, the transfer effect of the errors of the initial data is minimized.

The above set of detectors was used to study 15 spectra of several reactors and critical assemblies differing in the number of transferred slow, moderate, and fast neutrons. The most characteristic spectra are shown in Fig. 1. The error made in the reconstruction of given spectra was determined in the energy intervals 0.4 eV-10 keV, 10 keV-0.5 MeV, 0.5-1.5 MeV, and 1.5-10 MeV. The error was essentially below 10%.

The errors made in reconstructing spectra in the presence of errors in the experimental data were

Translated from Atomnaya Énergiya, Vol. 35, No. 5, pp. 343-348, November, 1973. Original article submitted December 28, 1972; abstract submitted June 20, 1973.

calculated. It was shown that when the mean-square error amounts to ±10% and has a normal distribution, the maximum differential error of the reconstruction amounts to 10-15% above 10 keV, but is less than 26-28%. The corresponding averaged errors are two times smaller.

A NEUTRON SPECTROMETER ON THE BASIS OF SPLITTING ISOTOPES

T. V. Koroleva, K. K. Koshaeva, and S. N. Kraitor

UDC 539.125.164

In experiments which relate to modeling of reactor accidents, studies of the radiation conditions in reactor sites and critical assemblies, and the calibration of individual neutron dosimeters, the effective neutron spectra must be measured and the accurate values of their dosimetric characteristics must be determined. The article describes the DISNEI neutron spectrometer based on splitting isotopes (the name DISNEI is taken from the initial letters of the key words "splitting isotopes" and "neutron spectrometry"). The detectors comprise ^{235}U, ^{235}U + Cd, ^{235}U + 1 g/cm^2 ^{10}B, ^{237}Np, ^{238}U, and ^{32}S. The article describes a method of treating track detectors of glass, the design of the spectrometer, and its calibration. In order to determine both the neutron transfer and the neutron dose, a modified effective cross section method and a threshold-energy method are used, which are more accurate than the usually employed method. The DISNEI spectrometer makes it possible to measure both the transfer and the dose of neutrons having energies ranging from thermal energies to 10 MeV (measurement error 5-15%). The results were confirmed in international comparisons of dosimetric systems for accidents in Oak Ridge (USA) in 1971.

The article outlines the results of measurements of neutron spectra in air and on the surface of a phantom (measurements made on the fast-neutron pulsed reactors of the Joint Institute of Nuclear Research and of the HPRR). The measurements on the fast-neutron pulsed reactor were made in the collimated extracted neutron beam which is practically free of secondary radiation. The transfer of all neutrons with energies above 0.4 eV on the front (relative to the active zone) surface of the phantom is therefore about 35 times greater than the neutron transfer on the rear surface. In the case of the HPRR reactor in which measurements were made directly in the experimental hall behind a 12 cm plastic shield, the considerable contribution of the scattered radiation increased the transfer of fast neutrons 7 times and that of moderate neutrons 3 times. Figure 1 shows the neutron spectrum of the HPRR reactor.

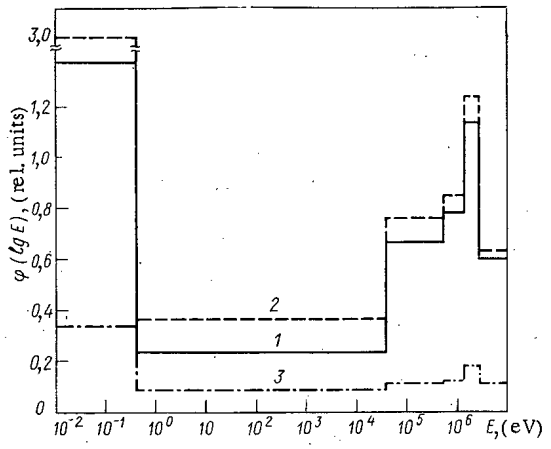

Fig. 1. Neutron spectrum of the HPRR reactor (1) with a 12 cm plastic shield in air, (2) at the front, and (3) at the rear surfaces of a phantom.

Ways of increasing the accuracy of the spectrometric measurements were considered. In the case of fast neutrons, the accuracy can be increased by introducing into the spectrometer detectors with splitting ^{231}Pa and ^{236}U isotopes. The measurement error of the spectra and of the neutron dose can be reduced 3-4 times in the energy range 0.5-1.5 MeV. In the case of moderate neutrons, the use of an additional ^{235}U + 0.08 g/cm^2 ^{10}B detector is proposed. A method is described for determining the spectra of these neutrons which are approximated by a step function of the form E^{-n}. It is shown that in the case of a relative error of the detector readings of 2-5%, the error in the determination of the spectral exponent n is less than 1-9% for $0.7 \leq n \leq 1.2$.

Original article submitted December 28, 1972; abstract submitted June 20, 1973.

ELECTROLYTIC PRODUCTION OF ALLOYS OF URANIUM WITH NICKEL IN MOLTEN SODIUM AND POTASSIUM CHLORIDES

G. N. Kazantsev, S. P. Raspopin, and O. V. Skiba

UDC 621.039.59:621.3.035.45

Liquid alloys of uranium with nickel are produced by the electrolysis of molten chlorides of the alkali and alkaline earth metals, containing oxygen-free chlorides of uranium, using metallic nickel as the cathode at a temperature of 800-900°C [1-3].

The optimum conditions of electrolysis were detected according to the results of measurements of the cathode polarization of metallic nickel, and were verified in experiments on the determination of the composition of the liquid alloys of uranium with nickel obtained as a function of the temperature, the cathodic current density, and the uranium trichloride concentration in the melt. The electrolysis of a salt melt containing 10% by mass uranium was conducted until 5-6 g of a uranium–nickel alloy, flowing from the cathode, was obtained, consuming 1.5-2 A·h. The current strength should not exceed 4 A, since the nickel cathode had a surface of up to 5 cm^2 immersed in the electrolyte.

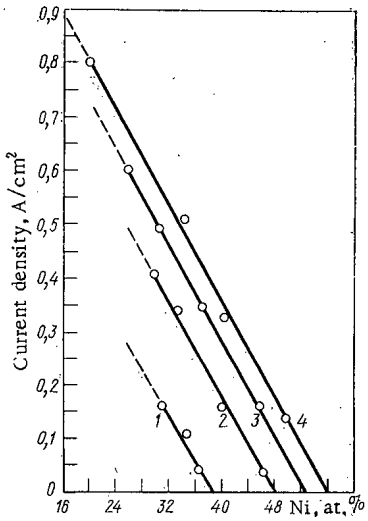

Fig. 1. Dependence of compositions of a cathodic alloy of uranium with nickel on the current density, °C: 1) 750; 2) 800; 3) 850; 4) 900.

By comparing the results of measurements of the cathodic polarization and current density at which uranium–nickel alloys could be obtained in the liquid state, it was established that electrolysis can be conducted with substantially larger current densities than those recommended on the basis of a study of polarization. This indicates a trapping by the alloy flowing from the cathode of fine crystals of metallic uranium, formed on the surface of the cathode and then assimilated by the alloy.

Thus, the most uranium-rich alloys are formed at the maximum current density and substantial cathode potentials, corresponding to the deposition of pure uranium. The linear dependences found (see Fig. 1) permit the selection of the conditions for the production of alloys with a set composition or the determination of the composition of an alloy under set conditions of electrolysis.

LITERATURE CITED

1. L. Niedrach and A. Glamm, Industr. and Engng. Chem., 48, 977 (1956).
2. L. Neidrach and A. Glamm, J. Electrochem. Soc., 103, 521 (1956).
3. L. Niedrach, Chem. Engng. Progr., 2, 411 (1958).

Original article submitted January 23, 1973; abstract submitted April 25, 1973.

TERNARY SYSTEMS OF LITHIUM CHLORIDE, SODIUM CHLORIDE, URANIUM TRICHLORIDE, AND URANIUM TETRAFLUORIDE

V. N. Desyatnik, S. P. Raspopin, I. I. Trifonov, and A. M. Tsybizov

UDC 541.123.3:546.131.33.34:791.3.4

Melts containing uranium tetrachloride with additions of lithium chloride and sodium chloride, and also uranium trichloride, can be used as electrolytes in electrolytic production or electrolytic refining of uranium. But the lack of data on the behavior of uranium tetrafluoride in melts of alkali metals, when uranium chlorides are present, is responsible for certain difficulties in the use of electrolytes of this type. That is why a study was undertaken of $LiCl–UCl_3–UF_4$ and $NaCl–UCl_3–UF_4$ systems by the differential thermal analysis method, backed up to a partial extent by x-ray analysis. The results were that melts of the system $LiCl–UCl_3–UF_4$ form two eutectic points and two peritectic points (Fig. 1) upon crystallization. The eutectic E_1 is characterized by the melting point 350 ± 2°C, and corresponds to the composition LiCl 43 mole %, UCl_3 25 mole %, and UF_4 32 mole %. The eutectic E_2 corresponds to the composition LiCl 13 mole %, UCl_3 34 mole %, and UF_4 53 mole % and melts at 455 ± 2°C. The melt of the peritectic point P_1 crystallizes at 465 ± 2°C and corresponds to the composition LiCl 14 mole %, UCl_3 36 mole %, and UF_4 50 mole %. At the peritectic point P_2, a melt of the composition LiCl 25 mole %, UCl_3 5 mole %, and UF_4 70 mole % crystallizes at 600 ± 2°C. A determination was made of the quasibinary section $UCl_3–LiCl \cdot 2UF_4$, which divides the ternary system $LiCl–UCl_3–UF_4$ into two secondary subsystems.

The primary crystallization surface of the ternary system $NaCl–UCl_3–UF_4$ is represented by seven fields (Fig. 2). The quasibinary section $UCl_3–3NaCl \cdot 2UF_4$ divides the system into two secondary subsystems. Two eutectic points, two peritectic points, and a single "transitory" point were determined in the system. The eutectic point E_1 crystallizes at 415 ± 2°C and corresponds to the system NaCl 34 mole %, UCl_3 21.5 mole %, and UF_4 44.5 mole %. The eutectic E_2 crystallizes at 430 ± 2°C, corresponding to the composition NaCl 55 mole %, UCl_3 22.5 mole %, and UF_4 22.5 mole %. The melts at the "transitory" point are of composition NaCl 16 mole %, UCl 34 mole %, and UF_4 50 mole % and crystallize at 530 ± 2°C. At point P_2 for the composition NaCl 42 mole %, UCl_3 14 mole %, and UF_4 44 mole %, crystallization takes place by a four-phase peritectic reaction at 470 ± 2°C.

The melt at point P_3, of composition NaCl 36 mole %, UCl_3 24 mole %, and UF_4 44 mole %, crystallizes at 440 ± 2°C.

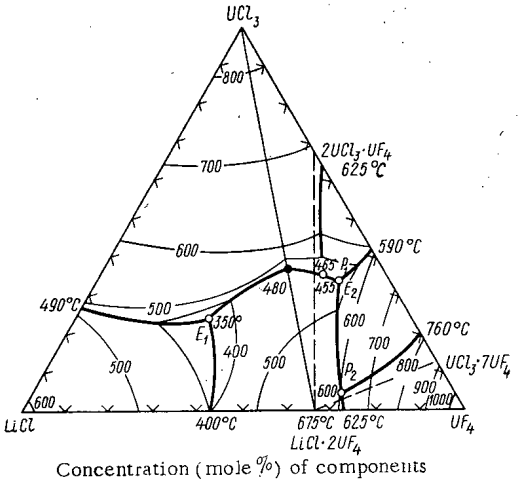

Fig. 1. Melting point diagram of system $LiCl–UCl_3–UF_4$.

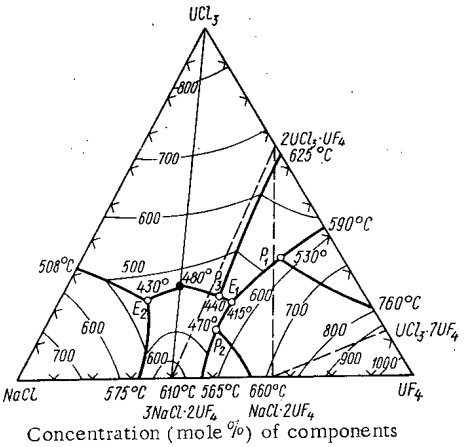

Fig. 2. Melting point diagram of system $NaCl–UCl_3–UF_4$.

Original article submitted February 8, 1973.

NONSTATIONARY TRANSPORT OF NEUTRONS IN A BLOCK OF MODERATOR CONTAINING A LARGE CAVITY

K. D. Ilieva and M. V. Kazarnovskii

UDC 539.125.52:621.039.51.12

We consider the transport of neutrons from a pulsed source in a spherical block of moderator of thickness H containing a large spherical cavity of radius R. The residence time of a neutron in the moderator is much shorter than the transit time in the cavity. It is assumed that: 1) the cross sections can be taken as constants in treating neutron transport in the moderator; 2) the spectrum k(v) ($\int_0^\infty k(v)dv = 1$) of the neutrons emerging from the moderator into the cavity does not depend on the spectrum of the incident neutrons. Then the flux of neutrons emerging from the moderator into the cavity can be described by the equation

$$N^-(\mu, v, t)=k(v)\int_0^\infty dv'\int_0^1 d\mu' K(\mu'\to\mu)\,N^-\left(\mu', v', t-\frac{2R\mu'}{v'}\right)+k(v)\,K(1\to\mu)\,\delta(t-R),$$

where $\cos^{-1}\mu$ is the angle of emission with respect to the inner surface of the moderator, v is the neutron velocity, t is the time, $K(\mu'\to\mu)$ is the flux of neutrons emerging at an angle $\cos^{-1}\mu$ produced by a neutron entering the moderator at the angle $\cos^{-1}\mu'$. In the one-velocity approximation $K(\mu'\to\mu)$ is given by familiar formulas for the albedo problem.

It is shown that the neutron flux can be calculated with sufficient accuracy in the isotropic approximation, i.e., by assuming $K(\mu'\to\mu) = 2k_0\mu$, where k_0 is the average albedo. In this approximation the flux of neutrons emerging from the moderator into the cavity is given by

$$N^-(\mu, v, B)=\frac{2k_0\mu v^3 e^{-v^2}}{R}\left(\sum_i \mathrm{Res}\left[\frac{e^{Bx}}{1-4k_0I(x)}\right]_{x=x_i}+\frac{4k_0}{\pi}\int_0^\infty \frac{\mathrm{Im}\,[I(-x)]\,e^{-Bx}dx}{\{1-4k_0\,\mathrm{Re}\,[I(-x)]\}^2+\{4k_0\,\mathrm{Im}\,[I(-x)]\}^2}\right).$$

Here $I(x)=\int_0^\infty dv v^3 e^{-v^2}\int_0^1 d\mu\mu e^{-\frac{\mu x}{v}}$ for $\mathrm{Re}[x] > 0$, $B = (t-R)/2R$, and the sum of the residues is taken for $\mathrm{Re}[x_i] < 0$.

An analysis of the expression given shows that a quasisteady neutron distribution is established in a time $1 \leqslant B \leqslant 4/x_1$, where x_1 is the root of the equation $1-4k_0I(x) = 0$ in the left half-plane which has the smallest absolute value. This root agrees closely with the first root of the equation $1-2k_0\int_0^1 \mu e^{-\mu x}d\mu = 0$, which is a solution of the analogous problem in the one-velocity approximation. The total neutron flux is attenuated according to the law

$$N_0^-(\mu, B)=\frac{\mu k_0 x_1 e^{Bx_1}}{2R(k_0e^{x_1}-1)}.$$

At large times the attenuation will become nonexponential since slow neutrons accumulate in the cavity. Then the total flux is given by

$$N^-(\mu, B)=N_0^-(\mu, B)+\frac{4k_0^2\mu}{R(1-k_0)^2}\left\{\frac{4!}{B^5}-\left[x_1^5+\frac{x_1^4}{B}+\frac{4x_1^3}{B^2}+\frac{4\cdot 3x_1^2}{B^3}+\frac{4!\,x_1}{B^4}+\frac{4!}{B^5}\right]e^{-Bx_1}\right\}.$$

The results of the calculation are compared with experimental data.

Original article submitted February 9, 1973; abstract submitted June 4, 1973.

ASYMPTOTIC NEUTRON FLUX FROM A PULSED SOURCE IN A MODERATOR WITH AN INFINITE PLANE SLOT

K. D. Ilieva and M. V. Kazarnovskii

UDC 539.125.52:621.039.51.12

Using the method described earlier [1], and with the same approximations, we consider the transport of neutrons in a system of two slabs of homogeneous moderator separated by a wide plane slot of width 2b with an infinite uniformly distributed pulsed source in the plane of symmetry of the system.

In this arrangement the flux of neutrons emerging from the moderator into the cavity is described by the equation

$$N^-(\mu, \nu, t)=k(\nu)\int_0^\infty d\nu'\int_0^1 d\mu' K(\mu'\to\mu)\,N^-\left(\mu', \nu', t-\frac{2b}{\mu'\nu'}\right)+k(\nu)\,K(\mu_s\to\mu)\,\delta\left(t-\frac{b}{\mu}\right).$$

The notation is the same as in [1]. The analytical expression for the neutron flux in the isotropic one-velocity approximation has the form

$$N^-_{\text{approx.}}(\mu, B)=\frac{k_0\mu}{b}\left(\sum_i \operatorname{Res}\left[\frac{e^{Bx}}{1-a(x)}\right]_{x=x_i}+k_0\int_0^\infty \frac{x^2e^{Bx}\,dx}{\{1-\operatorname{Re}[a(-x)]\}^2+(k_0\pi x^2)^2}\right);$$

$$a(x)=k_0\left\{e^{-x}(1-x)-x^2\left[0.5772+\sum_{n=1}^{\infty}\frac{(-1)^n x^n}{n!n}\right]-x^2\ln x\right\},$$

where the sum of the residues is taken for Re $[x_i] < 0$. In particular for asymptotically long times

$$N^-(\mu, B)\to\frac{2\mu k_0}{b(1-k_0)^2B^3}.$$

It is shown that taking account of the energy dependence by assuming a Maxwellian distribution of the neutrons emerging from the moderator into the cavity leads to exactly the same expression for the total neutron flux as $B\to\infty$.

Since as μ and $\mu'\to 0$ in the one-velocity approximation $K(\mu'\to\mu)=\mu/(\mu+\mu')$, it would seem that the anisotropy of the angular distribution should strongly affect the time dependence of the neutron flux in the penetration of neutrons through a plane slot at glancing angles. However, taking account of this effect for asymptotically long times makes only an insignificant change in the angular dependence of the flux of emerging neutrons and does not affect its time dependence. This is related to the fact that the main contribution to the asymptotic neutron flux comes from neutrons which have passed through the slot only once at a glancing angle.

Since one should expect the strongest effect of the energy and angular distributions of the emerging neutrons on the time dependence of the total flux for asymptotically long times, the results obtained give us confidence that direct numerical calculations of neutron fluxes for specific cases, in particular taking account of the finite size of the moderator, can be performed in the first approximation in the one-velocity model and under the assumption of isotropy of the neutron flux emerging from the moderator.

LITERATURE CITED

1. K. D. Ilieva and M. V. Kazarnovskii, this issue p. 1029. Brief Communications on Physics [in Russian], Vol. 3 (1973), p. 19.

Original article submitted March 20, 1973; abstract submitted June 4, 1973.

PROPAGATION OF NEUTRONS IN AN ANISOTROPIC MEDIUM*

A. S. Dolgov

UDC 621.039.51.12:539.125.52

In certain cases the anisotropy of a medium of microscopic or macroscopic character leads to the dependence of the mean free path on the direction of motion of a particle, which can be taken into account by introducing anisotropic cross sections for the processes. We consider an analytical solution of the problem of the transport of isotropically diffusing particles with orientational inhomogeneity of the properties of the medium. The method used is related to the method of Fourier transforms and the method of elementary solutions [1]. We find a solution of the problem for arbitrary boundary conditions and arbitrary geometry. Solutions in the corresponding limiting cases reduce to known solutions for a homogeneous medium.

In the appendices we consider features of the application of the methods of spherical harmonics and discrete ordinates to problems of transport in an anisotropic medium.

A general form of the equations of the P_n-approximations of the method of spherical harmonics is established, and calculation relations of the method of discrete ordinates are found. It is explained that unlike the method of spherical harmonics, the use of the method of discrete ordinates does not lead to a significant increase in volume of calculations in comparison with the corresponding case for an isotropic medium.

LITERATURE CITED

1. K. Case, Ann. Phys., 9, 1 (1960).

THE APPLICABILITY OF PHENOLFORMALDEHYDE RESIN AS AN INERT MATRIX FOR COMPARISON STANDARDS IN ACTIVATION ANALYSIS†

M. A. Kolomiitsev, T. S. Ambardanishvili,
V. Yu. Dundua, T. Ya. Zakharina,
G. M. Gromova, and N. V. Pachuliya

UDC 539.1.074.8

Neutron activation analysis is widely employed at the present time in making determinations of microelements in various materials. When neutron activation analysis of high resolving power semiconductor detectors is put into practice, its instrumentation severely restricts the region of application of methods based on prior radiochemical separation of the materials being studied. The construction of comparison standards for neutron activation analysis which can be used to make a direct measurement of activity and to record γ-spectra after irradiation by high integral neutron fluxes of up to 10^{19} neutrons/cm^2 is therefore a problem of current interest.

It is shown in the present work that the synthesis of phenolformaldehyde bakelite resin (PBR) under the special conditions in which contact of the monomers and catalyst (ammonia) with the glass is excluded enables one to obtain a polymer with a low content of neutron-sensitive impurities which are activated under the action of neutrons to form γ-emitting isotopes. It was found that prior to the synthesis the monomers

*Original article submitted February 13, 1973.
†Original article submitted April 4, 1973.

TABLE 1. Content of Admixtures of Neutron-Sensitive Elements in PBR

Element	Specific content of element in the resin, grams of element /grams of resin	Amount of element contained in a 50 mg tablet, g
Sodium	$1 \cdot 10^{-8}$	$5 \cdot 10^{-10}$
Chlorine	$1 \cdot 10^{-4}$	$5 \cdot 10^{-6}$
Scandium	$2 \cdot 10^{-12}$	$1 \cdot 10^{-13}$
Iron	$5 \cdot 10^{-6}$	$2{,}5 \cdot 10^{-7}$
Cobalt	$2 \cdot 10^{-12}$	$1 \cdot 10^{-13}$
Zinc	$5 \cdot 10^{-11}$	$2{,}5 \cdot 10^{-12}$
Arsenic	$4 \cdot 10^{-8}$	$2 \cdot 10^{-9}$
Bromine	$8 \cdot 10^{-9}$	$4 \cdot 10^{-10}$
Silver	$4 \cdot 10^{-12}$	$2 \cdot 10^{-13}$
Tin	$1 \cdot 10^{-8}$	$5 \cdot 10^{-10}$
Antimony	$7 \cdot 10^{-11}$	$3{,}5 \cdot 10^{-12}$
Cesium	$3 \cdot 10^{-13}$	$1{,}5 \cdot 10^{-14}$
Gold	$1 \cdot 10^{-10}$	$5 \cdot 10^{-12}$

and catalyst must be purified by distillation in a quartz dish, since the impurities present in them cannot be eliminated by subsequent reprecipitation of the PBR (the metals are connected by phenol hydroxyls, but the bromine enters into the composition of the bromophenols entering the polycondensation together with the basic monomers). The PBR obtained by a technique which has been developed can be used as an inert matrix (activated weakly by neutrons) in the preparation of comparison standards for neutron activation analysis. Phenolformaldehyde bakelite resin forms actual solutions with many elements [1]. The treatment of the compositions of the PBR element in the tablet standard is not difficult. The tablets are radiation-resistant to integral neutron fluxes of up to $\sim 10^{19}$ neutrons /cm^2, and are mechanically stable.

The content of admixed neutron-sensitive elements in the PBR was measured by irradiating large samples of the polymer (of up to 10-15 g) with integral neutron fluxes of $\sim 10^{19}$ neutrons/cm^2, and then analyzing the γ-spectra of these samples. A germanium–lithium semiconductor detector with a resolving power of 2.5 keV was used to record the spectra (see Table 1).

The high activation frequency of the matrix makes it possible to prepare on its base practically any standard for neutron activation analysis which is applicable for the direct measurement of activity. The error in the measurement of the main isotope's activity is at most 1% in the worst case (where the photopeaks of the main element and the admixture are not resolved).

The authors wish to thank L. M. Mosulishvili and T. K. Tevziev for the help which they rendered.

LITERATURE CITED

1. T. S. Ambardanishvili et al., "Metrology of neutron radiation in reactors and accelerators," in: Theses of the Proceedings of the First All-Union Coordinated Conference on the Metrology of Neutron Radiation [in Russian], All-Union Scientific Research Institute of Physicotechnical and Radiotechnical Measurements Press, Moscow (1971), p. 70.

NEUTRON ACTIVATION ANALYSIS OF DINOSAUR BONES FOR URANIUM, THORIUM, AND RARE EARTH ELEMENTS

Zh. Ganzorig, T. Gun-Aazhav,*
Sh. Gérbish,* O. Otgonsurén,
Zh. Séréeter,* I. Chadraabal,*
and D. Chultém

UDC 543.53

The uranium content in dinosaur bones was investigated earlier by recording the fragments of the fission of ^{235}U with thermal neutrons [1], and also according to the γ-radiation of the decay products of ^{238}U [2]. In this work we investigated the content of U, Th, rare earth elements (REE) in these bones by the method of activation analysis.

Activation with resonance neutrons permits a nondestructive determination of uranium and thorium in materials with a complex chemical composition [3]. Using this method, a quantitative analysis of U and Th in dinosaur bones was conducted on the IBR-30 reactor (United Institute of Nuclear Research). Figure 1 shows the γ-spectra of a sample of bone and a standard, measured under the same conditions. By a comparison of the areas of the corresponding peaks on these spectra we determined the concentration of the elements to be analyzed, which proved equal to: $(2.2 \pm 0.2) \cdot 10^{-4}$ and $(1.7 \pm 0.5) \cdot 10^{-4}$ g/g for U and Th, respectively, in the investigated samples.

For an analysis for rare earth and other elements, the bone sample was irradiated on the thermal channel of the reactor with a flux of $1.3 \cdot 10^{13}$ neutrons/cm$^2 \cdot$ sec for 5 min. Spectra a and b (Fig. 2) were measured two days after irradiation and correspond to a standard with a weight of 10 μg U and to the bone sample.

On spectrum a the lines of the products of the reactions $^{238}U(n, \gamma; \beta^-)$ [4] and $^{235}U(n, \gamma)$ [5, 6] are clearly visible (Table 1).

On spectrum b these lines appear less distinctly on account of the large background of natural radioactivity of the bone; the lines 658, 495, 773, 290, and 350 keV were masked by this background; the lines 512, 556, and 743 keV, on the contrary, were more pronounced than on the spectrum a, which is an indication of the presence of Sr and Zr in the ancient bones. The intensification of the lines 512 and 556 keV can be explained by the contribution from the reaction $^{84}Sr(n, \gamma)$ and by the result of the accumulation of the long-lived radioisotope ^{91}Sr (28 years) in the bones. The intensification of the line 743 keV is due to the reaction $^{96}Zr(n, \gamma)$, the cross-section of which is approximately equal to 0.1 b. The presence of zirconium is evidenced by the appearance of a new line, 755 keV of ^{95}Zr on spectrum b. Although this isotope is one of the fission products of ^{235}U, it can be assigned as the reaction product of $^{94}Zr(n, \gamma)$, since the line

TABLE 1. Origin of the Peaks in the γ-Spectrum a

Isotopes	Eγ, keV
^{239}Np	106, 120, 210, 228, 278, 333
^{91m}Y (^{91}Sr)	556
^{97}Nb	658
$^{97}Zr + ^{99}Mo$	743
$^{99}Mo + ^{99}Tc$	140
^{103}Ru	495
^{106}Rh (^{106}Ru)	512
^{132}Te (^{239}Np)	228
^{132}I	773
$^{133}I + ^{135}Xe$ (^{135}I)	530
^{135}Xe	250
^{143}Ce	290, 350

*Co-workers of Mongolian State University, Ulan-Bator.

Translated from Atomnaya Énergiya, Vol. 35, No. 5, pp. 349-351, November, 1973. Original article submitted August 22, 1972; revision submitted June 11, 1973.

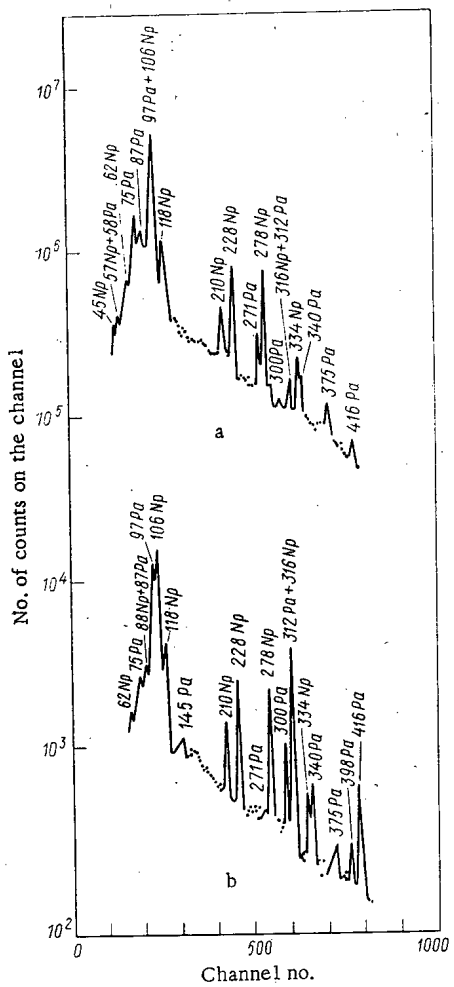

Fig. 1. γ-Spectra of dinosaur bone (a) weighing 20 g and a standard (b) weighing 10 μg U + 100 μg Th, irradiated with a flux of resonance protons. (Time of irradiation 2 days, exposure 2 days, measurement 1 h.)

TABLE 2. Origin in the Peaks in the γ-Spectrum b

Isotopes	Eγ, keV
Fission products of ^{235}U	
^{95}Zr (65,2 days)	725, 755
^{97}Zr (17 h)	743
^{99}Mo (2,8 days)	373, 743, 773
^{103}Ru (39,4 days)	495
^{106}Rh (^{106}Ru, 1 year)	512
^{131}I (8,1 days)	365
^{132}I (^{132}Te, 3,2 days)	668, 773
^{140}Ba (12,8 days)	132, 162, 304, 420, 435, 537
^{143}Ce (1,4 days)	290, 350
Products of the reaction (n, γ)	
^{46}Sc (83,9 days)	889, 1120
^{59}Fe (45,6 days)	1100, 1295
^{60}Co (5,5 years)	1175, 1333
^{140}La (1,7 days)	333, 435, 815, 867, 925; $1595-2mc^2$, $1595-mc^2$, 1595
^{141}Ce (32,5 days)	147
^{143}Ce (1,4 days)	290, 350
^{147}Nd (11,1 days)	537
^{152}Eu (12,7 years)	350, 867, 965, 1086, 1110, 1274, 1407
^{154}Eu (16 years)	725, 1295
^{160}Tb (72,3 days)	197, 216, 299, 879, 965, 1175, 1274
^{175}Yb (4,2 days)	290, 397
^{239}Np (2,34 days)	106, 210, 228, 278, 333

TABLE 3. Origin of the Peaks in the γ-Spectrum d

Isotopes	Eγ, keV
^{153}Gd	97, 103
^{152}Eu	123, 245, 296, 344, 367, 411, 444, 779, 867, 964, 1086, 1110, 1213, 1274, 1407, $40K_{\alpha}Sm+43K_{\alpha}Gd$
^{154}Eu	123, 723, 998, 1005, 1295, 1458, $43K_{\alpha}Gd$
^{170}Tm	84
^{46}Sc	889, 1120
^{60}Co	1173, 1333

755 keV is not present in spectrum a. The "disappearance" of two lines (250 and 530 keV) in spectrum a is evidently due to the diffusion of xenon in the porous structure of the bone.

The standard of uranium contained Na and K, while their lines 315, 1522 keV for ^{42}K and 857, 1368, 1732 keV for ^{24}Na on spectrum a served for internal calibration. It is evident that ancient bone contains much sodium and little potassium. The appearance of five lines of ^{140}La (333, 435, 485, 815, 1595 keV) on spectrum b is evidence that the investigated samples contain a large amount of rare earth elements. Spectra c and d were measured for the detection of other rare earth elements (Tables 2 and 3) 15 and 400 days after irradiation, respectively [4, 7, 8]. Actually, these measurements show that ancient bones contain not only U and Th, but also rare earth elements of the cerium and yttrium groups, including scandium. This fact is evidence of the well-known geochemical correlation between the actinide and lanthanide elements. The joint presence of all the detected elements in the bones (U, Th, REE, Sr, Zr, Na, Ba, Fe, Co) may be associated with the phenomenon of polymorphism. Therefore, an analysis of the ancient bone for Li, Be, Mg, Al, Ca, Ti, Y, and Ni is of great interest.

Let us note that the analysis for the rare earth elements is only qualitative. The quantitative analysis necessary for the detailed investigation of the nature and mechanism of the accumulation of these elements in bones requires their preliminary chemical separation [9]. This is due, in particular, to the fact that isotopes of the most widespread REE (^{140}La, ^{143}Ce) are formed not only as a result of the (n, γ) reaction,

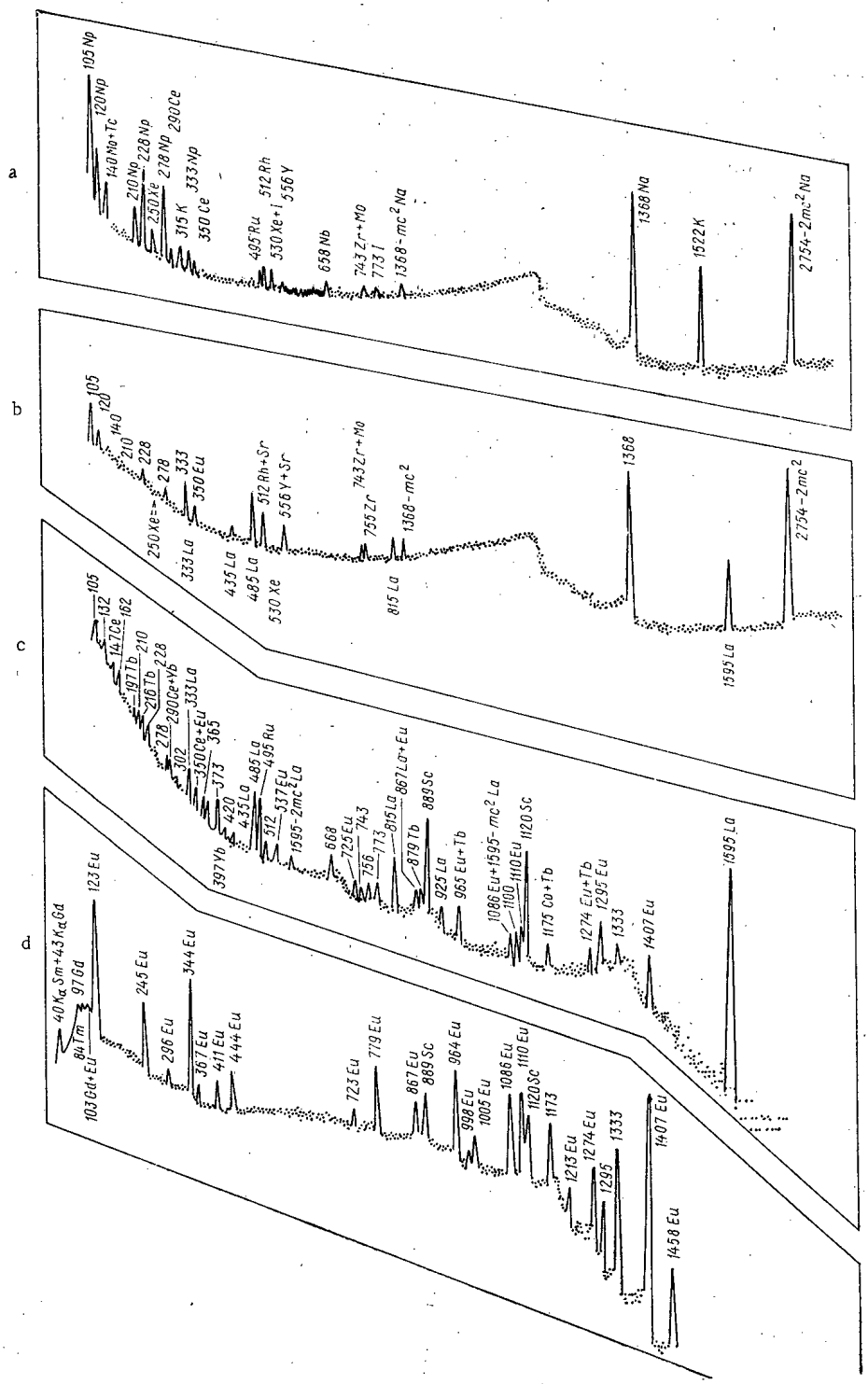

Fig. 2. γ-Spectrum of a sample of dinosaur bone irradiated with thermal neutrons.

but also in the reaction $^{235}U(n, f)$, as well as the decay of fission products. The high intensity of the lines of ^{140}La on spectrum c is explained by the accumulation of this isotope as a result of the decay of ^{140}Ba (~12 days), formed with a large yield in the fission of uranium [10].

LITERATURE CITED

1. O. Otgonsurén, V. P. Perelygin, and D. Chultém, At. Énerg., 29, No. 4, 301 (1970).
2. T. Gun-Aazhav et al., ibid., 35, No. 2, 130 (1973).

3. Zh. Ganzorig et al., Preprint of the United Institute of Nuclear Research 6-7040 [in Russian], Dubna (1973).
4. F. Adams and R. J. Dams, Radioanal. Chem., 3, 99-125 (1969).
5. G. Gordon et al., Nucleonics, 24, No. 12, 62 (1966).
6. F. Adams and R. J. Dams, Radioanal. Chem., 3, 271-285 (1969).
7. R. Dams and F. Adams, ibid., 7, 127-160 (1970).
8. I. V. Mendis, Reference Tables for Neutron Activation Analysis [in Russian], Zinatne, Riga (1969).
9. H. Higuchi et al., J. Radioanal. Chem., 5, 207-222 (1970).
10. A. A. Greshilov, V. M. Kolobashkin, and S. N. Dement'ev, Products of Instantaneous Fission of ^{235}U, ^{238}U, and ^{239}Pu [in Russian], Atomizdat, Moscow (1969).

ANALYSIS OF URANIUM AND THORIUM ORES USING A GAMMA RAY SPECTROMETER WITH A Ge(Li) DETECTOR

O. V. Gorbatyuk, E. M. Kadisov, V. L. Miller, and V. L. Shashkin

UDC 550.8:553.495:539.1.55:539.122.164

Because of their high energy resolution, spectrometers with Ge(Li) detectors are widely used in the analysis of radioactive ores by means of their γ-ray spectra. In particular the character of the spectrograms of the γ-radiation from ore samples (Figs. 1 and 2) permits the determination of the uranium, radium, radon, and thorium contents from a single measurement. This is done by using characteristic lines in the γ-ray spectra of the elements being determined or their decay products in equilibrium with them.

The uranium content can be determined from the characteristic γ-ray lines accompanying the decay of uranium itself (^{235}U) or its decay products ^{234}Th(UX$_1$) and ^{234}Pa. Radium is determined by using the single 186.2 keV line produced in the decay of ^{226}Ra. Radon is determined from the intense γ-ray lines

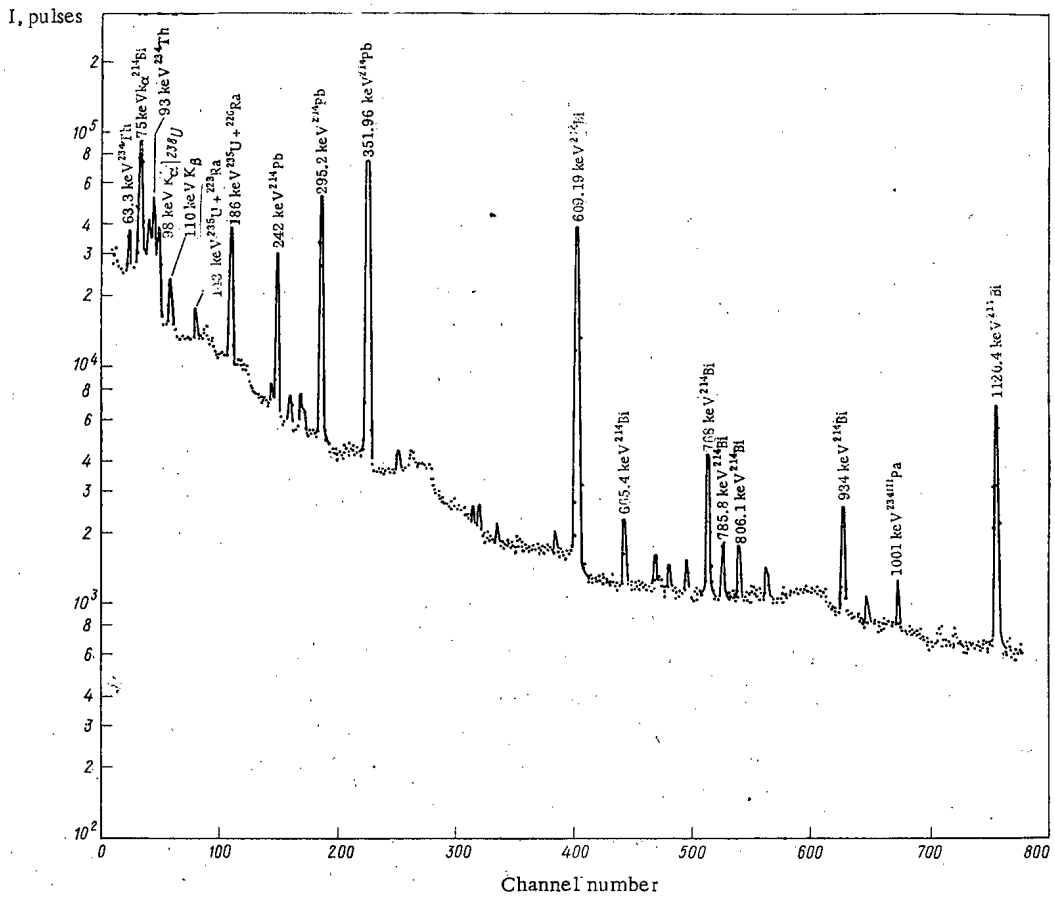

Fig. 1. γ-Ray spectrum of a specimen of pitchblende.

Translated from Atomnaya Énergiya, Vol. 35, No. 5, pp. 352-355, November, 1973. Original article submitted August 22, 1972; revision submitted May 29, 1973.

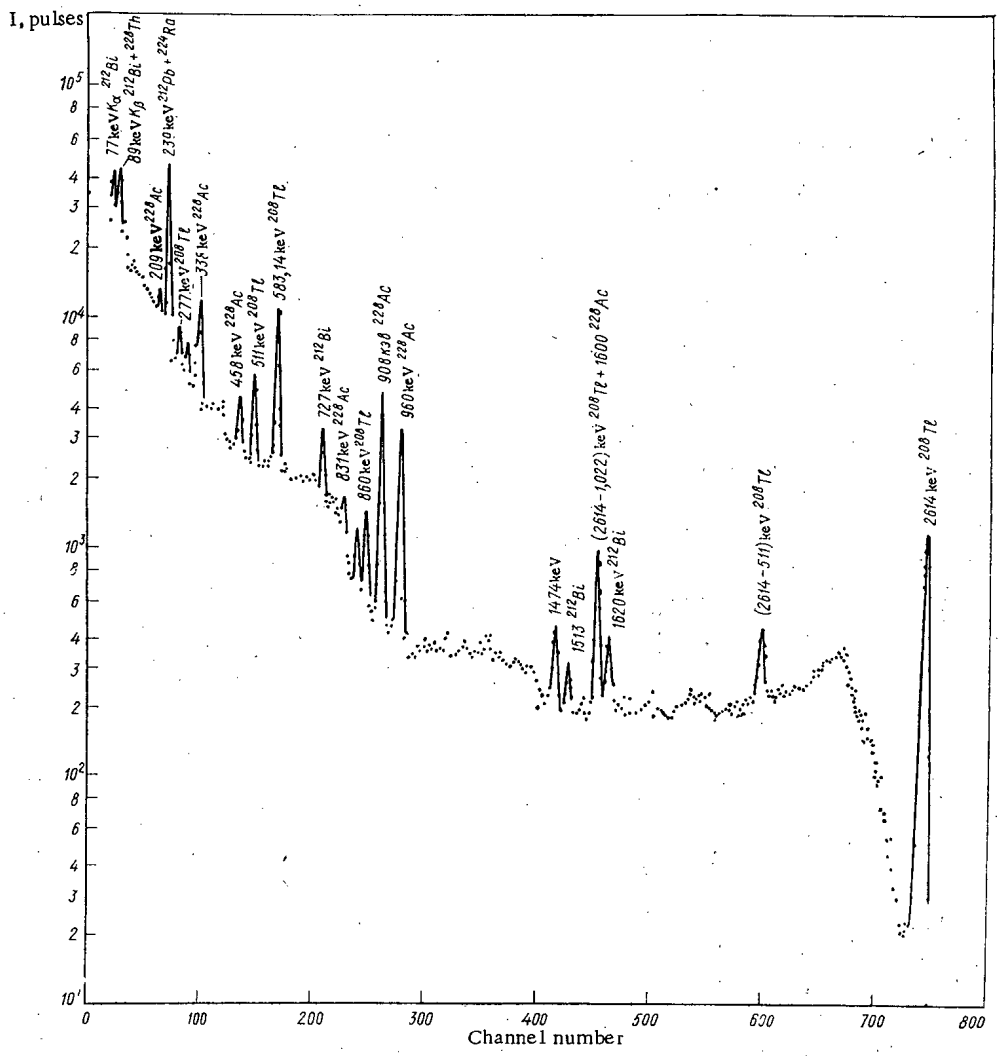

Fig. 2. γ-Ray spectrum of a specimen of thorium in equilibrium with its decay products.

accompanying the decay of ^{214}Pb(RaB) or ^{214}Bi(RaC). Thorium can be determined from the γ-radiation of ^{208}Tl(ThC") or ^{228}Ac(MsTh$_2$). There are many intense lines in the γ-ray spectra of these isotopes [1].

In choosing a line for determining an isotope it is necessary to take account of the quantum yield of this line, the efficiency of its recording, the background in its vicinity, and the contribution of unresolved γ-ray lines of other radioisotopes to the composite peak on the spectrogram.

Table 1 shows the lines which are most convenient for determining the isotopes listed.

Let us consider one of the possible ways of making an independent determination of uranium and radium in samples of uranium ore. Uranium is determined by using the 63.3 keV line of ^{234}Th which is practically single. For a spectrometer resolution of 2 keV the contribution to the peak of this line from the main interfering isotope ^{231}Pa is no more than 1% [2].

Since for the usual resolution of semiconductor spectrometers (2.5 keV in this region) the only ^{226}Ra line at 186.2 keV is merged with the 185.7 keV line of ^{235}U, the radium content of the sample is determined after subtracting the uranium contribution to the composite spectrogram peak found from the 63 keV line. It is assumed that the relative ^{238}U and ^{235}U contents in the ores are practically unchanged.

If the experimental conditions are such that the absorption of γ-rays of a given energy in the sample can be neglected, the area of the photopeak of the analytic line is proportional to the amount of γ-radiation of the isotope. In this case the uranium content of the sample is given by

$$q_U^{sa} = q_U^{st} \frac{S_{sa}^{63}}{S_{st}^{63}} \cdot \frac{P_{st}}{P_{sa}}, \quad (1)$$

TABLE 1. Main Analytic Lines in the γ-Ray Spectra of Radioactive Ores

Energy, keV	Isotope	Relative sizes of photopeaks from measurements with a 27 cm^3 Ge(Li) detector
	Uranium series	
63,3	UX_1 (^{234}Th)	0,16
186,2	^{226}Ra	0,26
295,20	RaB (^{214}Pb)	0,64
351,96	RaB (^{214}Pb)	1,00
609,19	RaC (^{214}Bi)	0,60
1120,4	RaC (^{214}Bi)	0,10
	Uranium-Actinium series	
185,7	^{235}U	0,18
	Thorium series	
208	$MsTh_2$ (^{228}Ac)	0,36
583,14	ThC″ (^{208}Tl)	1,00
909	$MsTh_2$ (^{228}Ac)	0,49
960	$MsTh_2$ (^{228}Ac)	0,43

where q_U^{sa} and q_U^{st} are respectively the uranium content of the sample and of the standard; S_{sa}^{63} and S_{st}^{63} are the areas of the 63 keV photopeaks in the sample and in the standard; P_{sa} and P_{st} are the weights of the sample and of the standard.

The standard can be a well analyzed sample of uranium ore. The radium content in units of equivalent uranium is given by

$$q_{Ra} = \frac{q_U^{st} \frac{S_{sa}^{186}}{S_{st}^{186}} \cdot \frac{P_{st}}{P_{sa}} - q_U^{sa}(1-a)}{a}, \quad (2)$$

where a is the fraction of the radium γ-radiation in the composite photopeak of the 186 keV U–Ra_1 line for equilibrium ore; S_{sa}^{186} and S_{st}^{186} are the areas of the 186 keV photopeaks in the sample and in the standard.

It should be noted that the factor a is independent of the detector efficiency, the sample composition, and the conditions of measurement.

The error in the analyses is determined mainly by the statistical error in the calculation of the area of the photopeak above the background. For an appreciable sample thickness the difference of the self-absorption of the line in the sample and in the standard can introduce a further error if the material composition of the sample and standard are different. In this case appropriate corrections must be introduced.

To determine radium by this method it is necessary to have as accurate a value as possible for the relative contributions of uranium and radium (E_γ = 185.7 and 186.2 keV respectively) to the composite photopeak (the factor a in Eq. (2)).

Special measurements were performed to determine the contribution of radium radiation to the composite peak. Then (~85 mg/cm^2) hermetically sealed samples of equilibrium pitchblende and radium were prepared. The γ-ray spectra of these preparations were measured and calculations were made of the ratio of the areas of the 186 keV peaks, normalized to one of the peaks, corresponding to the γ-ray lines of ^{214}Pb or ^{214}Bi. As a result of some self-absorption of γ-radiation in the samples the contribution of the radium γ-radiation to the composite peak turned out to be different for normalization to different lines. The final value of this quantity was determined by extrapolating the values obtained with different normalization

TABLE 2. Results of Analysis of Ore Samples for Uranium and Radium

	No. of samples *			
	1	2	3	4
Weight of sample, g	34.1	30.1	31.2	35.6
U content in % from chemical analysis	0.609	0.270	0.220	0.396
No. pulses in photopeak of 63 keV line	3520	1384	1073	2024
Background at 63 keV lines	10900	4514	3912	6742
U content in % at 63 keV lines, from Eq. (1)	—	0.27± ±0.02	0.20± ±0.02	0.34± ±0.03
U content in % of equilibrium U by radiochemical analysis	0.609	0.240	0.200	0.376
No. pulses in photopeak of 186 keV line	9260	3540	2947	5712
Background at 186 keV line	6020	2458	2240	3465
Ra content in % of equilibrium U by Eq. (2)	—	0.26± ±0.02	0.22± ±0.02	0.38± ±0.03

*Sample 1 was taken as a standard.

peaks. The contribution of radium to the composite 186 keV peak is 0.592 ± 0.005. The error cited is the mean square error.

Four samples of uranium ore were analyzed. The measurements were made using a γ-ray spectrometer with a 27 cm^3 Ge(Li) detector. The energy resolution of the spectrometer at 186 keV was 2.2 keV. The statistical error of determining the areas of the photopeaks did not exceed 6-7%. Self-absorption of γ-rays was neglected. The time to measure one sample was 60 min. The measured values show good agreement with the results of chemical and radiochemical analyses (Table 2).

The possibility of separating the 186.2 keV line of ^{226}Ra from the 185.7 keV line of ^{235}U is of interest from the point of view of independent determinations of uranium and radium. Since the handbook values of the energies of these lines contradict one another special measurements were undertaken to refine the absolute values and the energy difference. The measurements, performed by a method similar to the one described in [3, 4], gave the following results: the energy of the uranium line is 185.705 ± 0.015 keV; the energy of the radium line is 186.215 ± 0.015 keV. The difference is 510 ± 20 eV. Recording these lines separately thus requires a spectrometer with a resolution of about 500 eV, i.e., a spectrometer based on a Ge(Li) detector with a cooled internal preamplifier.

LITERATURE CITED

1. C. Lederer and J. Hollander, Tables of Isotopes, Wiley, New York (1967).
2. R. Lange and G. Hagee, Nucl. Phys., A124, 412 (1969).
3. R. Greenwood et al., Nucl. Instrum. and Methods, 77, 141 (1970).
4. R. Helmer et al., ibid., 96, 173-196 (1971).

POSSIBILITIES OF DETERMINING URANIUM AND RADIUM CONTENT OF ORES BY MEASURING GAMMA RADIATION IN A BOREHOLE USING A SPECTROMETER WITH A Ge(Li) DETECTOR

O. V. Gorbatyuk, E. M. Kadisov, V. V. Miller, and S. G. Troitskii

UDC 550.8:553.495:539.122.164

At the present time the first borehole γ-ray spectrometers with Ge(Li) detectors are being developed to analyze radioactive ores under natural conditions.

The possibility of an independent determination of uranium and radium from borehole measurements of the γ-radiation from ore strata using spectrometers with Ge(Li) detectors was examined in [1, 2]. It

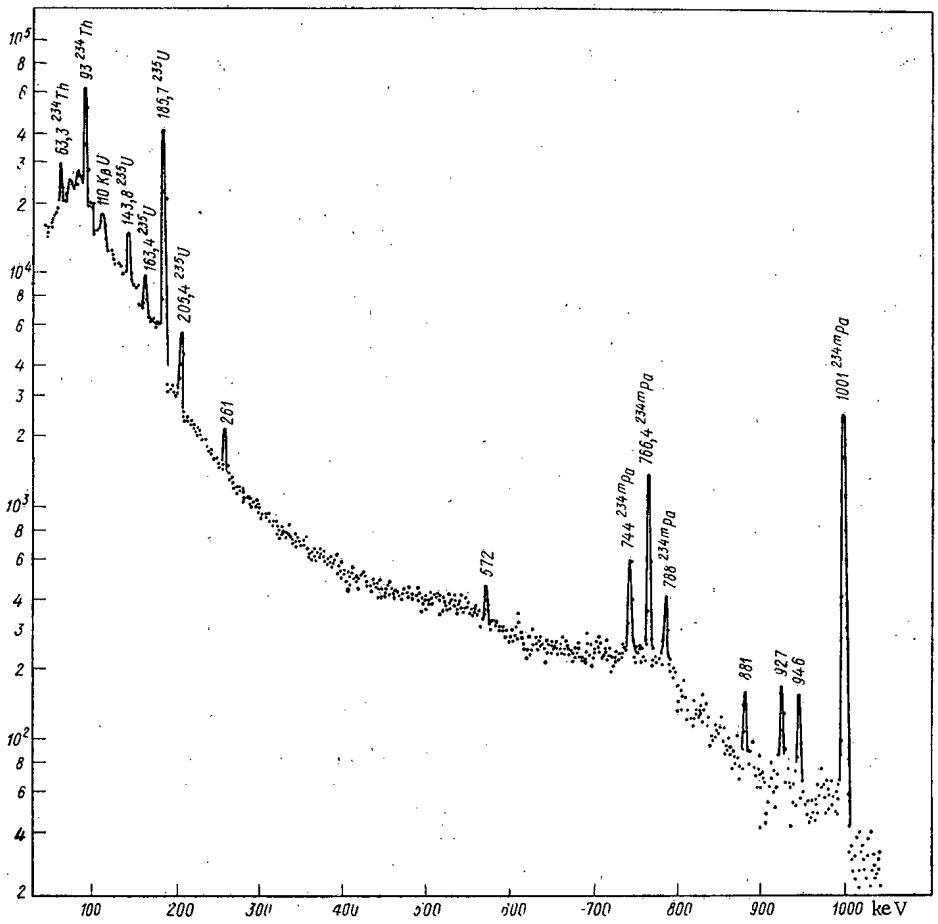

Fig. 1. γ-Ray spectrum from model of a stratum of uranium ore with radium leached out (model 2). T_{meas} = 60 min.

Translated from Atomnaya Énergiya, Vol. 35, No. 5, pp. 355-357, November, 1973. Original article submitted August 22, 1972; revision submitted May 29, 1973.

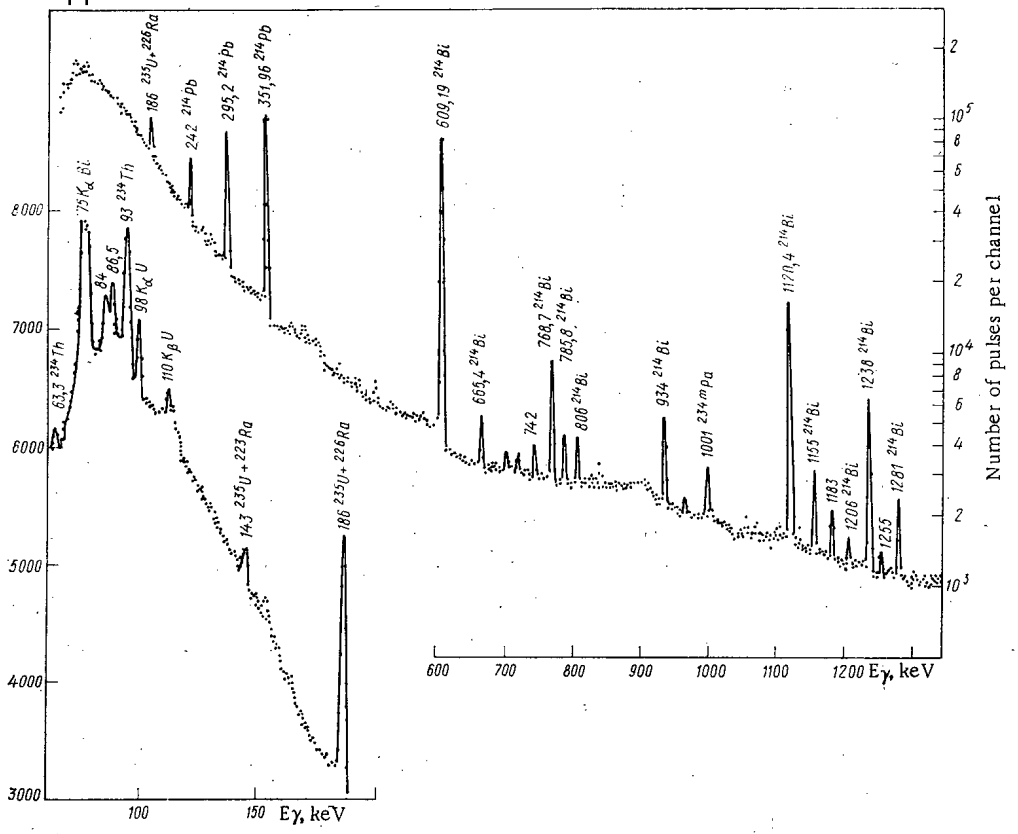

Fig. 2. γ-Ray spectrum from model of a stratum of equilibrium uranium ore (model 1). T_{meas} = 120 min.

was proposed to determine the radium content of ore from the γ-ray lines of the radon decay products ^{214}Pb(RaB) and ^{214}Bi(RaC); the uranium content from the size of the 186 keV peak due to the 185.7 and 186.2 keV γ-rays from ^{235}U and ^{226}Ra respectively. The contribution of the radium γ-radiation to the composite peak is taken into account.

The radium and uranium content can be determined by this method only for weak emanation of the ore since the disturbance of equilibrium between radium and radon is neglected.

There is another possible way of making an independent determination of uranium and radium which does not depend on weak emanation of the ore. In this method the uranium content is determined first from the intensities of the γ-ray lines from isotopes which are always in equilibrium with ^{238}U in ores, and then the radium content from the size of the 186 keV peak, taking account of the contribution of the uranium γ-radiation. In this case the uranium and radium contents and the emanating power of the ore can be determined by comparing the intensities of the γ-ray lines of ^{214}Pb or ^{214}Bi and ^{226}Ra.

To study the possibility of such a procedure the γ-ray spectra of three models of ore strata were measured. The first model was a mixture of sand and ore concentrate of equilibrium uranium (0.05% U), the second model was a mixture of sand and U_3O_8 with U in equilibrium with the short-lived deacy products (0.3% U), and the third model was a mixture of sand and the salt $Ba(Ra)SO_4$ (0.316% Ra units of equilibrium uranium). In all the models the bulk density of the material was 1.65 g/cm^3 and the effective atomic number was 13.36. The models with ore and radium salt were 40 × 40 × 50 cm and were hermetically sealed. The measurements were performed in a borehole which penetrated into the center of the model parallel to its long edge using a spectrometer with a 27 cm^3 Ge(Li) detector having an energy resolution of 2.5 keV at the 1.33 MeV ^{60}Co line.

The lines of ^{234}Th(UX$_1$), ^{235}U(AcU), and ^{234m}Pa are clearly separated in the spectrum of the γ-radiation from model 2 (Fig. 1). The measurements in model 1 (Fig. 2) showed that for analytic purposes it is necessary to use the 1001 keV line of ^{234m}Pa since it is not masked by radiation from uranium decay products or by scattered radiation in the spectrum of the ore stratum.

The absolute counting rate in the 1001 keV photopeak was 21 pulses/min for a ratio of peak height to background of 0.67. The corresponding values for the composite 186 keV peak were 570 pulses/min and 0.56. The sensitivity of determining uranium from the 1001 keV peak was 4.2 pulses/min for 0.01% U.

The threshold of sensitivity in the experiment was about 0.02% U for a 10 min measurement. The threshold of sensitivity was taken as that concentration of uranium for which the number of pulses recorded in the peak was three times the mean square error in the determination of the background under the peak.

The content of radioactive isotopes was calculated by comparing the areas of the corresponding peaks in the spectra measured opposite the ore stratum and in the standard model with known uranium, radium, and radon contents. In doing this the dependence of the detector efficiency on the γ-ray energy is automatically taken into account.

To take account of the possibility of different absorption of γ-radiation in the stratum and in the standard model the areas of the corresponding peaks were corrected by constructing a curve of the ratio of the areas of the peaks of the γ-ray lines of the radon decay products obtained by measurements opposite the ore stratum and in the model. The curve of the ratios extrapolated to 186 keV gives the correction factors for the 1001 and the 186 keV peaks.

The authors thank Yu. S. Shimelevich and V. L. Shashkin for helpful advice and a discussion of the work.

LITERATURE CITED

1. Yu. F. Baryshev et al., Preprint OIYaI 18-5199, Dubna (1970).
2. P. Dumesnil and C. Andrieux, Industr. Atomiques, 14, 29-40 (1970).

INVESTIGATION OF THE CHARACTERISTICS OF LAVSAN TRACK DETECTORS

V. P. Koroleva, V. S. Samovarov, and L. A. Chernov

UDC 539.1.074.88

Among solid track detectors used for the recording of fission fragments, the most widespread are various types of glass and mica. The properties of these materials have been comprehensively studied in [1, 2]. However, in many experiments it is preferable to use a film of Lavsan (polyethylene terephthalate), which has some advantages over glass and mice. Since it is strong and flexible, the film can take on any configuration without introducing any appreciable disturbances into the neutron fluxes in the closely spaced lattices of a nuclear reactor, whereas glass cannot always be bent to the desired shape and mica loses its detecting properties when it is deformed, as a result of cracks. The uranium content of Lavsan is approximately one-tenth that of glass and one-hundredth that of mica [3]. Consequently, for practical purposes, there is no background of spontaneous or induced fission introduced by the film into the neutron flux.

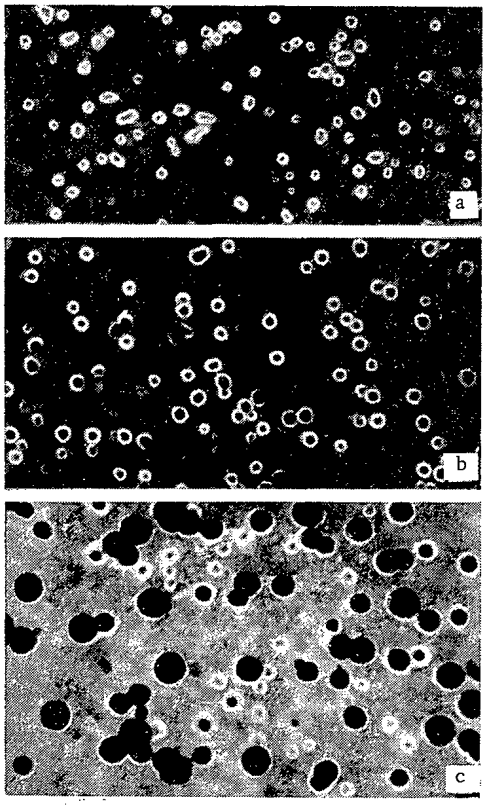

Fig. 1. Tracks of fragments from the fission of a layer of ^{235}U recorded on Lavsan for various etching times: a) 4 h; b) 6 h; c) 11 h.

In the study described in this report, we investigated the detecting properties of transparent Lavsan films 15, 20, and 35 μ thick, produced in the Soviet Union. The irradiation was carried out in a reactor, with the Lavsan mounted on uranium metal foil 0.1 mm thick. After etching, the fragment tracks were examined under an MIM-7 microscope at a magnification of 130.

Figures 1a, b, and c show the tracks of fragments from the fission of a layer of ^{235}U on Lavsan for various etching times (for t_e = 6 h we observe straight-through tracks). In Figs. 2-4 we show how the dimensions of the tracks vary with etching time (for two solvents), with solvent temperature, and with solvent concentration. The properties after

TABLE 1. Efficiency of Recording of Fission Fragments by Lavsan

Thickness of Lavsan, μ	Recording efficiency, %	Critical angle, degrees*	Factory of origin (in Moscow)
15	95±4	3	Kuskov
20	83±4	10	Dorogomilov
35	88±3	7	"

*The minimum angle between fragment trajectory and film surface for which tracks are recorded.

Translated from Atomnaya Énergiya, Vol. 35, No. 5, pp. 357-359, November, 1973. Original article submitted November 9, 1972.

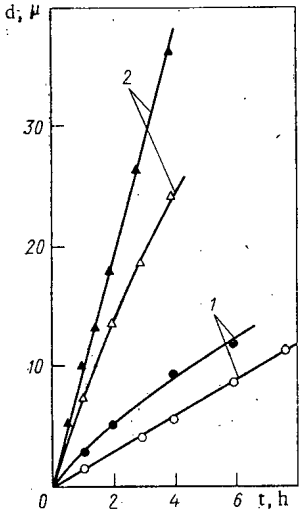

Fig. 2

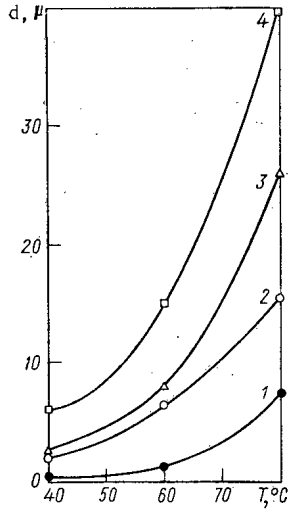

Fig. 3

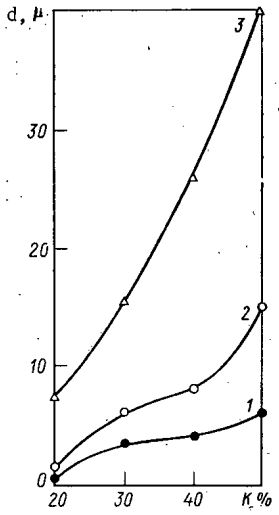

Fig. 4

Fig. 2. Dimensions of tracks of fragments from the fission of a layer of ^{235}U as a function of etching time for various chemical solvents (T = 60°C, concentrations 20 and 40% for curves 1 and 2, respectively): ●, ▲) NaOH; ○, △) KOH.

Fig. 3. Dimensions of tracks of fragments from the fission of a layer of ^{235}U as a function of the temperature of the KOH solvent at various concentrations (t_e = 1 h): 1) 20%; 2) 30%; 3) 40%; 4) 50%.

Fig. 4. Dimensions of tracks of fragments from the fission of a layer of ^{235}U as a function of the concentration of the KOH solvent at various temperatures (t_e = 1 h): 1) 40°C; 2) 60°C; 3) 80°C.

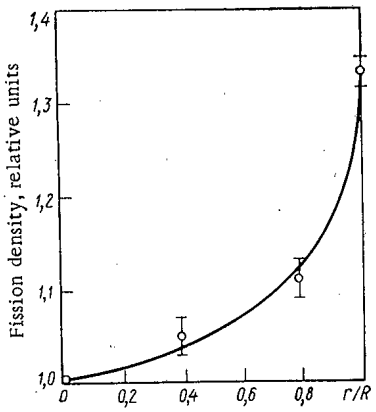

Fig. 5. Distribution of fission density as a function of fuel-element radius, as measured by means of Lavsan.

etching were found to be about the same for all the films we investigated, and the clearest picture of the tracks is obtained for the following etching conditions: solvent KOH, solvent concentration in water 30%, T = 60°C, t_e = 4 h.

The efficiency of recording of fission fragments by Lavsan when it was mounted on a source of fragments was determined by comparing the number of tracks produced by the fragments on the Lavsan to the fragment count obtained with a gold–silicon semiconductor counter having 100% efficiency, which was confirmed by the spectrum of pulses produced by the fission fragments. The fragment source used was a specimen of ^{252}Cf having an activity of $2.12 \cdot 10^4$ spontaneous fissions per hour; the specimen was 6 mm in diameter and was mounted on a tantalum backing. The results for the etching conditions selected are shown in Table 1, which also shows the mean-square error. The differences in efficiency may be due to the process of manufacture of the Lavsan.

The energy threshold for the recording of the fragments was determined by the method of slowing-down in aluminum foils of various thicknesses placed between the source and the Lavsan. Making use of the relation between the path length in aluminum and the energy of the fragments [4], we found that the fragment recording threshold for all three types of film was approximately 8 MeV.

As an example of the use of Lavsan in physics measurements, we may consider the distribution of fission density as a function of fuel-element radius (Fig. 5), obtained on a critical assembly [5]. The average point on the surface of the fuel element (r = R) was obtained by averaging the azimuthal distribution measured by means of a narrow strip of Lavsan wrapped around the fuel element half-way up its height. Similar measurements using Lavsan are of special interest for nonuniform reactor lattices.

LITERATURE CITED

1. V. P. Perelygin et al., Pribory i Tekh. Éksperim., No. 4, 78 (1964).
2. M. Debeauvais et al., Rad. and Isotopes, 5, 289 (1964).
3. A. Kapustsik et al., Pribory i Tekh. Éksperim., No. 7, 43 (1968).
4. C. Fulmer, Phys. Rev., 108, No. 5, 1113 (1957).
5. A. I. Mogil'ner et al., At. Energ., 24, No. 1, 42 (1968).

STABILITY CONDITIONS FOR THE STEADY STATE OF CONNECTED REACTORS

N. A. Babkin and V. D. Goryachenko

UDC 621.039.516

In the present paper sufficient conditions are determined for the stability "in the small" of a group of an arbitrary number of different nuclear reactors for quite general assumptions concerning the form of the neutron interactions and the internal feedbacks within each reactor.

Our starting point is the theorem of Hadamard [1], according to which the determinant $\Delta = \det(a_{ij})$ is different from zero if

$$|a_{ii}| > \sum_{j \neq i}^{n} |a_{ij}|; \quad i = 1, \ldots, n.$$

We consider the determinant $\Delta(s) = \det[\psi_{ij}(s)]$, where the function ψ_{ij} of the complex variable s obeys the inequality

$$|\psi_{ii}(s)| > \sum_{j \neq i}^{n} |\psi_{ij}(s)| \text{ for } \operatorname{Re} s \geqslant 0; \quad i = 1, \ldots, n. \tag{1}$$

According to the theorem, the determinant $\Delta(s)$ cannot equal zero when $\operatorname{Re} s \geq 0$; consequently, all the roots of the equation

$$\Delta(s) = \det[\psi_{ij}(s)] = 0$$

have negative real parts.

The last equation can be considered as the characteristic equation of a multivariate linear dynamical system with either lumped parameters, or a deviation argument, or with distributed parameters. For each of these cases in turn the function $\psi_{ij}(s)$ will be a polynomial, a quasipolynomial, or a function of s of a more complex nature, respectively.

We use these results to obtain the stability conditions for the steady state of a group of reactors. We restrict ourselves to the analysis of stability "in the small" and make use of the previously obtained [2] form of the linearized dynamical equations of the group of reactors

$$\frac{dx_i}{dt} = -\int_0^t f_i(t-\tau)\, x_i(\tau)\, d\tau + \int_0^t g_i(t-\tau)\, x_i(\tau)\, d\tau - \frac{\beta_i}{l_i} x_i + \sum_{j=1}^{M} \varkappa_{ij} \left[\int_0^t \varphi_{ij}(t-\tau)\, x_j(\tau)\, d\tau - x_i \right]; \tag{2}$$

$$i = 1, \ldots, M; \quad j \neq i.$$

Here x_i is the relative deviation of the power of the i-th reactor from its stationary level; β_i and l_i are, respectively, the delayed neutron source fraction and the neutron lifetime in the i-th reactor. The kernels f_i and g_i respectively describe the internal feedbacks and the delayed neutron sources in the reactor with index i; $\varkappa_{ij}$ is a positive constant proportional to the neutron coupling coefficient between the reactors with indices i and j. The function φ_{ij} describes the distribution (in time) of the probability of transition of neutrons from the j-th to the i-th reactor. It is evident that

$$\varphi_{ij}(t) \geqslant 0; \quad \int_0^{\infty} \varphi_{ij}(t)\, dt = 1; \quad i, j = 1, \ldots, M. \tag{3}$$

The characteristic equation of the system (2) is

Translated from Atomnaya Énergiya, Vol. 35, No. 5, pp. 359-360, November, 1973. Original article submitted February 7, 1973.

$$D(s)=\begin{vmatrix} w_1(s)+\sum_{j\neq 1}^{M}\varkappa_{1j} & -\varkappa_{12}\Phi_{12}(s) & \dots & -\varkappa_{1M}\Phi_{1M}(s) \\ -\varkappa_{21}\Phi_{21}(s) & w_2(s)+\sum_{j\neq 2}^{M}\varkappa_{2j} & \dots & -\varkappa_{2M}\Phi_{2M}(s) \\ \dots & \dots & \dots & \dots \\ -\varkappa_{M1}\Phi_{M1}(s) & -\varkappa_{M2}\Phi_{M2}(s) & \dots & w_M(s)+\sum_{j=1}^{M-1}\varkappa_{Mj} \end{vmatrix}=0, \tag{4}$$

where

$$w_i(s)=s+\frac{\beta_i}{l_i}+F_i(s)-G_i(s),$$

and Φ_{ij}, F_i, and G_i are Laplace transformations of the functions φ_{ij}, f_i, and g_i, respectively. Because of the conditions (3), the functions Φ_{ij} satisfy the inequalities

$$|\Phi_{ij}(s)|\leqslant 1 \text{ for } \operatorname{Re} s\geqslant 0;\ i,\ j=1,\dots,M, \tag{5}$$

this is easily established directly from the definition of the Laplace transformation.

We remark that when there is no interaction between the reactors (all $\varkappa_{ij}=0$), Eq. (4) breaks up into M independent equations

$$w_1(s)=0,\ \dots,\ w_M(s)=0,$$

each of which is a characteristic equation for an individual reactor isolated from the other reactors of the group.

The stability conditions for the group of reactors is formulated in the form of the following assertion.

The solution of the system (2) is zero, and consequently the steady state of the group of reactors is asymptotically stable if

$$\operatorname{Re} w_i(s)>0 \quad \text{for} \quad \operatorname{Re} s\geqslant 0;\ i=1,\dots,M. \tag{6}$$

The proof of this assertion is established by direct verification of the condition (1) for

$$\psi_{ii}=w_i(s)+\sum_{j=1}^{M}\varkappa_{ij};\ \psi_{ij}=-\varkappa_{ij}\Phi_{ij}(s);$$

$$i\neq j;\ i=1,\dots,M.$$

Taking into account the conditions (5) and (6) we have

$$|\psi_{ii}|=\sqrt{\left[\operatorname{Re} w_i(s)+\sum_{j=1}^{M}\varkappa_{ij}\right]^2+[\operatorname{Im} w_i(s)]^2}>\sum_{j=1}^{M}\varkappa_{ij}\geqslant\sum_{j=1}^{M}\varkappa_{ij}|\Phi_{ij}(s)|=\sum_{j=1}^{M}|\psi_{ij}|;$$

$$i\neq j;\ i=1,\dots,M.$$

Thus the inequalities (1) are satisfied. Consequently, when conditions (6) hold, Eq. (4) has no roots with $\operatorname{Re} s\geq 0$. The assertion is therefore proven.*

The characteristics of the results obtained are as follows.

1. The conclusion concerning the location of the roots of the equation $\det[\psi_{ij}(s)]=0$ in the left half plane of s (when condition (1) is satisfied) is a direct generalization of the sufficient stability condition obtained in [3] for a linear system with lumped parameters (in [3] $\psi_{ij}(s)=a_{ij}=\text{const}$; $\psi_{ii}(s)=s+a_{ii}$; $a_{ii}=\text{const}$).

2. The stability conditions (6) are a direct generalization of those of [2], in which the analogous result for the particular case of two connected reactors was obtained by a different method. The stability of a group of an arbitrary number of different reactors has not been considered in the literature.

3. The stability conditions (6) were obtained for any physically realizable values of the coupling coefficients $\varkappa_{ij}$ and arbitrary neutron interaction laws (satisfying the physically-required inequalities (3)).

* It is possible to allow the equality sign in conditions (6), but to stipulate that there are no zero roots of Eq. (4). This stipulation is quite natural, since the theory of stability in the small which we have used is not applicable when there are zero roots.

4. The criterion (6) is sufficient. It consists in the fulfillment of the sufficient conditions for stability for each of the M reactors within the group of reactors.

5. The stability criterion is not excessively restrictive. It is less restrictive than the frequency criterion of Velton for an individual reactor [2]. The proof of the condition (6) is simple: with some restrictions it leads to the proof of the frequency conditions

$$\operatorname{Re} w_i(j\omega) > 0 \text{ for all } \omega \geqslant 0$$

for each reactor of the group of reactors.

LITERATURE CITED

1. M. Parodi, The Localization of the Characteristic Numbers of Matrices and Its Application [in Russian], IL, Moscow (1960).
2. V. D. Goryachenko, "On the stability of connected nuclear reactors," At. Énerg., 30, No. 4, 381 (1971).
3. V. V. Dobronravov, "On the construction of sufficient stability criteria," Avtomatika i Telemekhanika, 17, No. 3, 211-216 (1956).

THE ROLE OF THE ACCOMMODATION COEFFICIENT IN CONTACT HEAT EXCHANGE

V. V. Kharitonov, L. S. Kokorev, and N. N. Del'vin

UDC 621.039.517.5

The simplest estimate of the heat conduction α through a layer δ shows that the magnitude of α is directly proportional to the thermal conductivity λ of the layer:

$$\alpha = \lambda/\delta. \quad (1)$$

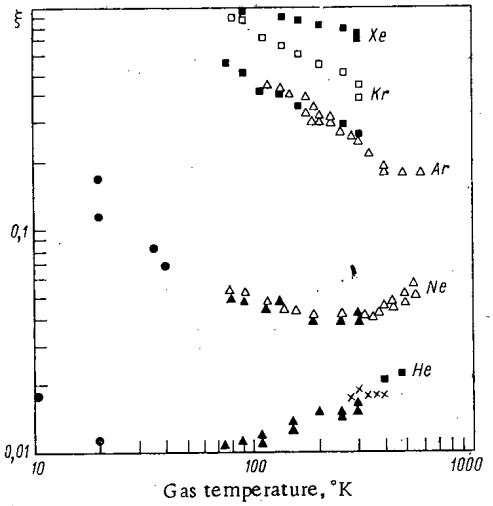

Fig. 1. Temperature dependence of quantity ξ of inert gases on pure tungsten surfaces.

However, on the basis of the results, analyzed in [1], of bench experiments and in-reactor experiments, we drew an unexpected, in our view, conclusion: the conduction of the gap between the fuel and the jacket in the fuel elements is independent of the composition of the gas mixture inside the jacket. It also proves to be unjustified to assume that there is a deterioration in the working characteristics owing to the changing composition of the gas during operation of the fuel elements [1].

We attempt to explain these results by the features of the interaction of the gas with the walls of the gap.

The length of the temperature jump at the gas–solid boundary [2] is a quantity of order

$$\delta_t \approx l/\xi, \quad (2)$$

where l is the mean free path of the gas molecule; ξ is the coefficient of accommodation, characterizing the mean fraction of energy exchanged during a single collision between the gas and the solid at the boundary. Thus, for helium at normal pressure and temperature 1000°C the quantity $l \approx 1\ \mu$. If

TABLE 1. Heat Conduction (3) of Gas Gaps at T = 500°K, Pressure 0.1 atm, and $\delta_t/\delta > 1$.

Gas, in gap	He	Ne	Ar	Kr	Xe	Wall material
$\xi\lambda$, mW/(m·deg) α, kW/(m²·deg)	4,6 1,5	3,2 2,0	4,0 3,4	3,1 2,9	4,1 4,0	Pure tungsten*
$\xi\lambda$, mW/(m·deg) α, kW/(m²·deg)	0,20 40 8,5	0,47 30 14	0,72 16 11	0,78 9 6,5	0,82 6 5	Platinum with gas adsorbed on the surface†

* The quantity ξ is taken from Fig. 1.

† The quantity ξ is taken from [4].

Translated from Atomnaya Énergiya, Vol. 35, No. 5, pp. 360-361, November, 1973. Original article submitted February 9, 1973.

$\xi = 0.01$, then $\delta_t = 0.1$ mm. If δ_t exceeds the mean thickness of the gas gap δ, the heat conduction of the latter can be estimated in the first approximation by the expression

$$\alpha \approx \xi\lambda/l \tag{3}$$

instead of (1). It is known that the coefficient of thermal conductivity of gases is inversely proportional to their atomic weight m; the ratio $\lambda/l \sim 1/\sqrt{m}$.

The quantity ξ depends on the properties of the gas and the solid, and also on the parameters of their atomic interaction. Figure 1 shows the temperature dependence of the coefficient of accommodation of inert gases on pure tungsten surfaces, constructed on the basis of experimental data of different authors from [3].* As can be seen from Fig. 1, the value of ξ, unlike the coefficient of thermal conductivity of gases, increases for increasing atomic weight of the gas. This holds both for pure and also for contaminated surfaces of solids (see Table 1).

Thus, the accommodation coefficients of different gases on the given surface for the same temperature are inversely related to their coefficients of thermal conductivity. As a result of this the heat conduction (3) of the gas gaps, the thickness of which is no greater than the length (2) of the temperature jump, depends weakly on the nature of the gas (see Table 1). The transport of part of the heat by radiation and through the point of direct contact of the fuel with the jacket makes this dependence even weaker. From Table 1 it follows that for Knudsen numbers (l/δ) of the order of or greater than unity the heat conduction of xenon in the gap, formed by pure surfaces of heavy metals, can slightly exceed the conduction of the gap with helium, although the thermal conductivity of the latter is thirty times greater than for xenon.

LITERATURE CITED

1. B. Lastman, Radiation Effects in Uranium Dioxide [in Russian], Atomizdat, Moscow (1964).
2. Yu. Yu. Abramov, Teplofiz. Vys. Temp., 8, No. 5, 1013 (1970).
3. L. Trilling, Surface Sci., 21, 337 (1970).
4. F. Reiter et al., Warme- und Stoffübertragung, 5, 116 (1972).

*On surfaces of uranium-containing compounds the quantity ξ should evidently be close to these values (see, for example, [1]).

FLUIDIZED OXIDATIVE DISAGGREGATION OF PELLETIZED NUCLEAR FUEL

A. T. Ageenkov, V. F. Savel'ev,
E. M. Valuev, N. A. Nilov,
E. N. Gal'perin, and E. I. Rybakov

UDC 621.039.54

Predispersal of nuclear fuel as a result of oxidation of uranium dioxide to uranyl uranate (mixed uranous–uranic oxide, U_3O_8) opens the way for more advantageous use of the advantages of fluidized-bed fluorinators [1-5]. This accounts for the search for an optimum-design fluidized-bed reactor and basic parameters of a process involving oxidative breakdown of pelletized nuclear fuel for power reactor fuel elements. The characteristics of the uranium dioxide employed in the work are listed in Table 1. The inert packing employed in the fluidized-bed fluorinator was aluminum oxide 100 μ mesh and 500 μ mesh.

Several models of fluidized-bed fluorinators (see Fig. 1) were tested with a view to arriving at a suitable reactor design for stable fluidization of a mixture of uranyl uranate and inert packing, taking advantage of the developed contact surface of the fuel pellets in the fluidized bed, and for eliminating any possibility of stagnant pockets forming in the reactor.

The tests revealed that, when no nuclear fuel is loaded, stable fluidization of the inert packing is achieved at a gas flowspeed of 0.03 to 0.05 m/sec, and 0.15 to 0.20 m/sec, for mesh sizes 100 μ and 500 μ, respectively.

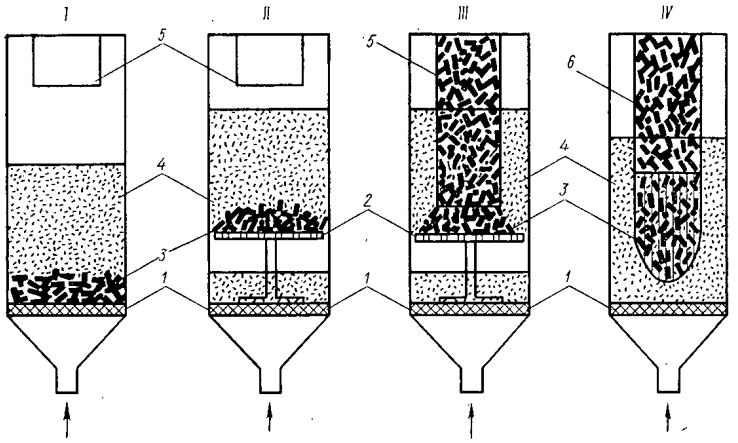

Fig. 1. Models of fluidized-bed fluorinators tested: I) UO_2 pellets rest on gas distributor grid, loading chute located outside fluidized bed zone; II) UO_2 pellets rest on elevated support grid, loading chute located outside fluidized bed zone; III) UO_2 pellets stacked up on support grid, loading chute located in interior of fluidized bed; IV) UO_2 pellets accommodated within slotted-grid oxidizing basket; 1) gas distributor grid; 2) elevated support grid; 3) UO_2 pellets; 4) fluidized bed; 5) loading chute; 6) oxidizing basket.

Translated from Atomnaya Énergiya, Vol. 35, No. 5, pp. 362-363, November, 1973. Original article submitted April 12, 1973.

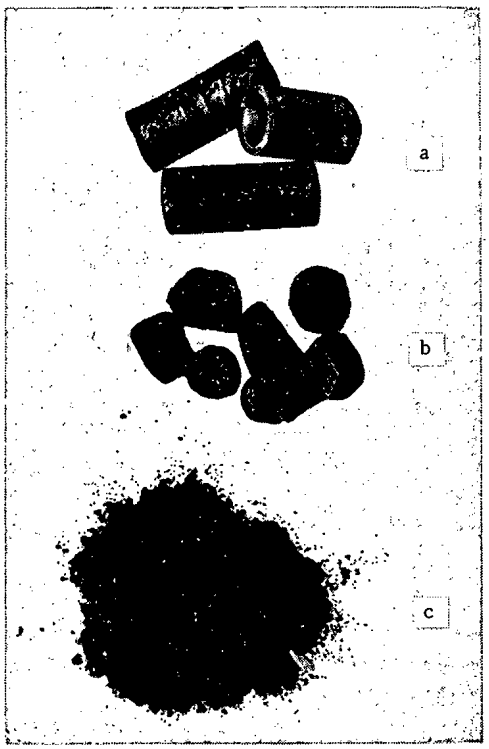

Fig. 2. Products of oxidative disaggregation: a) original UO_2 pellets; b) intermediate product; c) powdery uranyl uranate end product.

TABLE 1. Characteristics of Original Uranium Dioxide

Shape	Granulometic composition		Mean bulk density, g/cm³
	size, mm	amount, %	
Pellets	Diameter 12		
	Height 20–25	100	5,75
Lumps	−4 +2	46,5	6,90
	−2 +1	30,0	
	−1	23,5	
Pellets after thermal decladding of fuel elements	+6	29,0	6,70
	−6 +1	45,0	
	−1	26,0	

The way the uranium dioxide pellets are loaded into the reactor seriously affects the progress of fluidization of the packing in the reactor. Contact between the fluidized packing and the impinging uranium dioxide pellets is minimal in reactor models I-III. The fluidized packing is located outside the layer of fuel pellets in model II. The fluidized bed is separated into two distinct zones in models II and III: layers of UO_2 pellets are found at the top and at the bottom. Accumulations of sluggishly moving aluminum oxide powder, and voids alternately, are observed between the pellets within the uranium dioxide layer. In the type IV reactor, more homogeneous fluidization is achieved through the reactor volume, including in the layer of UO_2 pellets. Circulation of inert packing powder through the free space between pellets lodged in the oxidizing basket was reported. Subsequent investigations were staged in a type IV fluidized-bed reactor made from Kh18N10T, as a 100 mm diameter model. The oxidizing basket was made from steel rods spaced 3 to 5 mm apart.

At first weighed portions of 200 to 500 g uranium dioxide each were oxidized in air under the optimum fluidization conditions arrived at in the experiment. Complete breakdown of the compact uranium dioxide resulted at temperatures 420-450°C within 15 min, culminating in the formation of a finely dispersed uranyl uranate mixture uniformly distributed throughout the inert packing. While the experiment was in progress, some of the uranyl uranate formed was carried out of the reactor, entrained in the gas stream, to the filter. The dependence of the rate of breakdown of the UO_2 pellets and the rate of entrainment of the U_3O_8 formed, on the content of the material in the fluidized bed, for Al_2O_3 sized 100 μ, is expressed by the equations

$$V_{oxid} = 25 + 0.6\, e^{-0.02\, C};$$

$$V_{entr} = 0.0032\, C^2 - 0.008\, C,$$

where V_{oxid} is the rate of oxidative disaggregation of the UO_2 pellets, in g/dm³·min, V_{entr} is the rate of U_3O_8 entrainment out of the fluidized-bed reactor, in g/dm³·min, and C is the U_3O_8 concentration in the fluidized bed, in wt.% (from 3 to 35%).

It was shown that when the inert packing becomes saturated higher than 30-40% with uranyl uranate, the mixture becomes recalcitrant to fluidization, begins to cake up, and moves only sluggishly.

In subsequent experiments using weighed portions of UO_2 up to 10 kg, oxidative breakdown of the uranium dioxide was carried out to the point where not more than 35% of the U_3O_8 accumulated within the inert packing, after which pneumatic conveying was resorted to to move the mixture forming off to the oxidized product collector. The gas was scrubbed on a cermet filter of pore size 3-5 μ.

We infer from the experimental data and from analysis of the end product in the experiments that complete disaggregation of the fuel was achieved in all the experiments using pellets and lumps of uranium dioxide at temperatures 450-500°C. It was found that an increase in the size of the inert packing material

from 100 to 500 μ exerted a positive stabilizing effect on the oxidative process. In that case the process of abrasive stripping of the uranyl uranate from the surface of the uranium dioxide pellets and removal of the uranyl uranate from the oxidation reaction zone to the fluidized bed becomes intensified. The UO_2 pellets feature a rounded shape (see Fig. 2) in the intermediate stage of oxidation.

The disaggregation of the uranium dioxide following thermal decladding of the fuel elements also goes to completion to a rather great extent (99.7 to 99.8%). But the admixture of structural material from the cladding (0.5 to 0.7 wt.%) lends some special features to the process. First to break down are pellets containing no components derived from the cladding. Next follows oxidation of the remaining material, which includes partially collapsed UO_2 pellets with admixtures of zirconium, iron, and so forth. It is to be noted that particles of the fuel-element cladding material in amounts up to 70 g per 10 kg of oxidized nuclear fuel remain in the reactor after the mixture of uranyl uranate and aluminum oxide has been swept out by pneumatic conveying, i.e., there is some additional removal of impurities from the uranium.

Several batches of the resulting mixture of inert packing filler and uranyl uranate were fluorinated in the fluidized-bed fluorinator. Virtually complete conversion of the uranium to hexafluoride was achieved. The degree of fluorination of the inert filler and aluminum oxide was less than 1%, which made it possible to recycle the mixture through the oxidation–fluorination cycle.

LITERATURE CITED

1. U. D. Veryatin et al., "Basic problems in the fluoride method of reprocessing fuel elements from fast-reactor nuclear power stations," IV Geneva Conference (1971) on the Peaceful Uses of Atomic Energy, P/448.
2. J. Anastasia et al., Ind. and Engng. Chem., Process and Design Development, 4, No. 3, 338 (1965).
3. Nucl. Appl., No. 5, 320 (1968).
4. V. N. Prusakov, Report presented at the 36th International Congress on Industrial Chemistry, Brussels (1966).
5. V. N. Prusakov, O. G. Lebedev, and G. P. Guzhev, "Investigation of fluorination of uranyl uranate in a fluidized bed," Report to the II COMECON Symposium on Spent-Fuel Reprocessing, CSSR (1971).

RADIATION EFFECTS IN CESIUM IODIDE SINGLE CRYSTALS ACTIVATED BY THALLIUM UNDER GAMMA RADIATION

I. A. Berezin, V. M. Gorbachev, V. V. Kuzyanov, I. N. Sten'gach, and N. A. Uvarov

UDC 539.1.074.3

When thallium-activated single crystals of cesium iodide used for recording γ-rays are exposed to significant doses of penetrating radiation, there is an appreciable increase in the number of crystal defects that produce coloring and a change in the light yield and luminescence spectra of the crystal [1-3]; this may, in turn, change the γ-ray recording efficiency.

In the study presented here we investigated the luminescence spectra and light yield of CsI(Tl) crystals as functions of the γ-ray dose up to 10 Mrad, the recovery of the scintillation properties of single crystals during storage, the variation of the degree of radiation damage to the crystals as a function of thallium content, and the influence of prior heat treatment on increased radiation stability in a scintillator.

In our investigations we used the bremsstrahlung of electrons from a linear accelerator (electron energy approximately 15 MeV, current approximately 30 μA [4]) and γ-quanta from a cobalt gun (γ-quanta from ^{60}Co, E_γ = 1.27 MeV and 1.33 MeV). In the first case the irradiated specimens of CsI(Tl) crystals were placed at a distance of 20 cm from the lead target of the accelerator. The absorbed γ-ray dose rate at this point, as measured by an air-equivalent chamber, was $2.5 \cdot 10^3$ rad/sec. The irradiation doses reached values as high as 10 Mrad. The cobalt gun was used for investigating the effect of doses of less than $3 \cdot 10^5$ rad on the crystals. In this case the γ-ray doses were determined by means of glass dosimeters.

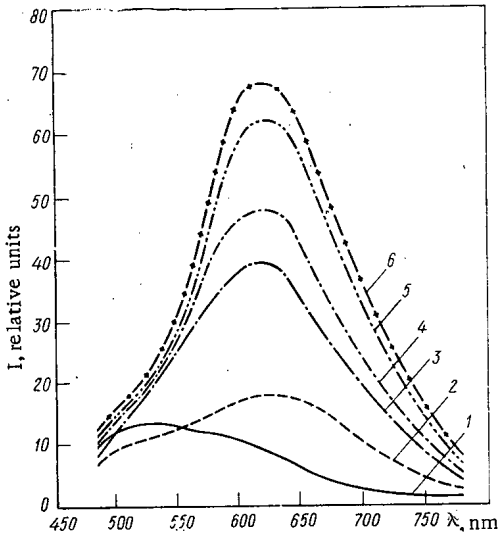

Fig. 1. Luminescence spectra of crystal A-197-69 after γ-ray irradiation: 1) before irradiation; 2-6) after irradiation with doses of 24, 100, 134, 260, and 380 krad, respectively.

The variation in the integral light yield of the CsI(Tl) crystals during the irradiation process was recorded by a photoelement with an antimony–cesium cathode, type FÉK-12 [5]. Only the scintillator was placed in the zone of the beam of bremsstrahlung quanta emanating from the lead target. Through an air-filled light guide with reflecting walls, the light of the luminescence reached the photoelement, which was shielded by lead against scattered radiation. The current in the photoelement, proportional to the light yield of the crystal, was recorded by means of an electrometric amplifier.

The luminescence spectra of the crystals were measured by means of an ISP-51 spectrograph with an FÉP-1 photoelectric attachment before and after the irradiation. The crystals were placed in front of the entry slit of the spectrograph. The luminescence of the crystals was excited by means of ultraviolet light from an SVDSh-250 mercury lamp with an ultraviolet light filter. The intensity of the

Translated from Atomnaya Énergiya, Vol. 35, No. 5, pp. 364-366. November, 1973. Original article submitted April 25, 1973.

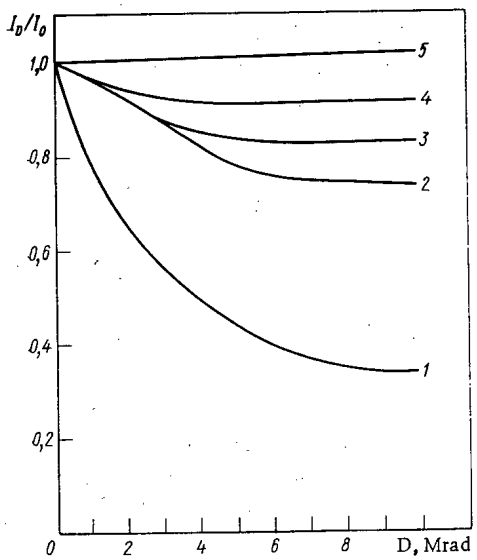

Fig. 2

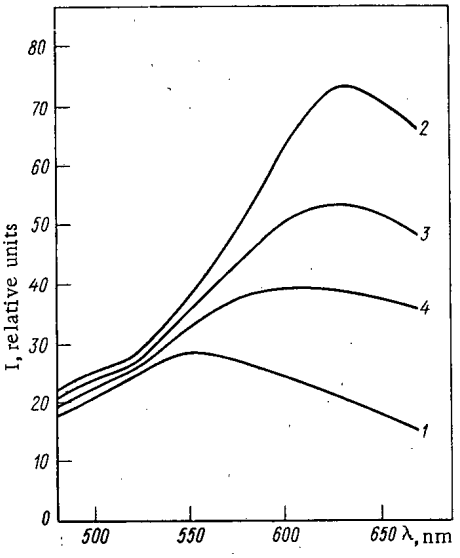

Fig. 3

Fig. 2. Variation in light yield of crystal A-460-69 as a function of γ-ray dose: 1) without annealing; 2) after first annealing (150°C, 14 h); 3) after second annealing (400°C, 30 h); 4) after fourth annealing (400°C, 70 h); 5) level of luminescence intensity without radiation damage.

Fig. 3. Luminescence spectra of crystal A-460-69 (γ-ray dose 10 Mrad): 1) unirradiated specimen; 2) specimen irradiated before annealing; 3) specimen irradiated after first annealing (400°C, 3 h); 4) specimen irradiated after second annealing (400°C, 6 h).

luminescence was recorded with an FÉU-22 photomultiplier.

In our study we used single crystals of cesium iodide activated thallium. Before the measurements the specimens were taken out of the containers in which they had been packed at the factory. The end faces of the crystals were polished. In a number of cases, especially for prolonged measurements, the specimens were sawed into two pieces; one was exposed to radiation, while the other was used as a control specimen.

We investigated 13 CsI(Tl) crystals, which had been produced between the years 1956 and 1969. Figure 1 shows the luminescence spectra of CsI(Tl) crystals after irradiation with various doses of ^{60}Co γ-rays ranging from $24 \cdot 10^3$ rad to $4 \cdot 10^5$ rad.

The spectra of the unirradiated crystals cover a wide range of wavelengths and have a broad peak at 480-550 nm, with a smooth decrease in intensity toward the short-wave and long-wave regions. After irradiation, the spectrum showed a second maximum in the neighborhood of 620 nm; the intensity of this maximum at first increases rapidly with increasing dose of absorbed radiation but then becomes stabilized and approaches a limit.

After the single crystals have been irradiated with a dose of 10^5 rad, the intensity of their luminescence in the orange and red parts of the spectrum increases considerably, while it decreases somewhat in the blue and violet regions. The pattern of increased luminescence intensity in the 550-700 nm region differs with crystals of different years of manufacture. In crystals dating from 1956 the increase factor is no more than 1.3-1.5, whereas in crystals dating from 1969 the increase factor reaches values of 3-10.

This indicates that crystals which have been stored for a long time are less affected by radiation.

The radiation effects produced in CsI(Tl) crystals depend to a large extent on the thallium content of the specimen. The data on thallium content* were compared with data on changes in the spectral composition of the luminescence from the crystals when exposed to γ-radiation. The criterion for the estimate

*The thallium content of 10 CsI(Tl) crystal specimens manufactured during the years 1956-1969 was determined by spectral analysis.

of radiation effects was taken to be the ratio of luminescence intensity in the orange region of the spectrum (λ = 620 nm) before and after irradiation: $\beta = I_\gamma(\lambda = 620\ \text{nm})/I_0(\lambda = 620\ \text{nm})$. In crystals manufactured in a given year the radiation effects are stronger when the thallium concentration is higher. Thus, when a radiation dose of $3 \cdot 10^4$ rad was applied to single crystals manufactured in 1969 and having thallium concentrations of 0.014%, 0.020%, 0.029%, and 0.037%, the ratio of intensities in the 620 nm region was 1.7, 2.5, 3.2, and 5.2, respectively. When the same dose was applied to crystals manufactured in earlier years, a similar change in intensity corresponded to higher concentrations (for example, crystal B-87-56, manufactured in 1956 and having a thallium concentration of 0.078%, changed in intensity in the 620 nm region by a factor of only 1.8).

Typical characteristics for the change in integral light yield of a crystal, as recorded by a photoelement with an antimony–cesium cathode, are shown in Fig. 2. As a rule, the light yield of the scintillator decreases continuously as the integral dose of radiation increases. For an integral dose greater than 5 Mrad, the light-yield level for most crystals stabilizes at a value of 30-40% of the initial values for crystals manufactured in 1969 and 60-70% for crystals manufactured in 1956.

The dispersion of the optical characteristics of the crystals when acted upon by γ-rays is very significant and is apparently determined by the manufacturing tolerances and storage times of the crystals. The degree of radiation damage depends only slightly on the size of the scintillator, and this indicates that the change in the spectrum and the light yield is caused primarily by a change in the character of the luminescence, not by poor transparency to the crystal's own radiation.

When the CsI(Tl) crystals are stored at room temperature, they are less strongly colored, and the radiation spectrum approaches the spectrum for the unirradiated specimens. However, restoration of the colored crystals is slow, and even when a month has passed after the irradiation, the initial properties are not completely restored. The process of color loss by the crystals is considerably accelerated if the temperature is increased. Thus, heating irradiated crystals for 1 h at 150°C completely restores their original color and their original luminescence spectrum.

When irradiated crystals of CsI(Tl) were annealed for a prolonged period, we observed a decrease in the effects produced by the radiation in the crystals. For investigation purposes, we cut the crystals into two parts: one was irradiated without prior annealing, the other was irradiated after annealing at 150°C or 400°C for various lengths of time ranging up to 70 h.

In all cases investigated, prior annealing of CsI(Tl) crystals brought an increase in their radiation stability, i.e., a smaller change in the spectral composition and light yield of the luminescence after irradiation with a dose of approximately 10 Mrad (Fig. 3). As the temperature and duration of the annealing was increased, an increase was observed in the radiation stability of the crystals. Thus, when a dose of 10 Mrad was applied to crystal A-460-69 before annealing, its integral light yield changed by a factor of 2.8. After the crystal had been annealed for 70 h at 400°C, the same dose reduced the light yield by only 10%.

The increase in the radiation stability of CsI(Tl) crystals after heat treatment can be clearly seen from the example of specimen A-273-69. The luminescence spectrum of this crystal before heat treatment was sharply changed even by exposure to ultraviolet rays. After annealing the luminescence intensity remained unchanged upon prolonged irradiation with ultraviolet light, and the amount of change produced in the spectrum by γ-rays became much smaller.

Heat treatment orders the structure in the crystal lattice and consequently reduces the probability of formation of coloring centers. X-ray investigations [6] confirmed that annealing improves the structure of the crystal. The fact that the radiation effects are less conspicuous in the 1956 crystals than in crystals produced in recent years is attributable to the fact that during a 15 year period of storage the process of structural improvement progressed to a considerable extent even at room temperature.

The effects noted in this article must be taken into account when radiometric studies are conducted in high-intensity γ-ray fields.

LITERATURE CITED

1. Z. L. Morgenshtern and I. P. Shchukin, Opt. i Spektr., 1, 190 (1956).
2. P. P. Feofilov, ibid., 1, 952 (1956).
3. A. N. Pisarevskii and V. D. Teterin, Izv. Akad. Nauk SSSR, Ser. Fiz., 32, 23 (1958).

4. T. N. Filimonova and A. M. Shmygov, Zh. Tekh. Fiz., 32, No. 12, 1438 (1962).
5. B. M. Stepanov et al., "Coaxial photoelements for recording rapid optical processes," in: Pulse Photometry [in Russian], Mashinostroenie, Leningrad (1969), p. 17.
6. L. M. Shamovskii, L. M. Rodionova, and A. S. Glushkova, Izv. Akad. Nauk SSSR, Ser. Fiz., 22, 3 (1958).

POSITRON SPECTRA GENERATED BY BREMSSTRAHLUNG WITH ENERGIES UP TO 800 MeV

G. V. Potemkin and S. A. Vorob'ev

UDC 539.124.6

In the majority of cases, positrons are obtained by conversion of a beam of high energy electrons in a linear accelerator [1, 2] or in a synchrotron [3, 4], using a material of high atomic number for the converter. When there is no extracted electron beam, positrons can be obtained by conversion of a beam of bremsstrahlung from a synchrotron [5-7]. The positron beam obtained in this way has a comparatively long radiation pulse time, which permits the study of the interaction of positrons with matter. In order to determine the parameters of such beams (parameters such as the positron energy distribution and the optimal converter thickness), studies of the conversion of bremsstrahlung into high energy positrons were conducted at the "Sirius" synchrotron of the Tomsk Polytechnical Institute; the results obtained are presented below.

Figure 1 gives a diagram of the layout of the experimental apparatus. A beam of bremsstrahlung, generated on an internal synchrotron target T (0.4 mm tantalum), is shaped by two collimators K_1 and K_2 (the hole diameters are 24 and 10 mm, respectively) and is cleansed of charged particles by the magnet OM of the type SP-58-01 with an interpolar gap of 50 mm and a magnetic field intensity in the gap of 30 kG. The narrow bremsstrahlung beam falls on the converter, situated in the analyzing magnet AM. The diameter of the bremsstrahlung beam is 17 mm at the converter, with a dispersion angle of the order of 0.8 mrad. The energy analysis of the positrons generated in the converter is performed with a magnetic spectrometer analogous to the electromagnet of the type SP-57-A-1 with triangular poles [8].

The positrons exiting from the magnetic spectrometer are recorded by a telescope of scintillation detectors C_1 and C_2 activated on coincidence. The scintillators used are plates of scintillation plastic with dimensions $20 \times 100 \times 10$ and $50 \times 100 \times 10$ mm. The beam of bremsstrahlung is monitored by the "transparent" ionization chamber M, calibrated by the Gauss photometer Q. The spectrum of synchrotron bremsstrahlung, measured by the pair magnetic γ-spectrometer, agrees well with the spectrum of Schiff [9]. Using the "transparent" ionization chamber, the number of equivalent γ-quanta of the beam of bremsstrahlung was determined; this number was held constant in each series of measurements, and was $N_{\gamma eq} = 0.72 \times 10^8$ for $E_{\gamma max} = 800$ MeV, and $N_{\gamma eq} = 1.22 \times 10^8$ for $E_{\gamma max} = 500$ MeV.

The energy dependence of the yield of positrons was measured for various thicknesses of Cu and Pb converters at zero angle relative to the direction of the bremsstrahlung beam incident on the target. The error of the measurement did not exceed 10 to 12%. The shape of the distribution curve is similar to the analogous curves for the energy dependence of electron–positron conversion [10], and differs only in a steeper fall-off on the decreasing side.

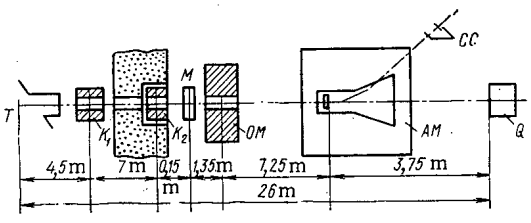

Fig. 1. Diagram of the experiment.

On the basis of the experimental number of equivalent γ-quanta determined, and the energy distribution of positrons, it is possible to find the conversion coefficient of bremsstrahlung to positrons

$$K(E_+) = \frac{N(E_+)}{N_{\gamma eq}\delta E_+ \Omega} \text{ MeV}\cdot\text{sterad}^{-1}.$$

Here $\delta = l_c/h_\varepsilon$ is the relative energy resolution of the magnetic spectrometer; this is determined by the horizontal

Translated from Atomnaya Énergiya, Vol. 35, No. 5, pp. 366-38, November, 1973. Original article submitted May 25, 1973.

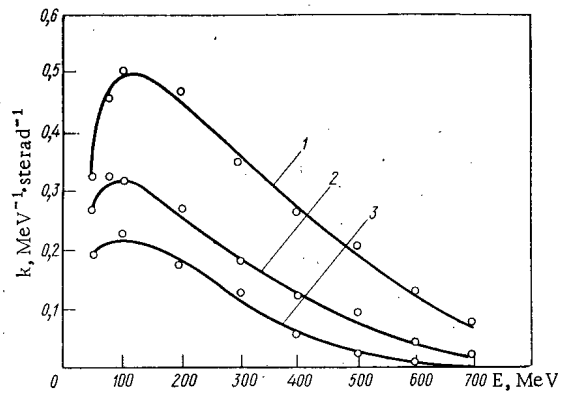

Fig. 2

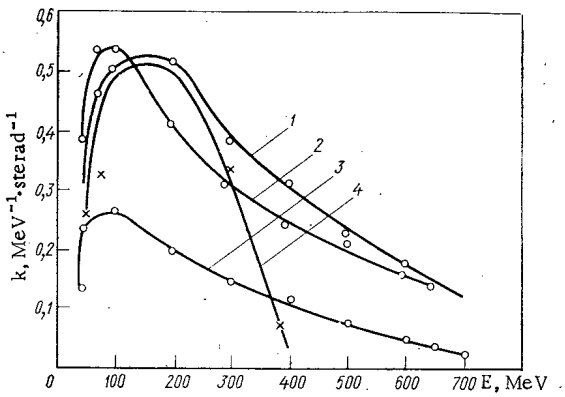

Fig. 3

Fig. 2. Dependence of the conversion coefficient on the positron energy for $E_{\gamma max}$ = 800 MeV and for a Cu converter: 1) 0.82 X_0; 2) 1.64 X_0; 3) 2.0 X_0.

Fig. 3. Dependence of the conversion coefficient on the positron energy for a Pb converter. For $E_{\gamma max}$ = 800 MeV: 1) 1.0 X_0; 2) 0.5 X_0; 3) 3.75 X_0. For $E_{\gamma max}$ = 500 MeV: 4) 1.0 X_0.

dimensions of the image, if the width of the counter l_c is greater than the horizontal dimensions of the image. The dispersion h_ε of the spectrometer is

$$h_\varepsilon = R(1-\cos\Phi) + l_2[\sin\Phi + (1-\cos\Phi)\operatorname{tg}\varepsilon_2],$$

where R = 163.5 cm is the radius of the trajectory of the particles in the magnetic field of the spectrometer; $\Phi = 38°$ is the angle of deflection of the particles; $\varepsilon_2 = 71°$ is the exit angle of the positrons from the magnetic field of the spectrometer; l_2 = 100.7 is the width of the scintillator of the first counter of the telescope. The luminosity of the spectrometer is given by

$$\Omega \approx 4\alpha_0\gamma_0,$$

where $\alpha_0 = 1 \cdot 10^{-2}$ rad and $\gamma_0 = 1 \cdot 10^{-2}$ rad are the maximum horizontal and vertical capture angles, respectively.

Figure 2 presents the dependence of the coefficient of conversion on the energy of the positrons for $E_{\gamma max}$ = 800 MeV, for Cu converters of various thicknesses. Figure 3 presents the same dependence for a Pb converter for $E_{\gamma max}$ = 500 and 800 MeV. A pronounced decrease in the coefficient of conversion is observed in the distributions obtained when $E_+ \leq 100$ MeV; this is caused by multiple scattering of the positrons in the material of the converter. Multiple scattering also leads to a relative increase in the high energy component of the positron energy spectrum when the thickness of the converter is increased.

It follows from the energy distributions obtained that the maximum coefficient of conversion lies in the range of positron energies $E_+ \leq 0.24\ E_{\gamma max}$ for thicknesses of the converter close to optimal.

In order to determine the optimal thickness, the dependence of the total coefficient of conversion (obtained by integration by computing the area under the corresponding curves for $K(E_+)$ on the thickness of the converter was obtained. The resultant distribution was of the "cascade type" with a maximum near $t_{opt} \approx 1.0\ X_0$. For an optimal Cu converter the total conversion coefficient is larger for $E_{\gamma max}$ = 800 MeV than it is for $E_{\gamma max}$ = 500 MeV. This agrees with the rule obtained earlier for the total optimal coefficient of conversion, which, for electron–positron conversion, has a linear character in the region of high energy [11]. However, an increase in the maximum energy of the bremsstrahlung quanta does not lead to a significant increase in the yield of positrons with energies near the maximum in the spectrum of the conversion coefficient. In general, the selection of the thickness and material of the converter should be determined by the conditions and intended use of the beam of positrons, taking into account their energy distribution.

LITERATURE CITED

1. R. Neal, Phys. Today, 20, No. 4, 27 (1967).
2. I. A. Grishaev et al., Usp. Fiz. Nauk, 13, No. 11 1926 (1968).
3. G. I. Budker et al., At. Énerg., 20, 206 (1966).
4. Yu. M. Ado et al., ibid., 23, 3 (1967).
5. B. Borgia, Nuclear Structure, University of California Press, Stanford (1964), p. 354.

6. A. A. Komar et al., Trudy FIAN, 22, 287 (1964).
7. A. A. Vorob'ev et al., The Program and the Texts of the Papers of the 21st Annual Conference on Nuclear Spectroscopy and the Structure of Atomic Nuclei [in Russian], Part 2, Nauka, Leningrad (1971), p. 134.
8. V. N. Kuz'min et al., in: Electron Accelerators – Papers of the 6th Interuniversity Conference [in Russian], Énergiya, Moscow (1968), p. 23.
9. A. F. Genning et al., in: Electron Accelerators – Papers of the 7th Interuniversity Conference [in Russian], Atomizdat, Moscow (1970), p. 31.
10. L. Katr and K. Lokan, Nucl. Instrum. Methods, 11, 7 (1961).
11. T. Aggson and F. Burnod, Report LAL-27 (1962).

breaking the language barrier

WITH COVER-TO-COVER ENGLISH TRANSLATIONS OF SOVIET JOURNALS

in physics

Title	# of Issues	Subscription Price
Astrophysics *Astrofizika*	4	$100.00
Fluid Dynamics *Izvestiya Akademii Nauk SSSR mekhanika zhidkosti i gaza*	6	$160.00
High-Energy Chemistry *Khimiya vysokikh énergii*	6	$155.00
High Temperature *Teplofizika vysokikh temperatur*	6	$125.00
Journal of Applied Mechanics and Technical Physics *Zhurnal prikladnoi mekhaniki i tekhnicheskoi fiziki*	6	$150.00
Journal of Engineering Physics *Inzhenerno-fizicheskii zhurnal*	12 (2 vols./yr. 6 issues ea.)	$150.00
Magnetohydrodynamics *Magnitnaya gidrodinamika*	4	$100.00
Mathematical Notes *Matematicheskie zametki*	12 (2 vols./yr. 6 issues ea.)	$185.00
Polymer Mechanics *Mekhanika polimerov*	6	$120.00
Radiophysics and Quantum Electronics (Formerly Soviet Radiophysics) *Izvestiya VUZ. radiofizika*	12	$160.00
Solar System Research *Astronomicheskii vestnik*	4	$ 95.00
Soviet Applied Mechanics *Prikladnaya mekhanika*	12	$160.00
Soviet Atomic Energy *Atomnaya énergiya*	12 (2 vols./yr. 6 issues ea.)	$160.00
Soviet Physics Journal *Izvestiya VUZ. fizika*	12	$160.00
Soviet Radiochemistry *Radiokhimiya*	6	$155.00
Theoretical and Mathematical Physics *Teoreticheskaya i matematicheskaya fizika*	12 (4 vols./yr. 3 issues ea.)	$145.00

Back volumes are available. For further information, please contact the Publishers.

SEND FOR YOUR FREE EXAMINATION COPIES

PLENUM PUBLISHING CORPORATION
227 WEST 17th STREET
NEW YORK, N. Y. 10011
Plenum Press • Consultants Bureau
• IFI/Plenum Data Corporation

In United Kingdom
Plenum Publishing Co. Ltd., Davis House (4th Floor)
8 Scrubs Lane, Harlesden, NW10 6SE, England